



UNIVERSITÀ DEGLI STUDI DI MESSINA
DIPARTIMENTO DI SCIENZE CHIMICHE, BIOLOGICHE,
FARMACEUTICHE ED AMBIENTALI

CORSO DI DOTTORATO DI RICERCA IN
BIOLOGIA APPLICATA E MEDICINA SPERIMENTALE
XXIX CICLO

**Probing the molecular interactions between
human Carbonic Anhydrases (hCAs) and a
novel class of designed benzenesulfonamides**

TESI DI DOTTORATO:
DOTT.SSA ELVIRA BRUNO

TUTOR:
PROF.SSA ROSARIA GITTO

COORDINATORE DEL CORSO DI DOTTORATO
CHIAR.MO PROF. SALVATORE CUZZOCREA

TRIENNIO 2014-2016

INDEX

Abbreviation	IV
Introduction	8
CHAPTER 1	10
<i>In the search of new therapeutics acting as Carbonic Anhydrase Inhibitors (CAIs) in human</i>	10
<i>1.1 Structure of Carbonic Anhydrase</i>	12
<i>1.2 Distribution of α-CA</i>	16
<i>1.3 Inhibition of the enzymatic activity</i>	19
<i>1.4 Characterization of the interactions between selected known inhibitors and hCA isoforms</i>	24
CHAPTER 2	34
<i>Results of the present thesis and Discussion</i>	34
<i>2.1 “In vivo” and “in silico” profiling of isoquinolinesulfonamides 13-31</i>	35
<i>2.1.1 Synthesis of isoquinolinesulfonamide derivatives 13-31</i>	36
<i>2.1.2 Biochemical screening and anticonvulsant effects</i>	39
<i>2.1.3 Prediction of biopharmaceutical parameters for compounds 13-31</i>	42
<i>2.2 Development of new arylsulfonamides inhibitors</i>	45

2.2.1 <i>Synthesis of 4-(3,4-dihydroisoquinolin-2(1H)-ylcarbonyl) benzenesulfonamides (70a-e) and 4-(3,4-dihydroquinolin-1(2H)-ylcarbonyl) benzenesulfonamides (71c-e)</i>	51
2.2.2 <i>Carbonic anhydrase inhibition assays against hCA isoforms and Structure-Activity Relationships (SARs) considerations</i>	54
2.2.3 <i>Enantiomeric separation and CA effects of each enantiomer</i>	58
2.2.4 <i>X-ray and docking studies</i>	60
Conclusions	70
CHAPTER 3	72
Experimental section	72
3.1 <i>Chemistry</i>	72
3.2 <i>CA inhibition assay</i>	79
3.3 <i>Anticonvulsant activity in DBA/2 mice</i>	79
3.4 <i>Enantiomeric resolution</i>	80
3.5 <i>X-ray studies</i>	81
3.5.1 <i>Co-crystal structures of inhibitors 70a, 70b, 70e, 71c and 71e in complex with hCAII</i>	81
3.5.2. <i>Co-crystal structures of inhibitors (R)-75d and (S)-75d in complex with hCA II</i>	82
3.6 <i>Molecular docking</i>	83
References	85

ANNEX	92
1.1 Recombinant protein	93
1.1.1 Procedure for protein expression in Escherichia coli - BL21(DE3)	95
1.1.2 Procedure to purify the protein	96
2.1 SDS-PAGE electrophoresis	97
3.1 Isothermal titration calorimetry (ITC)	99
References	100

Abbreviations

<i>ACC</i>	acetyl-coenzyme A carboxylase
<i>Ac-CoA</i>	acetyl coenzyme A
<i>ACE</i>	angiotensin converting enzyme
<i>AZM</i>	acetazolamide
<i>BBB</i>	brain blood barrier
<i>BBr₃</i>	boron tribromide
<i>CARPs</i>	carbonic anhydrase related proteins
<i>CD</i>	circular dichroism
<i>CNS</i>	central nervous system
<i>CSPs</i>	chiral stationary phases
<i>D&D</i>	Drug and Development
<i>D₂O</i>	deuterium oxide
<i>DCM</i>	dichloromethane
<i>DMF</i>	dimethylformamide
<i>DMSO</i>	dimethyl sulfoxide
<i>ED₅₀</i>	effective doses
<i>Et₂O</i>	diethyl ether
<i>EtOAc</i>	ethyl acetate
<i>EtOH</i>	ethanol
<i>FC</i>	Flash Chromatography
<i>GABA</i>	γ-aminobutyric acid
<i>HBTU</i>	<i>N,N,N',N'</i> -Tetramethyl- <i>O</i> -(1 <i>H</i> -benzotriazol-1-yl)uronium hexafluorophosphate

<i>hCAIs</i>	human Carbonic Anhydrase Inhibitor
<i>hCAs</i>	human Carbonic Anhydrases
<i>HPLC</i>	high performance liquid chromatography
<i>IOP</i>	intraocular pressure
K_i	inhibition constant
<i>LE</i>	ligand efficiency
<i>logBB</i>	brain-to-blood concentration ratio
<i>MBG</i>	metal binding group
<i>MMPs</i>	metalloproteinases
<i>MW</i>	microwaves
<i>nM</i>	nanomolar
<i>NMR</i>	Nuclear Magnetic Resonance
<i>PC</i>	pyruvate carboxylase enzyme
<i>PDB</i>	Protein Data Bank
<i>POCl₃</i>	phosphoryl chloride
<i>PSA</i>	polar surface area
<i>SARs</i>	structure-activity relationships
<i>TEA</i>	Triethylamine
<i>TFA</i>	trifluoroacetic acid
<i>TLC</i>	Thin-layer chromatography
<i>TPM</i>	topiramate
<i>TY</i>	tyrosinase
<i>ZBG</i>	Zinc-binding group

This PhD dissertation is entitled *“Probing the molecular interactions between human Carbonic Anhydrases (hCAs) and a novel class of designed benzenesulfonamides”* and is organized as follow. In the first chapter we have reviewed several previous works in the field of human Carbonic Anhydrase Inhibitors (hCAIs), which have been studied as innovative therapeutics for the treatment of several human diseases. The Chapter 2 describes the “results” of this research work concerning synthetic procedures, chemical characterization, structure-activity relationships (SARs), structural analysis of protein interaction of newer hCAIs. These compounds have been rationally designed on the basis of previous studies that have furnished suggestions about the key chemical features controlling inhibitory effects toward carbonic anhydrases. In this chapter we also discuss our main findings of our studies thus highlighting new suggestions for the development of hCAIs that could target specific and druggable CA isoforms.

In the Chapter 3 we report all experimental procedures for the synthesis and biochemical and pharmacological assays of the designed CA inhibitors. The “in vitro” biological assays have been performed at University of Florence in collaboration with Prof. Claudiu T. Supuran. The “in vivo “ properties of selected hCAIs have been tested in collaboration with Prof. Giovanbattista De Sarro from University of Catanzaro. The crystal structures of the synthesized compounds in complex with the hCA isoforms have been obtained in the laboratories of Prof. Pavlína Řezáčová at Academy of Sciences of the Czech Republic, Prague and in collaboration with Dr. Giuseppina De Simone from Institute of Biostructures and Bioimaging-CNR, Naples. Finally, in collaboration with Dr. Roberto Cirilli from the Istituto Superiore di Sanità, Rome, HPLC studies have been carried out.

In the last part of this dissertation, the Annex summarizes the main skills and competences that have been acquired during the six-months of external experience at University of Dundee, Division of Biological Chemistry & Drug Discovery, School of Life Sciences under supervision of Prof. Alessio Ciulli.

Key words: Carbonic Anhydrase, quinolines, isoquinolines, sulfonamides, HPLC, Docking studies, X-ray.

Introduction

Carbonic Anhydrases (CAs, EC 4.2.1.1) are a family of monomeric Zinc metalloenzymes that catalyze the reversible hydration of CO₂. The relevant role of this class of enzymes is the regulation of a broad range of physiological functions (gluconeogenesis, lipogenesis, and ureagenesis).^[1]

The family of human carbonic anhydrases (hCAs) comprises 15 different α -carbonic anhydrase isoforms: CA I-IV, CA VA and CA VB, CA VI-VII, CA IX, CA XII- XV and CARPs CA VIII, CA X, CA XI). In the last years, the attention toward this class of metalloproteins is in continuous growth because it was discovered their involvement in different diseases such as cancer,^[2] glaucoma,^[3] obesity,^[4] and epilepsy.^[5] Among the hCAs, the hCA VII is one of the least investigated cytosolic CA isoforms; it presents a limited distribution, being mainly expressed in the cortex, hippocampus, and thalamus regions within the mammalian brain where it is involved in generating neuronal excitation and seizures. Moreover hCA VII is expressed in other organs including the stomach, duodenum, colon, liver and skeletal muscle of mice.^[2, 5-7]

The hCA VII is currently considered to be involved in the mechanism of GABAergic generated seizures.^[5, 8] Recently, its involvement in neuropathic pain control has been proposed by a mechanism which is not completely known.^[6, 7, 9] Thereby, the investigation on hCA VII could also represent an interesting tool for the design of new pain killers useful for therapeutic applications. Several CA inhibitors such as acetazolamide (AAZ) and topiramate (TPM) have a long history as anticonvulsants, but their molecular targets and mechanisms of action at the neuronal network level are still poorly understood.^[10]

In the last years in the Department ChiBioFarAm – medicinal chemistry laboratories of the University of Messina, a collection of small molecules acting as carbonic anhydrase inhibitors had been discovered. The most active inhibitors displayed k_i values in the nanomolar range. Unfortunately, some of them showed poor selectivity toward the more druggable isoforms. These inhibitors possess the sulfonamide portion as key chemical portion that binds the Zinc²⁺ ion that is located at the bottom of a deep cleft of catalytic site (Figure 1).^[11]

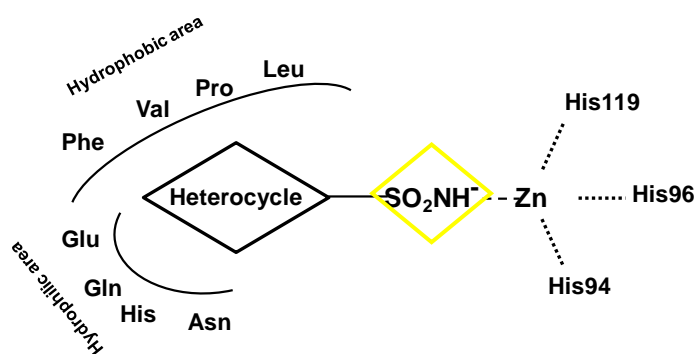


Figure 1. Representation of a hCA inhibitor with sulfonamide moiety.

The other moieties of these compounds control the major or minor interactions with the hydrophilic and/or hydrophobic regions of catalytic pocket. The degree of this pattern of contacts might be considered responsible of the inhibitory potency as well as selectivity toward specific CA isoforms.

During the three years doctoral course we chose to introduce new chemical moieties and modify these sulfonamides to obtain the new compounds. Specifically, we planned the synthesis of new compounds to improve inhibitory effects and isoforms selectivity.

Therefore, we planned the synthesis of a series of new sulfonamides bearing the quinoline and isoquinoline skeleton that has been variously decorated through the introduction of chemical fragment as hydrophilic/hydrophobic anchoring groups.

This series of novel hCAIs were in vitro tested against the hCA I, hCA II, hCA VII, hCA IX, hCA XII and hCA XIV. Structural and computational studies have been performed to explain the mechanism of inhibitory properties. Furthermore, in vivo studies were carried out to find new potential therapeutics for the treatment of brain pathologies.

CHAPTER 1

In the search of new therapeutics acting as Carbonic Anhydrase Inhibitors (CAIs) in human

Several metalloenzymes are involved in a wide array of in vivo functions, regulating blood pH, facilitating matrix degradation, modulating DNA transcription, and many others.^[12]

Moreover, given the relevance of these functions, an imbalance of the levels of these metalloenzymes plays a significant role in several diseases. In detail, pathologies for which metalloenzymes are implicated include cancer,^[13, 14] heart disease,^[15] epilepsy^[16] and obesity.^[17]

For this reason the development of metalloenzymatic modulators as new drugs for the treatment of these diseases could result in a good and innovative strategy in the Drug and Development (D&D) process.

Typically, metalloenzyme inhibitors are drug-like small molecules that incorporate a metal binding group (MBG) able to coordinate the metal ion within active site. By inducing an impairment of catalytic function, the MBG is appended to the drug-like portion of the inhibitor via a linker that can take on many forms, reflective of the diversity in enzyme active sites.^[18]

To represent a diverse range of MBGs we choose to analyze a small array of metalloproteins.

Matrix metalloproteinases (MMPs) are a group of Zn^{2+} -dependent endopeptidases known for their potential to disrupt angiogenesis in malignant tumors and represent a prototypical metalloenzyme target in medicinal chemistry. The MMP active site contains a catalytic Zn^{2+} ion coordinated by a His3 motif and a water molecule. The discovery of several potent broad-spectrum MMP inhibitors, have not successfully completed clinical trials for some disease (e.g. cancer, arthritis, etc.), due to problematic side effects, lack of efficacy in human trials, and other barriers.^[18]

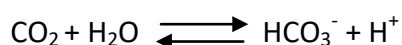
Angiotensin converting enzyme (ACE, EC 3.4.15.1) is a Zn^{2+} dipeptidyl carboxypeptidase in which the catalytic Zn^{2+} ion is bound to the protein by a His2 Glu motif. ACE functions endogenously to generate the biologically active polypeptide angiotensin II from angiotensin I. The cleaved product induces a vasoconstriction response that manifests as increased blood pressure. An important metalloenzyme inhibitor for treating hypertension, Captopril (Capoten, Squibb, patented in

1976),^[19] incorporates a thiol group capable of coordinating the catalytic Zn²⁺ ion in the active site of ACE.^[18]

Mushroom tyrosinase (TY) is a dinuclear Cu²⁺ oxidase controlling the production of melanin. The two active site Cu²⁺ ions are bound by six histidine residues (three to each metal ion). TY converts tyrosine to L-DOPA and subsequently L-DOPA to dopaquinone. Then dopaquinone, a highly reactive compound determinant in the melanogenesis, rapidly and spontaneously evolves towards the formation of various melanin pigments.^[20] Consequently, TY inhibitors are of interest to the cosmetics industry.^[18]

Discovered in the 1930s,^[21] Carbonic Anhydrases (CAs) represent the oldest known class of Zn metalloenzyme. In many organisms these enzymes are involved in crucial physiological processes connected with pH and CO₂ homeostasis/sensing; biosynthetic reactions, respiration and transport of CO₂/bicarbonate, electrolyte secretion in a variety of tissues/organs, bone resorption; calcification, tumorigenicity and many other physiological or pathological processes (thoroughly studied in vertebrates and some pathogens).^[22] The attention toward this family of enzymes is incremented due to the possibility to develop therapeutics in prevention and treatment of various diseases such as glaucoma, obesity, cancer, etc.

The family of carbonic anhydrases (CAs, EC 4.2.1.1) catalyse the interconversion between CO₂ and bicarbonate.^[23-25]



The physio/pathological relevance of this reaction is that the exceedingly high amounts CO₂ may damage cellular components, while its conversion to water soluble ions (bicarbonate and protons), may interfere with the pH balance of the cell through the generation of an acid (H⁺) and a buffering base (HCO₃⁻).^[22]

To date the CA enzymatic families are: α-, β-, γ-, δ-, ζ- and η classes. The α-CAs are present in vertebrates, protozoa, algae, cytoplasm of green plants and in many Gram negative bacteria,^[26-28] the β-CAs are found in both Gram negative and positive bacteria algae and chloroplasts of mono- as well as dicotyledons, and also in many fungi and some *Archaea*.^[23-25, 27] The γ-CAs were found in *Archaea*, cyanobacteria and most types of bacteria,^[26, 29] the δ- and ζ-CAs seem to be present only in marine diatoms,^[24, 30] whereas the η-CAs in protozoa.^[23, 31]

The class of α -CA is present in mammals; human carbonic anhydrase isoforms (hCAs) are subdivided in 15 different isoforms, that play an important physiological and patho-physiological functions “*in vivo*”.

1.1 Structure of Carbonic Anhydrase

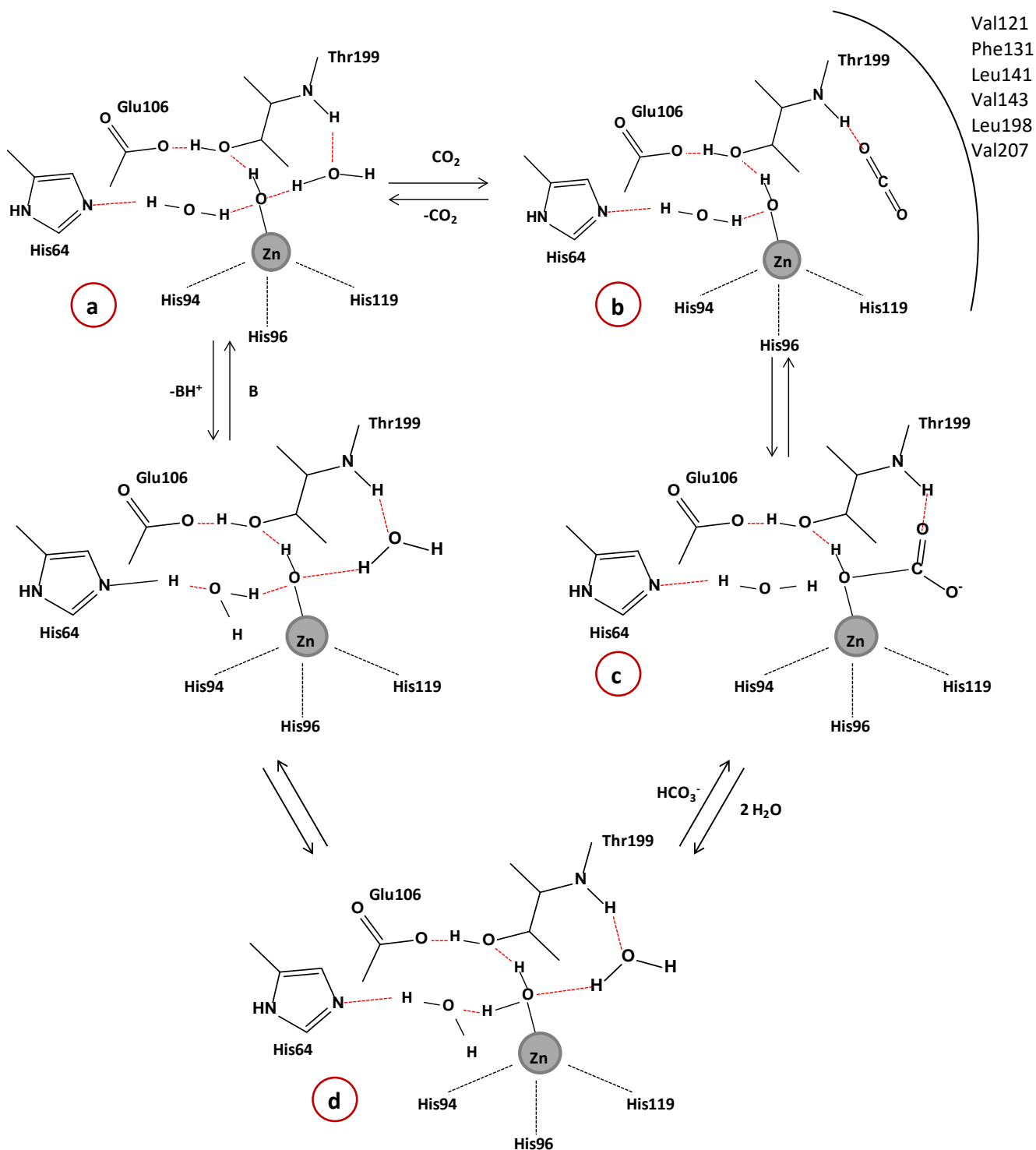
The active site of the CA shows a conical shape; it displays a 15 Å diameter entrance that tapers into the center of the enzyme. In the depth of the catalytic site we can find the MBG in a tetrahedral geometry. There are three amino acid residues (His94, His96 and His119) generating coordination bonds. Additionally, there is a water molecule/hydroxide ion that is coordinated with the metal ion.

The presence of Zn^{2+} ion characterizes all six CA genetic families, but Cd^{2+} is interchangeable with Zn^{2+} in the ζ -CAs, [25] Fe^{2+} seems to be present in γ -CAs, at least in anaerobic conditions, [32] whereas Co^{2+} may substitute the Zinc ion in many α -CAs without a significant loss of the catalytic activity. [23-25, 33-35]

The cavity is partitioned in to two very different environments. The area containing the zinc, in the depth of the active site, lies a cluster of hydrophobic amino acids (Val121, Phe131, Leu141, Val143, Leu198 and Val207), whereas on the other side of the zinc, leading out of the active site to the bulk solvent, the surface is lined with hydrophilic amino acids (Asn62, His64, Asn67, Gln92) (figure 2). [22, 36]

The bulky hydrophobic residue Phe131 divides the hydrophobic area in two sub-sites in which various classes of inhibitors bind in a specific manner. [36-39] Indeed, the mechanism where the zinc binds the CO_2 is supposed that the hydrophobic part is used to entrap the CO_2 molecule. [36]

The hydrophilic region facilitates the binding of the polar components generated from the CO_2 hydration reaction (bicarbonate and protons) and their release from the cavity, towards the environment. [22]



Scheme 1. Catalytic mechanism for the α -CA catalyzed CO_2 hydration. Hydrogen bonds are indicated by dashed lines in red. The hydrophobic cleft is indicated by an line.^[40]

The enzymatic mechanism of the CA is shown in the scheme 1. Zinc is the key of the enzyme reaction. The water bond to the Zn^{+2} ion is actually broken down to a proton and hydroxyl ion. Since zinc is a positively charged ion it stabilizes the negatively charged hydroxyl ion.^[40]

The active form of the enzyme is the basic one, with hydroxide bound to Zn^{2+} (**a**). This strong nucleophile attacks the CO_2 molecule that is bound in a hydrophobic pocket in its neighbourhood (**b**), leading to the formation of bicarbonate coordinated to Zn^{2+} (**c**). The bicarbonate ion is then displaced by a water molecule, leading to the acidic form of the enzyme, with water coordinated to Zn^{2+} (**d**), this form is catalytically inactive.^[23]

Generally, in the catalytically very active isozymes such as CA II, CA IV, CA VII and CA IX, occurs the regeneration of basic form (**a**), the His64 assists to the a proton transfer reaction from the active site to the environment or as well as by a cluster of histidines, which protrudes from the rim of the active site to the surface of the enzyme, assuring thus a very efficient proton transfer process for the most efficient CA isozyme, CA II.^[41, 42] Another pathway can transform the Zn^{2+} from the inactive form (**d**) to active form (**a**). Specifically, it can be by buffers present in the medium but this is the rate-limiting step in catalysis.

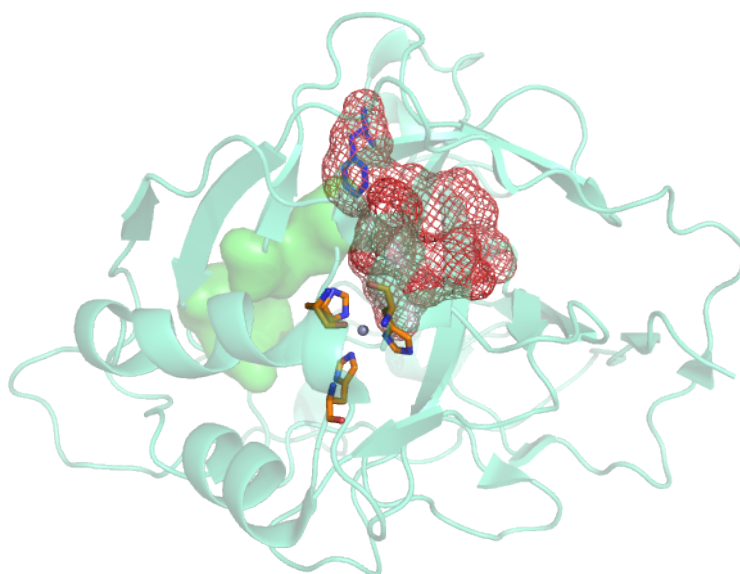


Figure 2. Catalytic pocket with the hydrophobic side in red and the hydrophilic region in green. The zinc is shown in grey with the three amino acid residues (His94, His96 and His119) and the Phe131 in blue. Picture modified from reference [36].

In the mechanism regenerating the zinc ion/hydroxyl in the catalytic process, there are several histidines called proton shuttling that are involved in this processes (such as the residue of His64).^[32, 35, 36, 38, 39]

Indeed, His64 is one of the few amino acid residues that has a flexibility within the catalytic pocket. This phenomenon has been demonstrated through x-ray studies where the imidazole moiety presents two conformations: an 'in' one, pointing towards the Zn²⁺ ion, and an 'out' one, pointing towards the exit of the cavity.^[43] The two conformations are part of the proton transfer mechanism by which this residue shuttles protons between the active site and the reaction medium (see Figure 3).^[38, 39, 43]

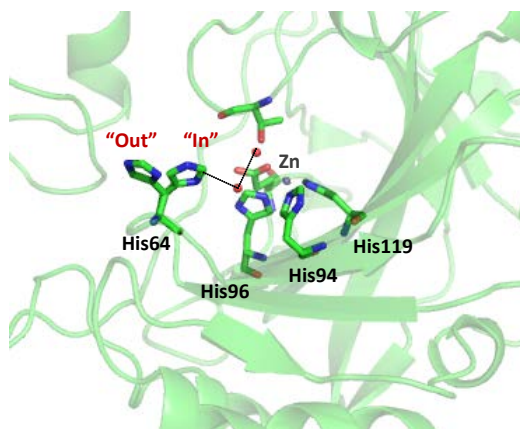


Figure 3. Catalytic pocket of hCA II, with zinc ion in grey, the molecules of water in red. His64 in both conformation, "In" and "Out". (PDB code 2CBA)^[44]

As shown in the Figure 3, the catalytic Zn²⁺ ion is located at the bottom of this cavity, coordinated by the three histidine residues and a water molecule/hydroxide ion. Moreover, the MBG is engaged in hydrogen bond interactions with another water molecule (called the deep water) and with the hydroxyl moiety of the threonine residue (Thr199), which in turn is bridged to the carboxylate moiety of a glutamic acid residue (Glu106) (figure 4).^[23, 34, 38, 39, 43]

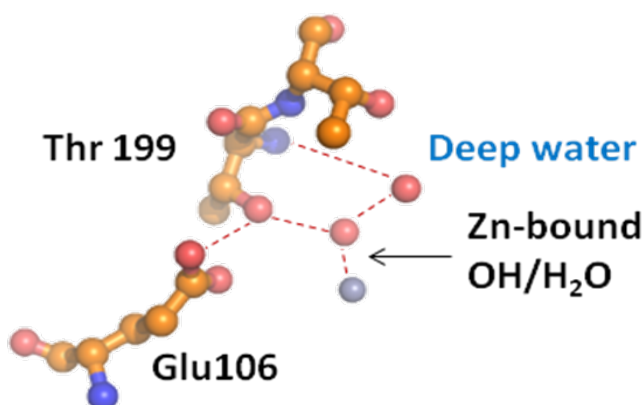


Figure 4. The ordered water network in the active site of hCA II. The zinc is represented by a grey sphere and the oxygen atoms of water molecules as smaller red spheres. Dotted lines are presumed hydrogen bonds with heavy atom distances given. Stick figures are selected amino acids of the active.^[45]

As displayed in the Figure 4, the presence of these two amino acids in the catalytic pocket results in an enhancement of the nucleophilicity of the Zn^{2+} bound water molecule, and orients the CO_2 substrate in a location favorable for the nucleophilic attack.

The residues Thr199 and Glu106 are important elements in the catalytic side for all α -CAs, so they are called gate-keeping residues.^[22]

1.2 Distribution of α -CA

In mammals, the different CA isozymes and CA-related proteins (CARP) display different tissue distribution, expression levels, and subcellular locations. In more details, there are five cytosolic forms (CA I, CA II, CA III, CA VII and CA XIII), five membrane bound isozymes (CA IV, CA IX, CA XII, CA XIV and CA XV), one mitochondrial forms (CA V), and a secreted CA isozyme (CA VI).^[42] In addition, there are the catalytically inactive isoforms of α -carbonic anhydrases known as carbonic anhydrase related proteins (CARPs) and classified as CA VIII, CA X, and CA XI. The hCA I, II and IV are involved in respiration and regulation of the acid/base homeostasis. These processes involve both

the transport of CO₂/bicarbonate between metabolizing tissues and excretion sites (lungs, kidneys), they facilitate CO₂ elimination in capillaries and pulmonary microvasculature, elimination of H⁺ ions in the renal tubules and collecting ducts, as well as reabsorption of bicarbonate in the brush border and thick ascending Henle loop in kidneys. ^[42]

Moreover, CAs are involved in vision and control the production of the bicarbonate-rich aqueous humor secretion (mediated by ciliary processes isozymes CA II, CA IV and CA XII) within the eye; so their malfunctioning leads to high intraocular pressure, and glaucoma. ^[42, 46] Specifically, the hCA II is also involved in the bone development and function, such as the differentiation of osteoclasts, or the provision of acid for bone resorption in osteoclasts.

CAs are involved in the secretion of electrolytes in many other tissues/organs, such as: saliva production in acinar and ductal cells; gastric acid production in the stomach parietal cells; bile production, pancreatic juice production, intestinal ion transport. ^[42, 46]

CAs also play a role in gustation and olfaction, protection of gastro-intestinal tract from extreme pH conditions (too acidic or too basic), regulation of pH and bicarbonate concentration in the seminal fluid, muscle functions and adaptation to cellular stress. Some isozymes, such as CA V, control molecular signaling processes, such as insulin secretion signaling in pancreas β cells. ^[42, 46]

Isozymes II and VA are involved in important metabolic processes, as they provide bicarbonate for gluconeogenesis, fatty acids de novo biosynthesis or pyrimidine base synthesis.

Finally, some isozymes (such as CA IX, CA XII, CARP VIII) are highly abundant in tumors, being involved in oncogenesis and tumor progression.

Currently, CA inhibitors are clinically used as antiglaucoma agents, diuretics, antiepileptics, in the management of mountain sickness, gastric and duodenal ulcers, neurological disorders, or osteoporosis among others. ^[42, 47, 48]

The development of carbonic anhydrase inhibitors (CAIs) are of growing interest since various isoforms of the enzyme are identified as promising drug targets for treatment of diseases. The principal drawback of the clinically used CAIs is the lack of isoform selectivity, which may lead to observable side effects. ^[49]

Table 1. Classification of the hCA isoforms.				
Isoform	Sub-cellular localization	Tissue/organ localization	Disease	Therapeutics
hCA I	Cytosol	Erythrocytes, GI tract	retinal cerebral edema	No drug
hCA II	Cytosol	Erythrocytes, eye, GI tract, bone osteoclasts, kidney, lung, testis, brain	glaucoma	acetazolamide, methazolamide, ethoxzolamide, dichlorophenamide, dorzolamide
			edema	
			epilepsy	acetazolamide, topiramate, zonisamide
			altitude sickness	No drug
hCA III	Cytosol	Skeletal muscle, adipocytes	oxidative stress	No drug
hCA IV	Membrane-bound	Kidney, lung, pancreas, brain capillaries, colon, heart muscle	glaucoma	acetazolamide, methazolamide, ethoxzolamide, dichlorophenamide, dorzolamide
			Retinitis pigmentosa	No drug
			stroke	No drug
hCA VA/VB	Mitochondria	Liver/Heart and skeletal muscle, pancreas, kidney, spinal cord, GI tract	obesity	topiramate, zonisamide
hCA VI	Secreted into saliva/milk	Salivary and mammary glands	cariogenesis	No drug
hCA VII	Cytosol	CNS	epilepsy	acetazolamide, topiramate, zonisamide
hCA VIII (CARP VIII)	Cytosol	CNS	neurodegeneration	No drug
			cancer	Indisulam (E7070)
hCA IX	Transmembrane	Tumours, GI mucosa	cancer	Indisulam (E7070)
hCA XII	Transmembrane	Renal, intestinal, reproductive epithelia, eye, tumours	cancer	Indisulam (E7070)
			glaucoma	acetazolamide, methazolamide, ethoxzolamide, dichlorophenamide, dorzolamide
hCA XIII	Cytosol	Kidney, brain, lung, gut, reproductive tract	sterility	No drug
hCA XIV	Transmembrane	Kidney, brain, liver	epilepsy	acetazolamide, topiramate, zonisamide
			retinopathy	No drug

1.3 Inhibition of the enzymatic activity

For a long period, the only mechanism of CA inhibition known was the interaction between the metal ion in tetrahedral geometry with the zinc-binding group (ZBG as MBG) or by adding to the metal coordination sphere and generating trigonal bipyramidal geometry, as reported in the Figure 5.^[22]

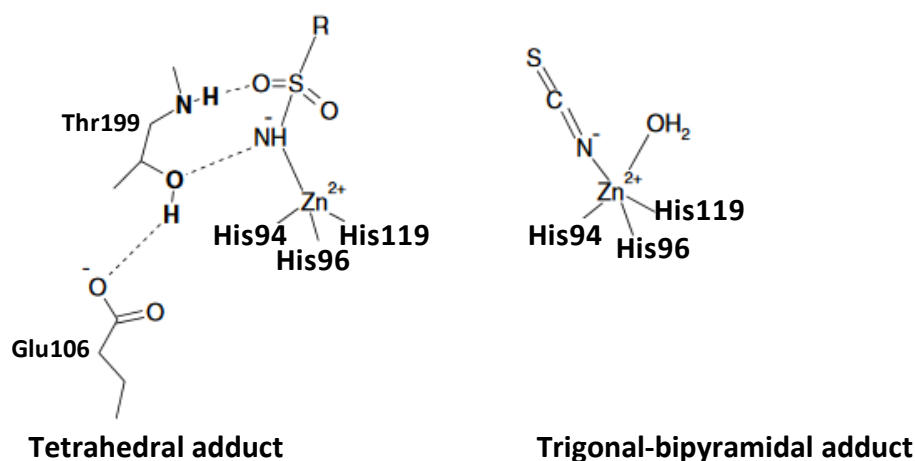


Figure 5. α -CA inhibition mechanism between the metal ion with the ZBG in two different geometries.

The anions may bind either in tetrahedral geometry of the metal ion or as trigonal–bipyramidal adducts, such as for instance the thiocyanate adduct shown in Figure 5.

Others examples of the inorganic anions are generally represented by halogens, such as chloride, iodide and bromide, or cyanate and the sulphur and anions characterized by less affinity for metal ions in solution (tetrafluoraborate, perchlorate, nitrate, fluoride and heavier halides, among others).^[42, 50] The application in therapy of anions is not possible due of the many side effects and even their use is limited by the small size which makes it difficult the optimization of their structure.

The tetrahedral geometry is formed by the unsubstituted sulfonamides that bind the Zn^{2+} ion replacing the non-protein ligand. Sulfonamides and their isosteres

(sulfamates, sulfamides),^[23, 29, 39] are the most important CAIs binding in a tetrahedral geometry. Krebs (1948) discovered that unsubstituted aromatic sulfonamides are inhibitors of the carbonic anhydrase.^[51]

The classical CA inhibitors (CAIs) are the primary sulfonamides, R-SO₂NH₂, which are in clinical use for more than 50 years as diuretics and systemically acting antiglaucoma drugs.^[52]

In fact there are ~30 clinically used drugs (or agents in clinical development). Some of them are shown in Figure 6, they belong to the sulfonamide or sulfamate, such as the classical inhibitors acetazolamide (**1**), methazolamide (**2**), ethoxzolamide (**3**), dichlorophenamide (**4**) and also more recent drugs/investigational agents such as dorzolamide (**5**), brinzolamide (**6**), indisulam (**7**), topiramate (**8**), celecoxib (**9**), sulthiame (**10**), saccharin (**11**), zonisamide (**12**) (figure 6).^[43, 53-59]

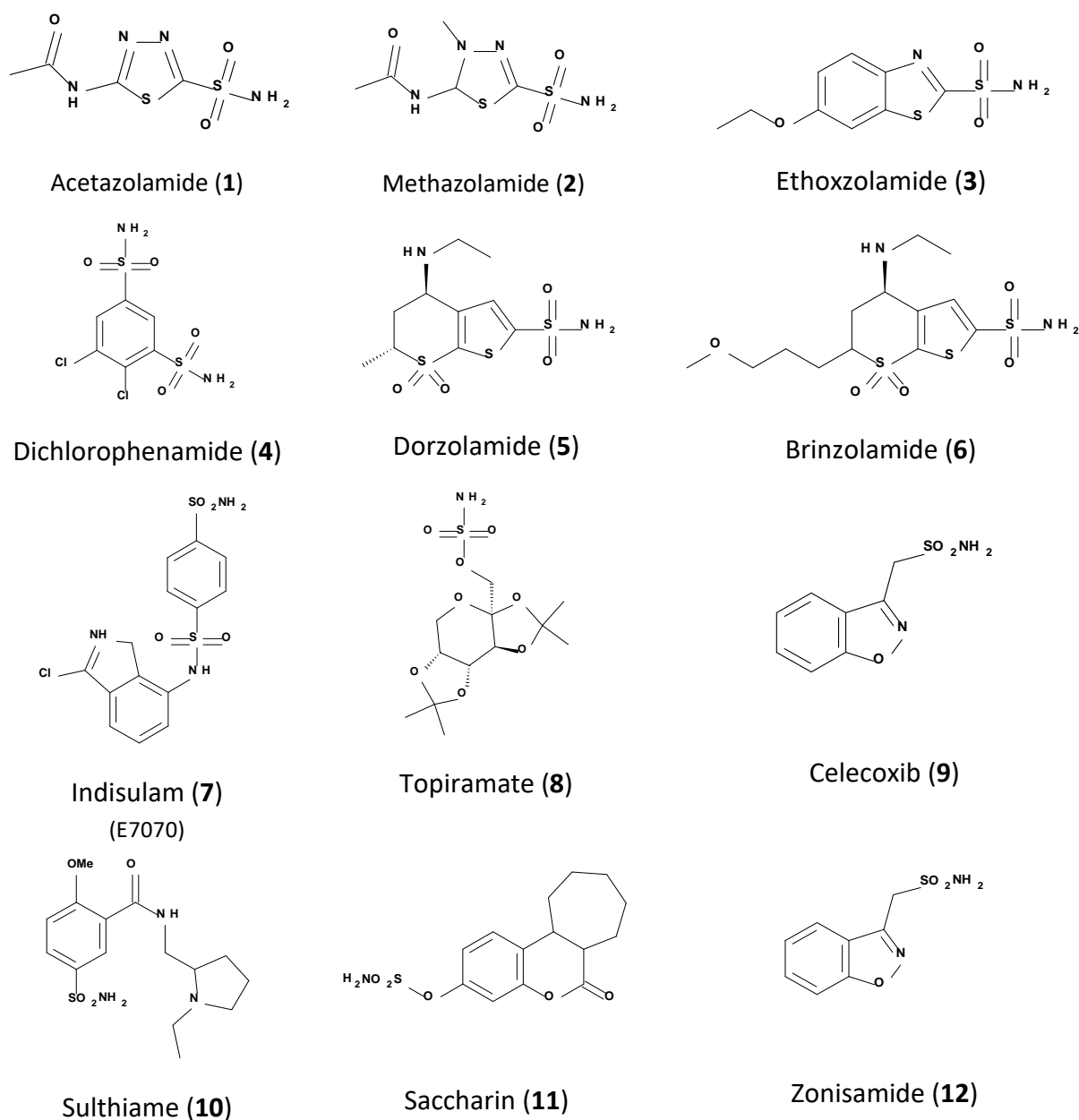


Figure 6. Classics sulfonamides CAIs

Some of these compounds are useful in reducing elevated intraocular pressure (IOP), but have a limited use due to numerous side effects that arise by inhibition of CAs other than those present in the eye ciliary processes (i.e., CA II, IV, and XII), leading to fatigue, paresthesias, and kidney stones.^[23] Moreover, can also be use as diuretic and, in addition, for the treatment of cancer, epilepsy, obesity, neuropathic pain and infections.^[2, 5, 9, 29, 59] However, critical barriers to the design of CAIs as therapeutic agents are related to the high number of isoforms in humans, their

rather diffuse localization in many tissues/organs, and the lack of isozyme selectivity of the presently available inhibitors of the sulfonamide/sulfamate type.^[52]

The interaction of the inhibitor with the metallic cofactor is described below.

In deprotonated state the $\text{-SO}_2\text{NH}^-$ moiety coordinates to Zn^{2+} ion and creates an extended network of hydrogen bonds, involving residues Thr199 and Glu106, also participating to the anchoring of the inhibitor molecule to the metal ion.

The largest majority of the designed sulfonamides possess an aromatic scaffold. This approach was really beneficial for the chemistry of this class of derivatives, as a large number of new ring systems that was and will be explored in this way. The development of new inhibitors of CA includes a “tail that might induce water solubility. Specifically, amino, hydroxyl, immino or hydrazino moieties can be bound to different scaffolds of well-known aromatic/heterocyclic sulfonamides; in this way these inhibitors maintain affinity for the CA active site, assuring in this way the possibility to modulate in greater details the physico-chemical properties of these pharmacological agents (figure 7).^[48]

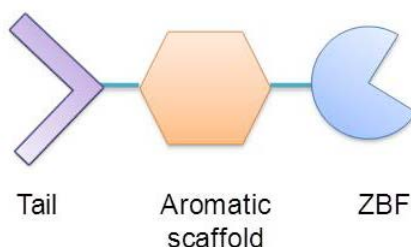


Figure 7. Generic skeleton of CAIs

The inhibition of hCAs can be carried out with others mechanism. In detail, several inhibitors can occlude the active site entrance that is located further away from the metal ion, at the entrance of the site cavity . Such compounds incorporate a “*sticky group*” which may be of the OH, amino, COOH and other types. This alternative mechanism of action was discovered for coumarins^[60, 61] and it was later shown that many other classes of structurally similar compounds, which bind to the enzyme in this manner (Figure 8).^[62, 63]

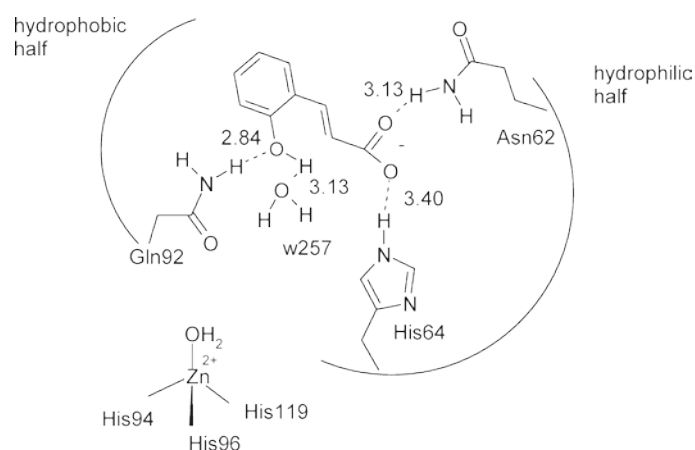
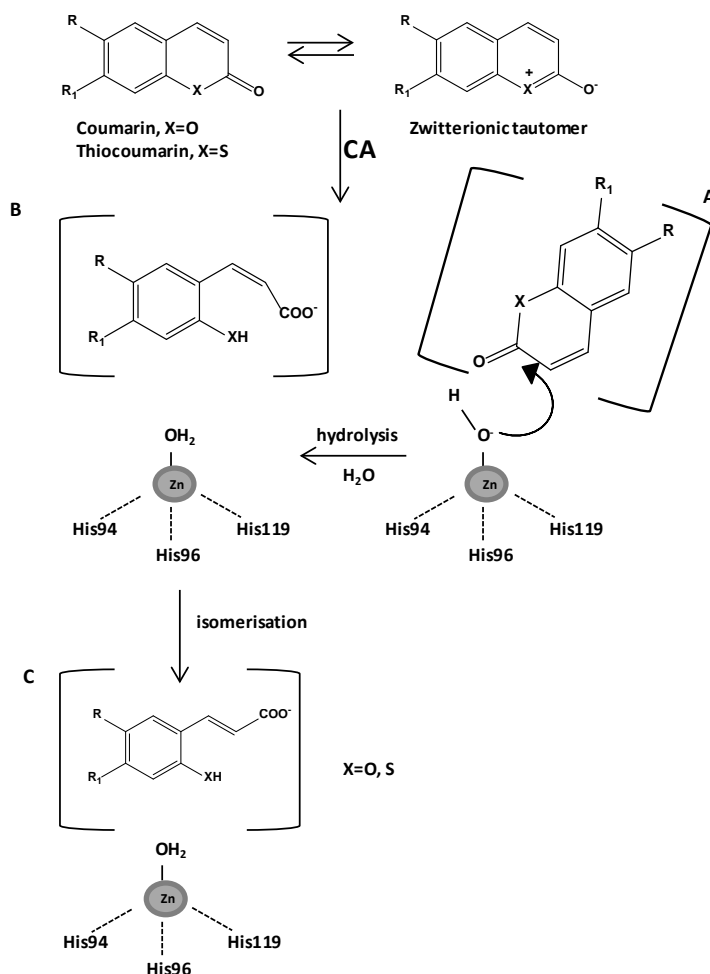


Figure 8. Hydrogen bonds in which the coumarin binds the residues into the hCA II active site.

The inhibition mechanism of this class of compounds can be explained as depicted in Scheme 2. Several coumarins/thiocoumarins may possess various tautomeric forms, such as the zwitterionic benzo(thio)pyrylium phenoxides, which may bind within the CA active site similarly to phenols by anchoring to the zinc-bound water molecule/hydroxide ion. In the first step, coumarins/thiocoumarin, shown in the step A, may undergo hydrolysis by the zinc-activated water molecule/hydroxide ion from the enzyme cavity, which acts as a very potent nucleophile. It can be hypothesized that a *cis*- or *trans*-2-hydroxy/mercapto-cinnamic acid intermediate is formed (step B), which cannot bind effectively in the restricted space near the Zn^{2+} ion due to its bulky skeleton, being thus reoriented toward the exit of the active site cavity. In the final step the compound suffers for a rearrangement of the enzyme-inhibitor adduct; step C, provided that the R and R_1 moieties from the initial (thio)coumarin are not too bulky to interfere with the binding to the enzyme active site.^[61]

The inhibitor *cis* or *trans* 2-hydroxy-cinnamic acid was found bound at the entrance of the active site cavity (Figure 8).^[60] In detail, the COOH moiety of the inhibitor interacts with two amino acid residues of the hydrophilic part of the hCA II active site (Asn62 and His64) by means of two hydrogen bonding interactions (Figure 8).^[60, 61]



Scheme 2. Proposed inhibition mechanism of CAs by coumarins/thiocoumarins.

1.4 Characterization of the interactions between selected known inhibitors and hCA isoforms

Many hCAIs bearing sulfonamide moiety possess high affinity for the most part of isozymes considered to play important physiological functions. However, the critical challenge for the design of novel pharmacological agents from this class is constituted by the lack of specificity of such compounds towards the different isozymes.^[48]

Some of these isoforms present the differences on aminoacidic residues that modulate the hydrophobicity and charge while others change the active site cavity volume and shape. These differences in active site environment in turn modulate inhibitor binding constants and their dynamics of entry.^[64]

To describe the main interactions within catalytic site of selected isoforms we report several specific binding poses for well-known hCAIs currently in therapy for treatment of epilepsy, obesity and cancer.

Acetazolamide (AZM, 1): AZM was initially discovered as a diuretic agent, but its clinical use was limited due to its transient action and onset of metabolic acidosis. However AZM corrects the significant metabolic alkalosis which occurs with loop diuretics such as furosemide, bumethanide, torasemide, and so on; so this this compound displays more clinical interest as a diuretic. Furthermore, the inhibitor **1** is highly efficient for the treatment of patients with hypercapnia and metabolic alkalosis. However, the main use of **AZM** and other first generation CAIs, such as methazolamide (**2**) and dichlorophenamide (**4**), is the therapeutic treatment of glaucoma.^[65] It is interesting to consider that AZM dissolved in water has three possible protonation states with two associated pK_a values (7.2 and 8.7) that are relevant to physiological pH (figure 9). It is thought that any of these forms can bind to hCA II.

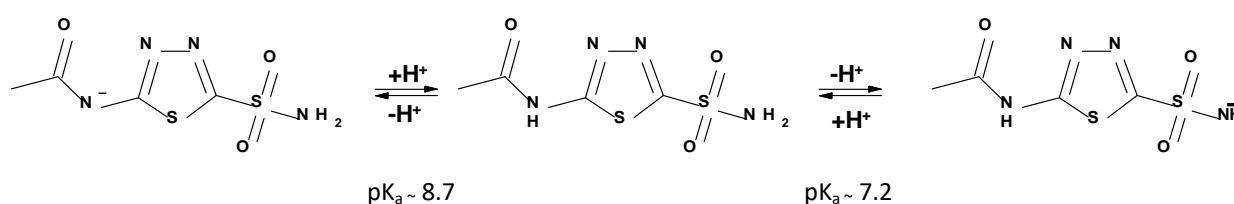


Figure 9. Ionization and pK_a of acetazolamide (AZM, **1**) in water.

The **AZM** was co-crystallized with the hCA II isoform and has been found that AZM was in the anionic form, with the negatively charged sulfonamide group coordinated to the zinc.

The lone pair of sulfonamide N is involved in a coordinating bond with the zinc of ~ 2.4 Å distance (figure 10 A), it makes the H bonding interaction with the oxygen of Thr199, which in turn acts as a H-bond donor to Glu106.

Moreover the amidic group binds a water molecule, W1120, which forms an H-bond bridge between AZM and hCA II. Indeed, W1120 interacts with the hydroxyl of Thr200 and with the carbonyl group of Pro201.

AZM also interacts through two very weak hydrophobic interactions: the first is a type of $-CH\cdots\pi$ interaction (~ 3.5 Å distance) between Leu198 and the thiadiazole ring of AZM. The other is a somewhat distorted $-CH\cdots\pi$ interaction between the terminal $-CH_3$ of AZM and Phe131. As weak as these interactions are, they contribute to the overall binding of AZM to hCA II (figure 10 B).

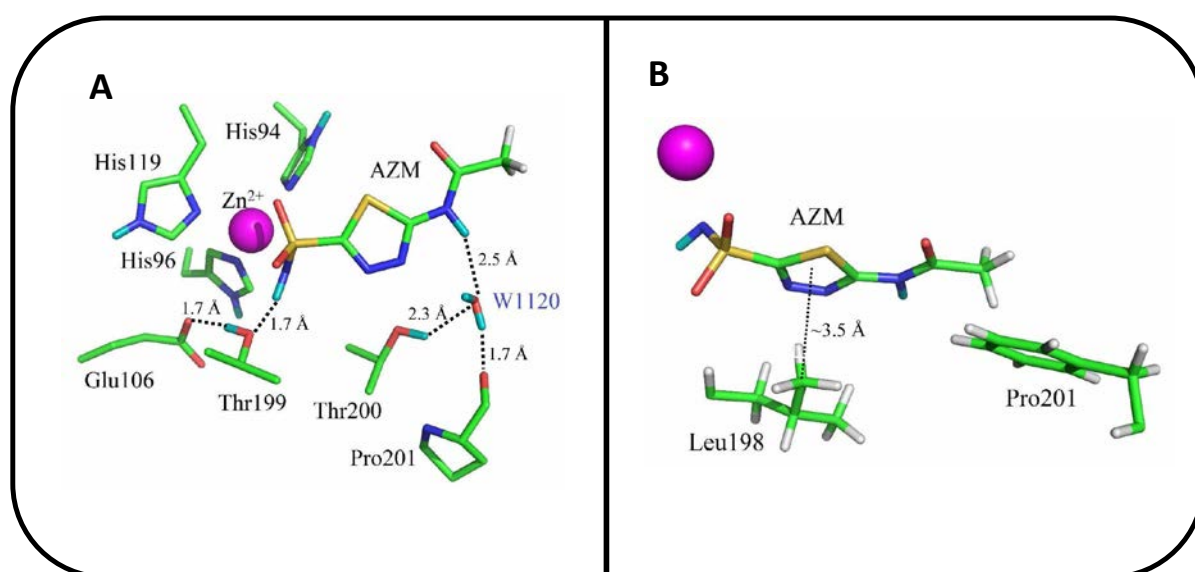


Figure 10. (A): Interaction between AZM and hCA II (PDB code 4G0C); zinc is shown as a magenta sphere. Hydrogen bonds as observed in the nuclear maps are indicated by dashed lines with distances as indicated. (B): AZM makes hydrophobic interactions within the active site of hCA II.^[66]

Moreover, AZM demonstrated a modulator in anticancer therapies in combination with different cytotoxic agents, such as alkylating agents, nucleoside analogs, platinum derivatives, etc. It was hypothesized that the anticancer effects of AZM (alone or in combination with such drugs) might be due to the acidification of the intra-tumor environment ensued after CA inhibition, although other mechanisms of action of this drug were not excluded.^[66, 67]

Figure 11 shows the comparison of the catalytic pocket between hCA II and hCA IX. Acetazolamide inhibits the hCA II and hCA IX with the K_i values in the range nM (12 and 25 nM, respectively). The comparison of the hCA II and hCA IX active sites shows that there are two main differences for

residues Phe131 and Val135, for which Val and Leu are present in hCA IX, respectively. Phe131 (in hCA II) is involved in very weak hydrophobic interactions with AZM and its absence in hCA IX could, in part, explain the small 2-fold difference in binding constants for AZM between hCA II and IX.^[66]

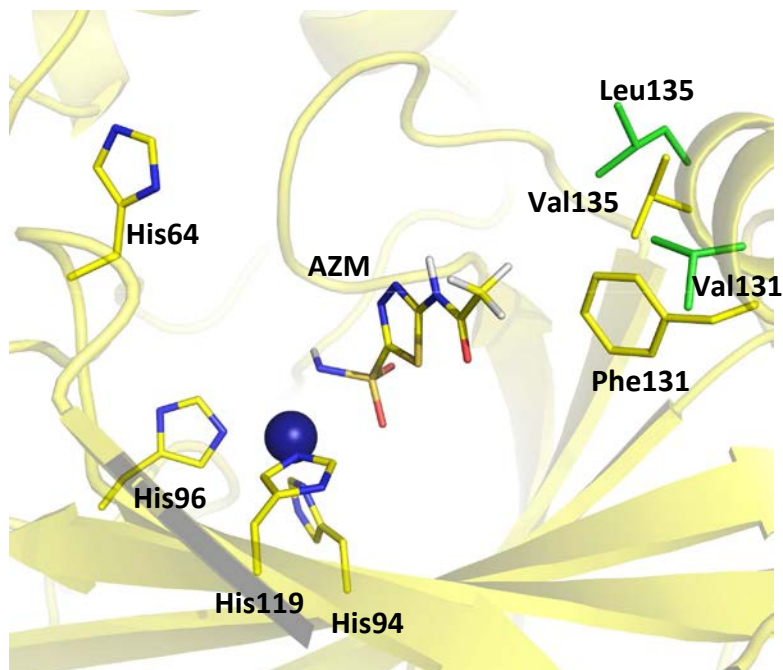


Figure 11. Complex between hCA II and AZM (yellow cartoon and sticks) and residues that are different residues in hCA IX are shown in green ball-and-stick (Val131 and Leu135). Zn²⁺ is shown as a blue sphere. (PDB code 3IAI)^[66]

Since several decades, coadministration of **1** with various antiepileptic drugs (AEDs), such as topiramate (**8**) and zonisamide (**12**), produced a remarkable increase of the anticonvulsant activity for barbiturates including barbital, mephobarbital, metharbital; phenytoin; valproic acid and trimethadione. The mechanism for which the AZM enhances the anticonvulsant effects of these AEDs are poorly understood but it was inferred that the difference in the potentiating effects of acetazolamide on the activity of various antiepileptics might be correlated to the effect that **1** has on the brain levels of these drugs as well as pH changes that acetazolamide may induce by inhibiting the many CA isoforms present in the brain.^[66, 67] Acetazolamide is still used in combination therapy with the AEDs or in refractory epilepsies.^[68]

Moreover, it was observed that AZM (**1**) displays K_i values at nanomolar concentration against hCA VII (2.5nM) and is characterized by hCA VII selectivity over hCA II. By analyzing the X-ray crystal

structure of **1** in complex with CA VII (PDB code 3ML5) the main interactions between the inhibitor and the protein were studied. Specifically, a structure-based pharmacophore model has been carried out using LigandScout and the results are displayed in Figure 12.^[69] As shown in this figure AZM binds the catalytic side with seven hydrogen bonding features including: four H-bond acceptors which bind residues Gln92, Thr199, Thr200, and a water molecule (W354); three H-bond donors pointed towards His94, Thr199, and a water molecule (W354).^[69]

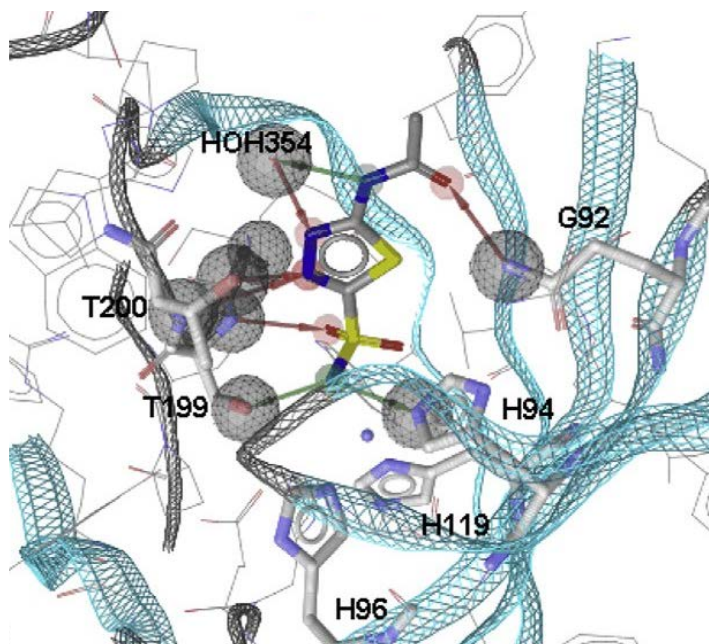


Figure 12. Structure-based pharmacophore model generated using LigandScout^[70] from the X-ray crystal structure of acetazolamide (**1**) and in complex with CA VII (PDB code 3ML5). Hydrophobic groups (light yellow spheres), H-bond donors (green arrow), H-bond acceptors (red arrow).^[69]

Topiramate (TPM, 8): TPM is a sugar sulfamate derivative possessing good anti-epileptic activity. It is derived from a monosaccharide (β -D-fructopyranose) and bears the sulfamate functional group that is considered to be responsible for its anticonvulsant properties, even if the mechanism of action of this drug seems to be rather complicated and not entirely understood. The anticonvulsant effects of topiramate are probably due to CO_2 retention secondary to inhibition of the red cell and brain enzymes, but other mechanisms of action were also hypothesized for TPM. In fact TPM shows a positive modulatory effect on some types of GABA_A receptors, antagonizes kainate/AMPA receptors and inhibits the generation of action potentials in neurons *via* antagonism of Na^+ channels activation.^[10, 71, 72]

In Figure 13 is reported the X-ray structure of the complex between **8** and hCA II. Beyond the known interaction between the nitrogen atom of the sulfonamide moiety of the inhibitor **8** and the Zinc ion at the tetrahedral vertex with a distance of 1.97 Å, it makes an extended network of hydrogen bonds between the inhibitor and some amino acid residues within the cavity strongly stabilize the complex. In detail, Asn62 with one of the oxygen (O₄) of topiramate (3.06 Å), Gln92 with the other oxygen (O₆) of topiramate (2.85 Å) and the water molecule 1134 that makes a bridge between the inhibitor and Thr200 through two hydrogen bonds, one with O₃ (2.84 Å) of the inhibitor and the other with the oxygen of the residue Thr200 (2.92 Å). The same oxygen of Thr200 makes hydrogen bond with the pyranose oxygen of topiramate (2.82 Å).^[72] In this case the interactions between the inhibitor and the hCA II are the same that have been shown previously.

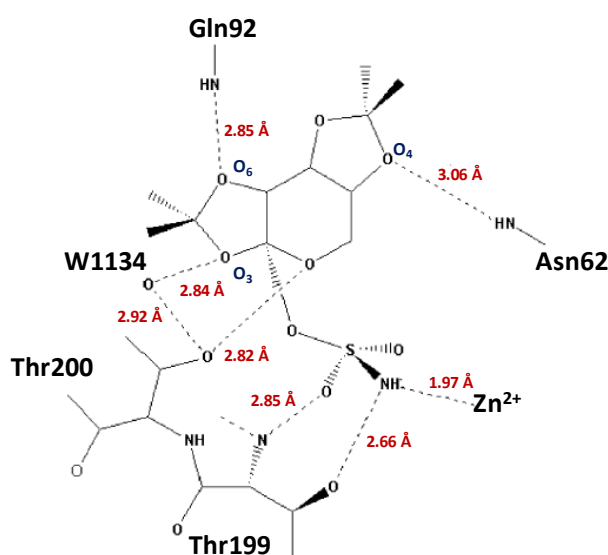


Figure 13. Complex between topiramate (**8**) and hCA II. In red the corresponding distances (in Å).

The inhibitory activity of TPM has been tested against other hCA isoforms and topiramate showed a K_i in subnanomolar concentration against the hCA VII (0.9 nM) thus corroborating its contribute to epileptic activity. There is not yet the crystal structure between the TPM and the hCA VII but this inhibitor was and is still used as antiepileptic drug.

TPM has recently been approved for a second clinical use, as an antiobesity agent. Indeed, it reduces lipogenesis by inhibiting CA isoforms involved in metabolic pathways such as the mitochondrial CA VA/B or the cytosolic CA II.

The role of mitochondrial CAs is to assist the mitochondrial pyruvate carboxylase enzyme (PC) affording carbon units, in the form of bicarbonate ions, which are incorporated in the pyruvate, to form oxaloacetate which in turn is then converted into citrate through the reaction with acetyl coenzyme A (Ac-CoA). Citrate, unlike oxaloacetate and Ac-CoA, is able to translocate from the mitochondria into the cytosol by means of the tricarboxylate transporter, and once in loco gets degraded back into oxaloacetate and CoA by the ATP- cytrate lisase. The oxaloacetate is then decarboxylated to afford pyruvate which is retaken into the mitochondria by the pyruvate carboxylase transporter. The cytosolic activated CoA is then converted into malonyl-CoA by means of the cytosolic acetyl-coenzyme A carboxylase (ACC) which uses the bicarbonate provided by the cytosolic CA II. The malonyl-CoA units are then elongated in the same manner to afford fatty acids. It has been demonstrated that sulfonamide/sulfamate CAIs inhibit this process in vitro and in vivo through modulation of this mechanism. As indicated in Figure 13, the TPM in complex with CA II assumes the classical tetrahedral coordination of the sulfamate group to the zinc ion, whereas the fructose part is entrapped into the enzymatic cleft by means of a large number of hydrogen bonding and van der Waals interactions. Using the TPM/hCA II adduct, molecular dynamic/docking studies have been carried out to observe the hypothetical binding mode between the inhibitor **8** and unexplored isoform hCA VA. This study strongly suggested that there is a similar mode of binding between the complex TPM/hCA II and TPM/hCA VA (figure 14), with exception of the hydrogen bond interaction Asn62 with one of the oxygen (O₄) of topiramate (figure 13) that is not retained in this case, as a consequence of the mutation Asn62 – Thr62 (figure 14) for hCA VA. The loss of this important polar interaction seems to be responsible for the lower binding affinity observed for TPM toward hCA VA with respect to that measured for hCA II (K_i = 13.8 nM against hCA II and 25.4 nM against hCA VA).^[73, 74]

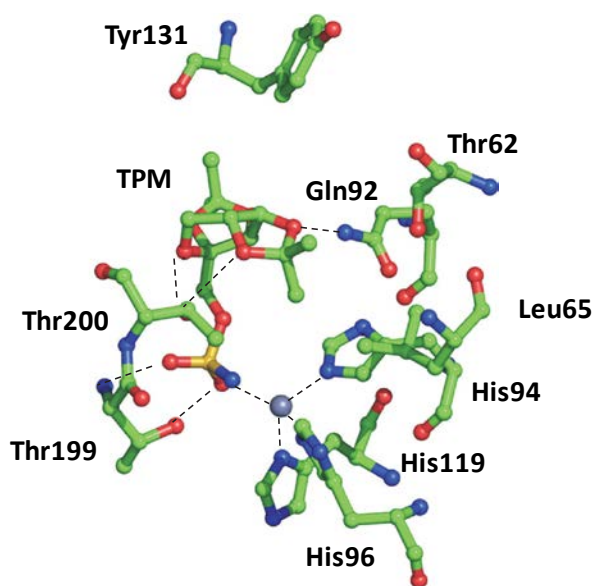


Figure 14. Molecular dynamic/docking studies between topiramate (**8**) and hCA VA.^[73, 74]

All these results strongly support the role that TPM inhibits mitochondrial CAs and, therefore, *de novo* lipogenesis, thus explaining the antiobesity effects of TPM.

Indisulam (7)(E7070): Indisulam is a novel sulfonamide anticancer agent in clinical development for the treatment of solid tumors. The inhibitor **7** was found to suppress the expression of cyclin E and the phosphorylation of CDK2, both of which are essential for the G1 to S transition. Fukuoka et al.^[75] clarified that **7** disrupted cell cycle progression at multiple points, including both G1/S and G2/M transitions, in a human non-small cell lung cancer cell line A549 (*adenocarcinomic human alveolar basal epithelial cells*). The compound **7** proved to inhibit pRb phosphorylation, to reduce the protein expression of cyclin A, cyclin B1, CDK2 and CDC2, and to suppress CDK2 catalytic activity with the induction of p53 and p21 proteins only in parental (drug sensitive) A549 cells.^[75, 76]

The relationship studies between the sulfonamides with the antitumor activity have so far clarified that the sulfamoyl group ($-\text{SO}_2\text{NH}_2$) is not an essential functionality for the *in vitro* growth inhibitory activity against cancer cells. However, there is still a possibility that the CA inhibitory properties of the compound **7** can contribute, at least in part, to its *in vivo* efficacy. The isozymes most abundant and considered to play a critical physiological/pathological role, such as CA II and CA IX, exhibit the highest affinity for **7**, with an inhibition profile quite similar to those of the

clinical drug **1** ($K_i = 12$ nM and 25 nM of AZM (**1**) toward hCA II and hCA IX respectively; $K_i = 15$ nM and 24 nM of E7070 (**7**) toward hCA II and hCA IX respectively).

So, the CA inhibition of **7** might be considered as a positive factor for the clinical strategy of antimetastasis and combination therapies.^[76]

The X-ray crystal structure of the adduct of hCA II with E7070 (**7**) revealed unexpected interactions. Three different conformations of the chloroindole fragment were found. As you can see in Figure 15, **E7070** binds within the hCA II active site in three different conformations that regards only the terminal, chloroindole fragment of the molecule, which is rather flexible and allows the three different spatial arrangements, whereas the benzenesulfonamide head binds unequivocally to the active site in one conformation, similarly to other sulfonamide CA inhibitors. About the known interaction between the zinc ion and the sulfonamide moiety the Zn–N bond is appreciably shortened in this complex as this distance is usually around 1.95–2.10 Å. This shortening may be considered as a first factor favoring the high affinity of **7** for hCA II.^[76]

The benzenedisulfonamide moiety of **7** lies in the hydrophobic part of the active site cleft, where it makes van der Waals interactions with the side chains of Val 135, Phe 131, Leu 204, Pro 202, Trp 209, Val 121, Leu 198 and Thr 200. In conformation A (Fig. 2A), the chlorine atom is engaged in a weak hydrogen bond with the COOH group of Glu69. In the second conformation of **7** (Fig. 2B), the NH group of the inhibitor is then involved in hydrogen bond (of 2.54 Å) with the -CONH₂ group of Gln92. The chlorine atom forms a shorter (1.88 Å) hydrogen bond with the -COOH group of Glu69. Finally, the third conformation of **7** bound to hCA II (Fig. 2C) involves only a network of four hydrogen bonds in which one oxygen atom of the secondary sulfonamide moiety and three water molecules participate.^[76]

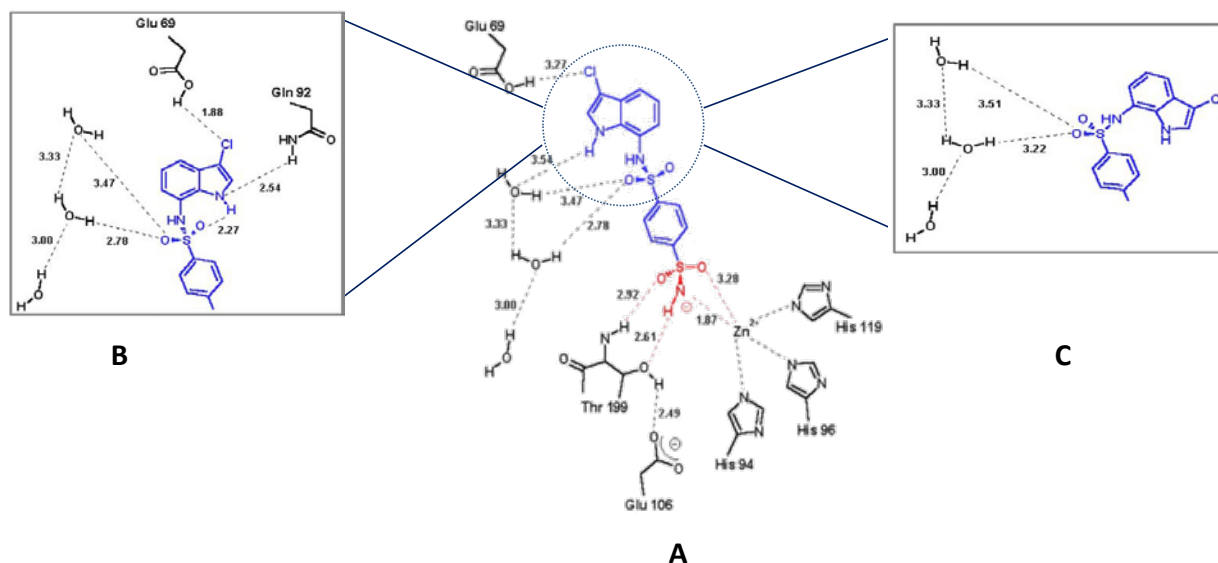


Figure 15. Complex between indisulam (**7**) and hCA II. A, B and C are the representation of the three conformation of the chloroindole portion of the inhibitor **7** within the hCA II active site. [76]

Currently, **7** is under clinical evaluation as antitumor agent in patients with colorectal cancer, non-small cell lung cancer, and so on. [76]

Therefore, the crystal structures of selected well-known inhibitors in complex with druggable isoforms have furnished interesting information about the binding pose within catalytic site of druggable isoforms. Overall, the sulfonamide/sulfamate moiety establishes the network of contacts that control the binding recognition of CA. Additional interactions can address the isoform selectivity thus highlighting both the volume and shape of catalytic site cavity for each isoform.

Chapter 2

Results of the present thesis and Discussion

To date numerous small molecules have been claimed to inhibit metalloenzymes such as human Carbonic Anhydrase (hCAs). Specifically, hCA inhibitors (hCAIs) are able to coordinate the Zn^{2+} ion and establish additional interactions promoted by the aryl substituents in the region nearby the catalytic site. [69, 77]

At the medicinal chemistry laboratory of the University of Messina previous studies allowed the identification of a new class of hCAIs. Actually, a large series of isoquinolinesulfonamides have been synthesized and these derivatives were tested as inhibitors of hCA I, hCA II, hCA IX and hCA XIV. [1, 77-80]

Therefore, the data obtained demonstrated that most of these compounds are good inhibitors with K_i in the range of nanomolar concentration. In particular, several synthesized sulfonamide derivatives showed high inhibitory activity toward hCA II, hCA IX and hCA XIV. [1, 77]

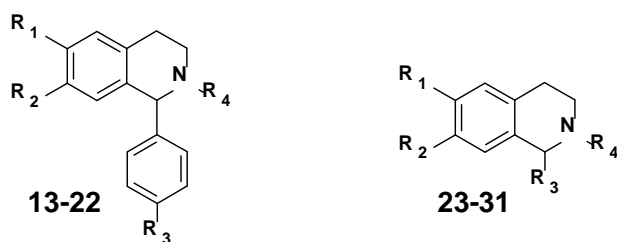


Figure 16. hCA inhibitors Isoquinolinesulfonamides 13-31.

2.1 “In vivo” and “in silico” profiling of isoquinolinesulfonamides 13-31

Our idea was to focus the interest on the development of new hCAIs able to produce neuroprotectant effects through a selective inhibition of hCA VII isoform, that is widely distributed in the brain. To achieve this objective, in the first step of this research project we decided to collect further biological data for the already synthesized isoquinolines **13-31**.^[1, 77-80]

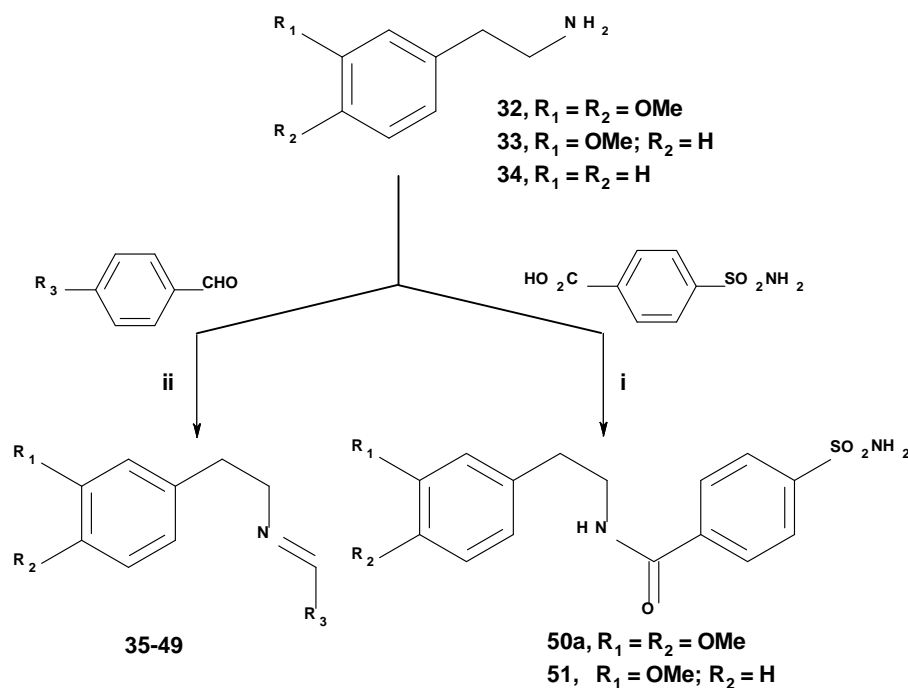
Specifically, we determined the inhibitory effects towards hCA VII for compounds **13-18**, for which these data are not yet reported in literature. Considering that the activity of carbonic anhydrase can be associated to neurological disorders, such as epilepsy, linked to excitatory neurotransmission, we further explored in vivo effects. In fact, it is well known that neuronal excitability is related to γ -aminobutyric acid (GABA)_A ergic depolarization and the prolonged activation of GABA_A receptors can lead the imbalance of the ions. This imbalance can determine the improvement of intracellular HCO₃⁻ ions that is consistently replenished by the activity of carbonic anhydrase. For this reason the inhibition of CA represents a good strategy for the treatment of epilepsy.^[81-83]

Several CA inhibitors such as acetazolamide (**AAZ**, **1**) and topiramate (**TPM**, **7**) have a long history as anticonvulsants, given that hCA II and hCA VII are specific isoforms involved in GABA-mediated neuronal excitation. So we herein hypothesize that the compounds **13-31** could represent an innovative template for the development of new anticonvulsant agents.^[11]

Following previously reported procedure, we re-synthesized compounds **13-31** and their anticonvulsant effects were tested against audiogenic seizures in DBA/2 mice.^[1, 77-80]

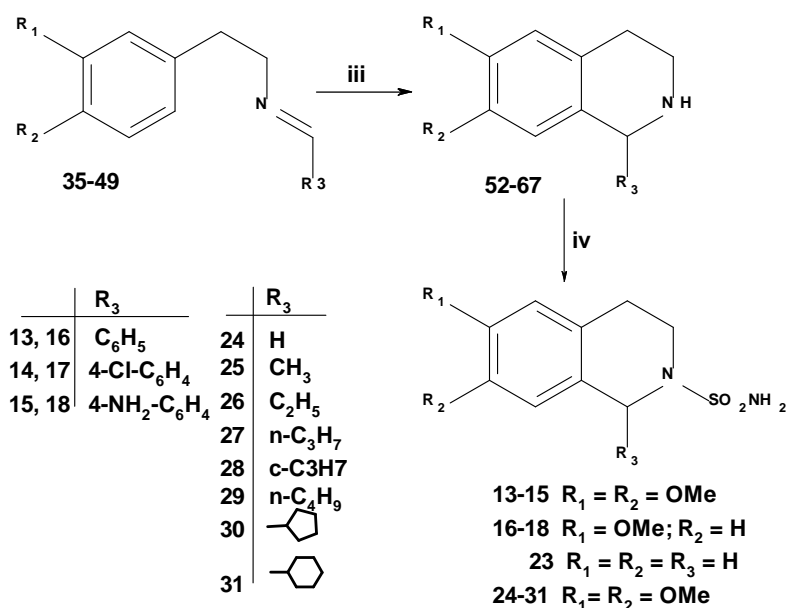
2.1.1 Synthesis of isoquinolinesulfonamide derivatives 13-31

The desired isoquinoline derivatives **13-31** were prepared *via* synthetic routes outlined in Schemes 3 and 4. We used the phenylethylamine derivatives (**32-34**) as starting reagents, that were converted into the two series of key intermediates **35-49** and **50a-51**. Following the well-known Pictet-Spengler approach, in the first step of the synthetic pathway the phenylethylamines **32-34** undergo a condensation with suitable aldehydes thus giving imines **35-49**.^[84, 85] The main feature of this reaction is that gives good yields, reducing the reaction time and the some reaction work without solvent.^[86] In a parallel route the starting amines **32-34** reacted with the 4-(aminosulfonyl)benzoic acid and furnished the corresponding 4-methyl-N-phenethyl-benzamide derivatives (**50a-51**) via *N,N,N,N*-Tetramethyl-*O*-(1*H*-benzotriazol-1-yl)uronium hexafluorophosphate (HBTU) coupling in the presence of triethylamine (TEA).



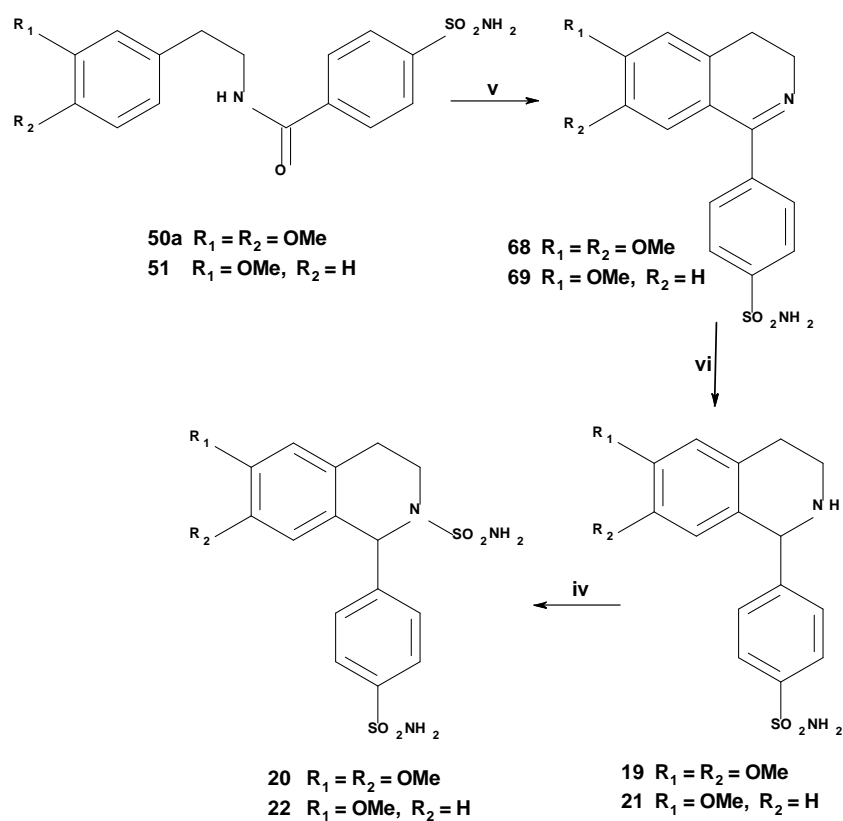
Scheme 3. Reagents and conditions: i) HBTU, DMF, Et_3N , rt, 2h; ii) MW: 5 min, 90°C, 200 Psi, 150 W.

In agreement with expected nucleophilicity of the amine, the imines **35-49** cyclized in the corresponding isoquinolines **52-67** through microwave irradiation (MW, 5 min, 90°C, 200 Psi, 150 W) in the presence of trifluoroacetic acid (TFA). Successively, these intermediates reacted with a large excess of sulfamide leading to the 3,4-dihydro-1H-isoquinoline-2-sulfonamide derivatives **13-18** and **23-31**.



Scheme 4. Reagents and conditions: **iii**) TFA MW: 5 min, 90 °C, 200 Psi, 150 W; **iv**) MW: 20 min, 100 °C, 200Psi, 150W.

By using the Bischler-Napieralski approach we prepared the desired isoquinolines **20-22** through a multistep procedure. Initially, the phosphoryl chloride (POCl₃) has been used to promote the intramolecular electrophilic aromatic substitution allowing the cyclization of the intermediates N-phenethyl-4-sulfamoyl-benzamides (**50a,51**). So, we obtained the corresponding dihydroisoquinolines derivatives **68,69**. Successively, the reagent NaBH₄ was used to convert the imine **68,69** in the corresponding secondary amine **19,21** (6,7-dimetossi-1-phenyl-1,2,3,4-tetrahydroisoquinoline and 6-metossi-1-phenyl-1,2,3,4-tetrahydroisoquinoline, respectively). Finally, compounds **19,21** were treated with sulfamide to give the 3,4-dihydro-1H-isoquinoline-2-sulfonamides derivatives **20-22**.



Scheme 5. Reagents and conditions: **v)** POCl_3 , Δ , toluene, 2h; **vi)** NaBH_4 , CH_3OH , 2h.

2.1.2 Biochemical screening and anticonvulsant effects

Table 2 reports the inhibitory effects of the isoquinolinesulfonamides **13-31** against hCA II and hCA VII isoforms. The inhibitory constants were obtained using a Durrum-Gibson stop-flow spectrophotometer that measures the hydration (or dehydration) of CO₂ and then the release (or removal) of protons.^[87, 88]

The inhibition constant (K_i) values determined for compounds **13-31** were compared with the K_i values of topiramate (TPM, **7**) as reference standard showing both CA inhibition and anticonvulsant properties (*Topamax*[®]).^[71, 72] Table 2 summarizes the effective doses (ED₅₀) determined for compounds **13-31** that were administered intraperitoneally 30 min before auditory stimulation using DBA/2 mice, a strain susceptible to sound induced-seizures. The ED₅₀ values were determined for the inhibition of clonic and tonic seizures, these data were compared with those measured for TPM.^[78]

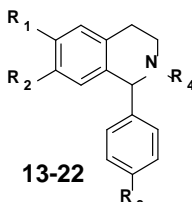
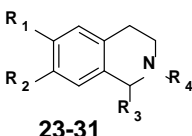
As you can see in Table 2, the monomethoxy compounds **16-18** are less efficacious inhibitors against the hCA VII isoform than corresponding dimethoxy analogues **13-15**, which proved to be potent hCA VII inhibitors at nanomolar concentration ($K_i < 8.2$ nM). Moreover, compounds **13-15** proved to be inefficacious to inhibit hCA II ($K_i > 5000$ nM). This unexpected isoform selectivity might be considered an advantage for the development of CA inhibitors lacking off-target effects related to activity toward ubiquitous isoforms such as hCA II. In particular, the compound **15**, which bears a 4-aminophenyl group at the C-1 position of the isoquinoline scaffold, displayed the highest selectivity for the hCA VII isoform (~2000-fold) over the hCA II isoform and showed relevant anticonvulsant effects in comparison with that shown by reference compound topiramate **7**.

The replacement of the optimized 4-aminophenyl substituent with the 4-benzenesulfonamide moiety gave compounds **19-22**. Similar to the results of previous SAR, we observed that the dimethoxy isoquinolines derivatives **19** and **20** were more selective inhibitors of hCA VII than monomethoxy analogues **21,22**.^[77] The “in vivo” screening revealed that compounds **19-22** were less potent anticonvulsant when compared with the active inhibitor **15**. The lacking of substituents on benzene-fused ring as well as nitrogen atom of isoquinoline nucleus results in low selective hCA VII inhibitors **23-24**, which were active agents just in preventing tonic phase.

Compounds **25-30** are characterized by the presence of (cyclo)alkyl substituent on isoquinoline skeleton. Overall, these compounds exhibited potent inhibitory effects toward hCA VII as well as high selectivity over hCA II.^[80] Specifically, n-propyl derivative **27** and n-butyl derivative **29** were the most interesting inhibitors; the cyclohexyl derivative **31** demonstrated low inhibitory effects as well as poor anticonvulsant efficacy. Unfortunately, compounds **25-30** generally displayed low *in vivo* efficacy to prevent audiogenic seizures with exception for compound **29**.

Summarizing all data displayed in Table 2, we found that the *in vivo* effects might be correlated with the significant effects of hCA VII inhibition. However, we found this correlation exclusively for compounds **13-15** and **28-29**, which proved to be efficacious against both the clonic and tonic phases of audiogenic seizures at doses higher or similar to those of topiramate (**7**). It appears not clear the poor *in vivo* efficacy for other potent hCA VII inhibitors falling in this series of sulfonamides **13-31**.

Table 2. K_i values (nM) against hCA II and hCA VII isoforms and anticonvulsant effects in DBA/2 mice XIV of tested compounds **13-31** and reference compound TPM (**7**).

 13-22					 23-31				
					K_i values (nM) ^a		ED ₅₀ (μmol/kg ip) ^b		
	R ₁	R ₂	R ₃	R ₄	hCAII	hCAVII	Clonic phase	Tonic phase	
13	OMe	OMe	H	SO ₂ NH ₂	15700 ^c	7.1	>100 ^c	7.82 (6.66–9.19) ^b	
14	OMe	OMe	Cl	SO ₂ NH ₂	5300 ^c	8.2	23.5 (14.4–38.5) ^c	7.25 (4.54–11.6) ^b	
15	OMe	OMe	NH ₂	SO ₂ NH ₂	11300 ^c	6.0	17.7 (9.80–30.1) ^c	3.60 (1.45–8.97) ^b	
16	OMe	H	H	SO ₂ NH ₂	422 ^d	302	93.1 (82.5–105)	82.6 (74.3–91.9)	
17	OMe	H	Cl	SO ₂ NH ₂	104 ^d	37.5	>100	>100	
18	OMe	H	NH ₂	SO ₂ NH ₂	222 ^d	14.8	>100	75.2 (46.9–121)	
19	OMe	OMe	SO ₂ NH ₂	H	3640 ^e	4.6 ^e	>100	48.2 (30.3–76.6)	
20	OMe	OMe	SO ₂ NH ₂	SO ₂ NH ₂	3130 ^e	7.0 ^e	>100	61.3 (45.0–83.4)	
21	OMe	H	SO ₂ NH ₂	H	8.8 ^f	5.7 ^f	92.9 (61.2–141)	39.4 (23.0–67.6)	
22	OMe	H	SO ₂ NH ₂	SO ₂ NH ₂	48.5 ^f	23.4 ^f	>100	79.0 (53.9–116)	
23	H	H	H	SO ₂ NH ₂	32.8 ^e	5.5 ^e	>100	65.6 (43.6–98.7)	
24	OMe	OMe	H	SO ₂ NH ₂	94.5 ^e	5.4 ^e	>100	88.2 (55.9–139)	
25	OMe	OMe	Me	SO ₂ NH ₂	87.3 ^e	6.4 ^e	>100	>100	
26	OMe	OMe	Et	SO ₂ NH ₂	1975 ^e	6.7 ^e	>100	>100	
27	OMe	OMe	propyl	SO ₂ NH ₂	235000 ^e	16.3 ^e	>100	56.9 (40.9–79.2)	
28	OMe	OMe	c-propyl	SO ₂ NH ₂	820 ^e	10.2 ^e	58.0 (39.7–84.7)	37.5 (27.0–52.0)	
29	OMe	OMe	Butyl	SO ₂ NH ₂	350000 ^e	13.6 ^e	63.8 (45.1–90.2)	51.4 (38.5–68.6)	
30	OMe	OMe	cyclopentyl	SO ₂ NH ₂	650 ^e	71.5 ^e	>100	>100	
31	OMe	OMe	cyclohexyl	SO ₂ NH ₂	18890 ^e	698 ^e	>100	51.5 (34.1–77.7)	
TPM (7)					10 ^c	0.9 ^c	47.7	29.2	

^aErrors in the range of $\pm 10\%$ of the reported value, from 3 different assays; recombinant full-length hCA II and hCA VII were used. ^bAll data were calculated following the Litchfield and Wilcoxon method; at least 32 animals were used to calculate each ED₅₀ 95% confidence limits are given in parentheses. ^cData are taken from reference [78]. ^dData are taken from reference [79]. ^eData are taken from reference [1]. ^fData are taken from reference [77]

2.1.3 Prediction of biopharmaceutical parameters for compounds 13-31

During the Drug Discovery (D&D) process an important step involves the compound selection, which is aimed to the identification of compounds more likely to be well absorbed and distributed in the human body. Although a considerable number of routes for absorption of drugs through membranes might exist, the transport by passive diffusion is the most common one. In order to be absorbed by this route, drugs must be lipophilic enough to penetrate the lipid cores of membranes, but not so lipophilic that they get stuck there.^[89]

By analyzing data displayed in Table 2, you can find that there is not a clear correlation between hCA VII inhibitory potency and anticonvulsant effects. Considering that the major distribution of the hCA VII is into the central nervous system (CNS), we decided to predict the capability of the synthesized hCA VII inhibitors to cross the brain blood barrier (BBB). Therefore, we decided to estimate several physicochemical properties for compounds **13-31** in comparison with reference compound **7**. Our idea was to rationalize the lacking of in vivo effects for some active hCA VII inhibitors. The results of these studies could furnish suggestions for the design of new hCA VII inhibitors as anticonvulsant agents.

Firstly, we calculated the values of LogP and LogD^[90], that is defined as the ratio of the concentrations of both the ionized and unionized species of the compound in the organic and aqueous phases.^[91]

As displayed in Table 3 these sulfonamide derivatives generally showed low estimated lipophilicity (<2.5), and the ranking score of their anticonvulsant effects does not fit with the lipophilic properties. Especially, there is no correlation between anticonvulsant efficacy and lipophilic properties of most active anticonvulsants **14**, **15** and **28** ($\log D_{7.4}$ =1.81, -0.05, and 0.65, respectively), thus suggesting the role of other biopharmaceutical parameters.

To explore other physicochemical properties we used further metrics such as the polar surface area (PSA),^[92] and derived values such as $\log BB$ ^[93, 94] that could be useful parameters to understand the ability of a small molecule to penetrate the brain.

The polar surface area (PSA) is a metric to optimize the drug's ability to permeate cells. The logarithm of the brain-to-blood concentration ratio (logBB) is a measurement of the drug permeation through the BBB.^[95]

In general, the central nervous system (CNS) drugs possess clog P values ranging from 2 to 4^[96, 97] and PSA of 60 Å² or less are completely absorbed, whereas those with at least 140 Å² are not.^[92] Moreover, the logBB threshold values were set to 0.3 and -1. So the compounds with logBB>0.3 cross the BBB easily and compounds with logBB<-1 are poorly brain distributed.

Table 3. Calculated physicochemical properties and lipophilic indices.

	LogD _{7.4} ^a	LogP ^a	PSA ^b [Å ²]	logBB ^c	LE ^d
13	1.22	1.645±0.49	90.2	-0.95	0.47
14	1.81	2.410±0.50	90.2	-0.83	0.45
15	-0.05	0.440±0.50	116	-1.51	0.46
16	1.41	2.153±0.47	81.0	-0.73	0.41
17	2.00	2.918±0.48	81.0	0.62	0.45
18	0.15	0.948±0.48	107	-1.30	0.48
19	0.01	1.042±0.56	99.0	-1.17	0.49
20	-0.69	-0.188±0.51	159	-2.24	0.30
21	-0.67	1.653±0.54	89.8	-1.29	0.52
22	-0.50	0.320±0.49	150	-2.16	0.41
23	0.08	0.560±0.42	71.8	-0.84	0.82
24	-0.21	0.055±0.47	90.2	-1.19	0.64
25	0.29	0.653±0.48	90.2	-1.10	0.60
26	0.82	1.162±0.48	90.2	-1.02	0.47
27	1.35	1.672±0.48	90.2	-0.94	0.45
28	0.65	1.044±0.48	90.2	-1.04	0.47
29	1.88	2.181±0.48	90.2	-0.86	0.50
30	1.78	2.098±0.48	90.2	-0.88	0.43
31	2.34	2.625±0.48	90.2	-0.80	0.36
7	2.97	2.157±0.67	124	-1.36	0.57

^aLogP and LogD_{7.4} data are predicted from a commercially available program (ACD/Lab). ^bPSA vlues are predicted by means of molinspiration calculator. ^cLogBB=-0.0148PSA + 0.152LogP + 0.139. (Clark Equation) ^dLE = -1.4 log K_i/number of heavy atoms.

As shown in Table 3, compounds **13**, **14**, **16**, **17**, **23**, **27**, and **29-31** were estimated to have the ability to cross the BBB; thus, they possess logBB values higher than the recommended threshold (>-1). Among them, we found that sulfonamides **13** and **14** protected DBA/2 mice in tonic seizures. On the contrary, compounds **15**, **18-22**, **25-27**, and **28** displayed logBB parameters below -1. Therefore, for most interesting anticonvulsant **15** the prediction of brain penetration is not coherent with the “*in vivo*” effects. Considering the failure of the *in silico* prediction of brain penetration of active anticonvulsant **15**, we can hypothesize that there are other ADME properties that influence the bioavailability of these potent hCA VII inhibitors. On the other hand the penetration of BBB is a complex procedure and logBB should be considered only indicative and not a measure that guarantees permeability through BBB.

With the aim to design new hCA VII inhibitors, for which the balance of lipophilic and hydrophilic features should be optimized, we calculated the ligand efficiency (LE) for all tested compounds.^[96, 98] Specifically, LE estimates the role of the molecular size with respect to biological effects. In fact, the LE index correlates the number of heavy atoms with the inhibitory effects. It is well known that good CNS drug candidates generally possess LE values ranging from 0.3 to 0.5. As shown in Table 3, the LE values are optimized for all compounds with the exception of inhibitor **31**, which displays low activity. The calculated values of the LE suggest the design of new isoquinolinesulfonamides bearing additional hydrophobic molecular fragments.^[10]

2.2 Development of new arylsulfonamides inhibitors

To explore the binding mode of these previously synthesized derivatives the X-ray studies have been carried out for selected inhibitors in complex with carbonic anhydrase.

In detail, two of the most active compounds, the 6,7-dimethoxy-3,4-dihydroisoquinoline-2(1H)-sulfonamide (**24**) and the 6,7-dimethoxy-1-methyl-1,2,3,4-tetrahydroisoquinolin-2-ylsulfonamide (**25**), have been co-crystallized with isoform hCA II. These two compounds differ only for the additional methyl group at C-1 position on isoquinoline nucleus for **25**. The comparison of the the crystal structures of the analogues **24** and **25** (green and pink, respectively, in Figure 17A) in complex with the hCA II in complex (PDB code 3IGP and 3PO6, respectively) gave the information about their binding modes in the enzyme active site.

The position of the sulfonamide group is well conserved in the two crystal structures; the major difference is in the arrangement of the isoquinoline moiety within the active site cavity.

The substantial change in position of **25** with respect to **24** within the hCA II active site consistent for the methoxy oxygen atoms in the compounds. The isoquinoline moiety of **24** forms numerous van der Waals interactions with residues Gln92, Val121 located on the bottom of the catalytic site and the side chain of Phe131 contributes to interaction with the unsubstituted methoxy groups. In contrast, the substituted isoquinoline moiety of **25** is stabilized by the amino acid residues located on the opposite side of the active site cavity (residues Asn62, Asn67, Gln92, Val121). The methyl substituent on the isoquinoline scaffold interacts with Leu198.

The comparison of the residues interacting with **24** and **25**, respectively, revealed that the isoquinoline moiety can achieve two different binding modes within the hCA II active site and it engage different amino acid residues in the interaction. This finding is quite striking considering that **24** and **25** are very similar in their structure and also in their inhibitory properties.

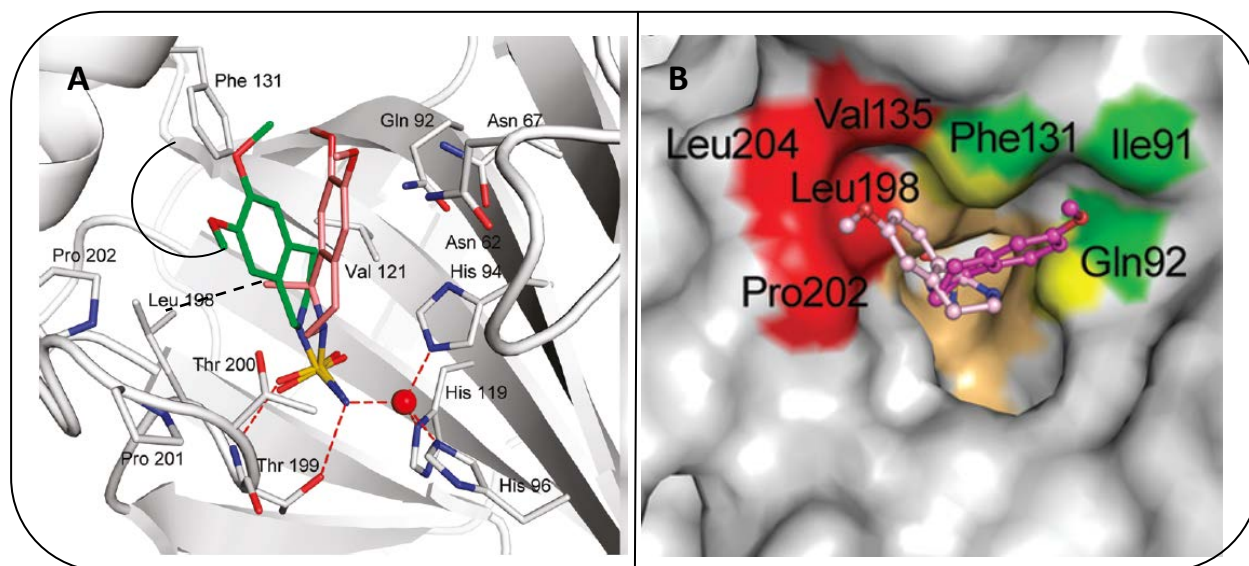


Figure 17: In the panel **A** there are the comparison of **24** (green) and **25** (pink) binding mode into the hCA II active site. the Zn^{2+} ion is red sphere and also the polar interactions are indicated with dashed lines. In the panel **B** the inhibitor **69** in the active site cavity involved in van der Waals interactions color coded as follows: residues involved in van der Waals interactions with arylsulfonamide moiety are colored light brown, residues forming interactions with both alternative conformations are colored yellow, residues forming interactions with alternative conformation.

To gain more information about the inhibitor/enzyme interactions for this class of sulfonamides we carried out further structural studies for selected newer compounds. Among the series of 1-aryl-isoquinolinesulfonamides, the intermediate compound 4-(6-methoxy-3,4-dihydroisoquinolin-1-yl)benzenesulfonamide (**69**) demonstrated a good inhibitory activity in the range of value of K_i 8.6 – 18.3 nM with all isoforms except the hCA I isoform ($K_i=681$ nM). The dihydroisoquinolinesulfonamide **69** was co-crystallized with the hCA II isoform. Compound **69** appeared in the cavity in two alternative conformations (pink and magenta, see Figure 17B) and each conformation occupies a different surface pocket located on the opposite side of the enzyme active site entrance. It's obvious that the nitrogen of the sulfonamide group binds the Zinc²⁺ ion and generated the interactions with the residues located at the bottom of the active site cavity (His94, His96, and His119), but the more interesting interactions concern the hydrophobic portion of the methoxy substituent on the benzene fused ring of the inhibitor **69** that established the contacts with the hydrophobic pocket (red area) formed by residues Phe131, Val135 (see the reference [1]). The presence of the two conformation of the inhibitor **69** in complex with hCA II was employed to decipher the CA inhibitory effects toward all studied isoforms. To explain the CA selectivity and the different degree of inhibitory effects displayed by the most one active

compound, **69**, we have superimposed the coordinates of hCA I (PDB code 3LXE, orange),^[99] hCA VII (PDB code 3MDZ, magenta), hCA IX (PDB code 3IAI, cyan),^[100] and hCA XIV (PDB code 1RJ6, green)^[101] onto the coordinates of hCA II (gray) in complex with both conformers of compound **69**. The relevant differences were in the amino acid composition within the catalytic site. Specially the superposition between the hCA I and the hCA II showed different amino acids in the hydrophobic area of the cavity and this can be an explanation of the reduction of the affinity of compound **69** with the hCA I isoform. The isoquinolinesulfonamide **69** proved to inhibit hCA VII isoform with a similar potency when compared with hCA II isoform ($K_i = 10.2$ vs 8.6 nM, respectively). The superposition between hCA II in complex with **69** and hCA VII pointed out the presence of the hydrophobic contact with Phe131 of compound **69** within the catalytic site of hCA VII.^[77]

To further explore how the modification can influence the interaction with hydrophilic/hydrophobic areas of the catalytic pocket, the *N*-(3,4-dimethoxyphenethyl)-4-sulfamoylbenzamide (**50a**), has been tested against the hCA I, hCA II, hCA VII, hCA IX and hCA XIV isoforms. Compound **50a** bears the arylsulfonamide portion as key chemical moiety shared with previously studied compounds. However there is the lacking of the heteroaromatic matrix different by the 4-(6-methoxy-3,4-dihydroisoquinolin-1-yl)benzenesulfonamide (**69**).^[69, 77]

As shown the Figure 18, compound **50a** generally maintains high affinity in the nanomolar range (K_i values ranging from 2.7 to 8.7 nM) but unfortunately, the active inhibitor **50a** failed to selectivity targets the most druggable hCA isoforms (hCA VII, hCA IX and hCA XIV) over ubiquitous hCAs (hCA I and hCA II).

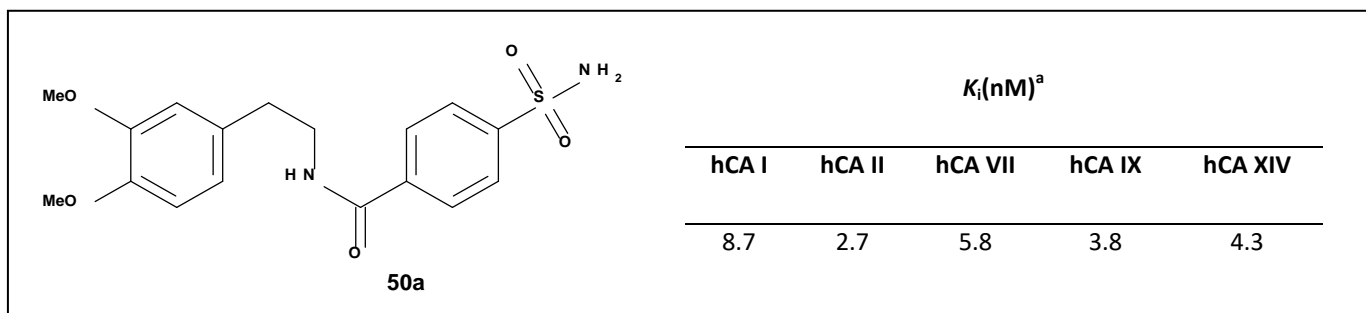


Figure 18: Inhibition of hCA I, hCA II, hCA VII, hCA IX and hCA XIV isoforms by *N*-[2-(3,4-dimethoxyphenyl)ethyl]-4-sulfamoylbenzamide (**50a**).

With the aim to investigate the inhibitor–protein interactions, we co-crystallized the active inhibitors **50a** with the isoform hCA II, and the crystal structures were determined at atomic resolution (PDB code 3V7X). The crystal structures of hCA II in complex with compound **50a** was determined by the difference Fourier method and refined using data to 1.03 Å.^[77] The *N*-(3,4-dimethoxyphenethyl)-4-sulfamoylbenzamide (**50a**) assumed two slightly different conformations within of the scaffold. The high quality of the experimental data allowed the interpretation of the electron maps by two alternative conformations of inhibitor, as displayed in the Figure 19A.

While in the Figure 19B, we can distinguish that the the *N*-(3,4-dimethoxyphenethyl)-4-sulfamoylbenzamide (**50a**) assumed two slightly different conformations (colored turquoise where the alternative conformation are shown in lighter shades) and are quite similar within of the cavity. The major interactions of the inhibitor **50a** with the active site of hCA II isoform are mediated through the deeply buried sulfonamide group, which makes polar interactions with the zinc ion and residues located at the bottom of the active site cavity (His94, His96, and His119), similar to those observed for other arylsulfonamides previously reported in the literature.^[37, 48, 102-104]

Moreover, the dimethoxyphenyl substituent is mostly solvent-exposed, having only minor van der Waals interactions with specific residues such as Phe131, Val135, and Pro202. The oxygen of the 3-methoxy group makes a water mediated hydrogen bond with residues Gly132 and Gln136.

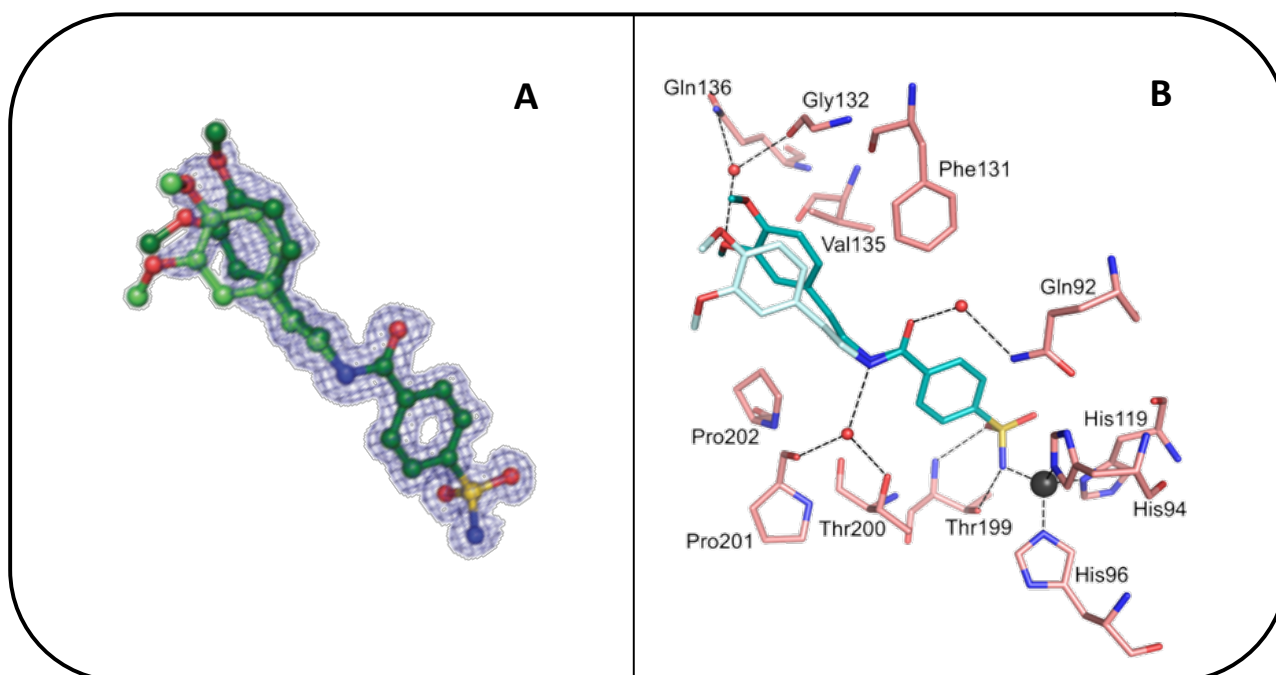


Figure 19: **A:** Electron density maps of the inhibitory compound **50a**. The $2F_o - F_c$ electron density map for compound **50a** is contoured at 0.9σ . **B:** Co-crystal structure of benzamide **50a** with hCA II in (PDB code 3V7X).¹ The inhibitor in stick representation has carbon atoms colored turquoise (alternative conformation is shown in lighter shades), other atoms are colored according to standard color coding: oxygen red; nitrogen blue; sulfur yellow. The amino acids residues involved in the interactions are also shown as sticks with carbon atoms in pink. Polar interactions are represented by dotted lines. Zinc ion and water molecules are represented by grey and red spheres, respectively.

To overcome the low hCA selectivity in this phase of the research work we planned the synthesis of new compounds and we chose to synthesize new direct analogues of inhibitor **50a** (Figure 20).

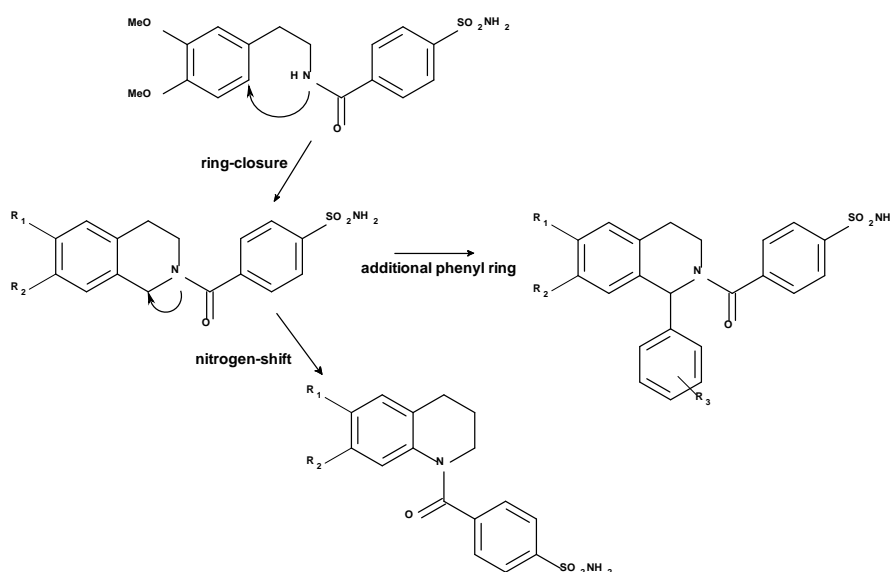


Figure 20: Designed CAIs structurally related to "lead compound" **50a**.

The new sulfonamides should be characterized by a reduced conformational mobility when compared to parent compound **50a**. Therefore, we have synthesized isoquinoline derivatives as corresponding cyclic analogues of prototype benzamide **50a**. Moreover, by shifting the nitrogen atom of isoquinoline ring we planned the synthesis of quinoline derivatives as positional isomers. In the end we have added the phenyl ring in the position C-1 of the isoquinoline derivatives that could add a new hydrophobic anchoring moiety, that might be useful to strengthen the network of non-polar interactions with hydrophobic residues within catalytic site.

Thus a set of mono- or dimethoxy-benzene derivatives and corresponding dealkyl-analogs has been prepared and tested to further study the role of substituents on the selectivity against some CA isoforms. These modifications could influence the interaction with hydrophilic/hydrophobic areas of catalytic pocket and control the activity/selectivity against some CA isoforms. To enhance the hydrophobic interactions we also examined the effects of an additional halo-substituent at para position of C-1 phenyl ring.

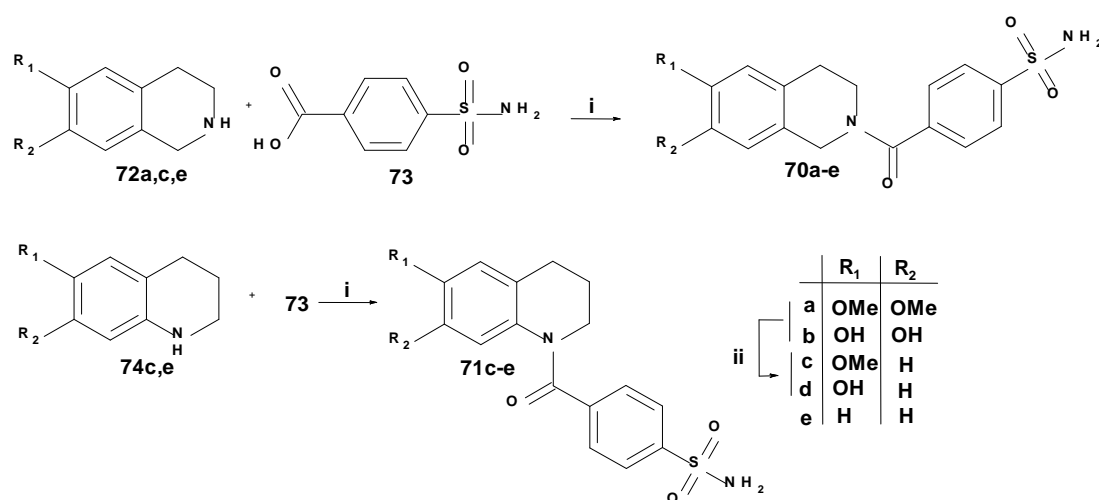
All compounds were obtained in good yields, the structural characterization and purity of tested compounds were supported by elemental analyses and spectroscopic measurements.

Afterwards, to evaluate the influence of the chirality on the CA inhibition we carried out the enantiomeric separation for selected compounds. Then, the inhibitory activity of the individual enantiomers has been assayed. Finally, computational and experimental studies have been carried out to furnish relevant structural insights about the recognition process in to the catalytic site.

2.2.1 Synthesis of 4-(3,4-dihydroisoquinolin-2(1H)-ylcarbonyl)benzenesulfonamides (70a-e) and 4-(3,4-dihydroquinolin-1(2H)-ylcarbonyl)benzenesulfonamides (71c-e)

A short and efficient synthesis of the designed 4-(3,4-dihydroisoquinolin-2(1H)-ylcarbonyl)benzenesulfonamides (**70a-e**) and 4-(3,4-dihydroquinolin-1(2H)-ylcarbonyl)benzenesulfonamides (**71c-e**) is depicted in the scheme 4. To prepare the designed amides **70a,c,e** and **71c,e** the *N,N,N,N*-tetramethyl-*O*-(1*H*-benzotriazol-1-yl)uronium hexafluorophosphate (HBTU) has been used as an activator of the acid group of the 4-(aminosulfonyl)benzoic acid **73** to prepare the designed amides 4-(3,4-dihydroisoquinolin-2(1H)-ylcarbonyl)benzenesulfonamides **70a,c,e** and 4-(3,4-dihydroquinolin-1(2H)-ylcarbonyl)benzenesulfonamides **71c,e**. In particular, suitable and commercially available 1,2,3,4-tetrahydroisoquinolines **72a,c,e** or 1,2,3,4-tetrahydroquinolines **74c,e** reacted with **73** in presence of triethylamine (TEA), the reaction has been conducted overnight at room temperature to bring the reaction to completeness.

The methoxy 4-(3,4-dihydroisoquinolin-2(1H)-ylcarbonyl)benzenesulfonamides **70a,c,e** and 4-(3,4-dihydroquinolin-1(2H)-ylcarbonyl)benzenesulfonamides **71c** have been dealkylated with the boron tribromide (BBr₃) under N₂ to lead the hydroxyl analogues **70b,d** and **71d**.



Scheme 4. Reagents and conditions: i) HBTU, DMF, TEA, rt, overnight; ii) BBr₃(1M in DCM), DCM, rt, overnight.

By inspection of the $^1\text{H-NMR}$ spectra of the isoquinoline derivatives **70a-e** we observed a complex pattern of signals. We have attributed this behavior to the presence of the two possible rotamers (**A e B**). As displayed in Figure 21, a possible rotation about the amide $-\text{CO-NH}$ bond can occur, thus generating the presence of two stable rotamers, and a rotamer appears to be present in a higher concentration.

The $^1\text{H-NMR}$ spectra have been conducted at room temperature and they showed that there are two different sets of peaks for the protons of the aromatic ring of the benzenesulfonamide moiety and the protons of the alkyl cycle ring of the isoquinoline. This phenomenon has been discussed by other researchers for *N*-acyl- and *N*-formyl-tetrahydroisoquinolines.^[104, 105]

For the derivatives **71c-e** the $^1\text{H-NMR}$ spectra did not reveal the presence of rotamers.

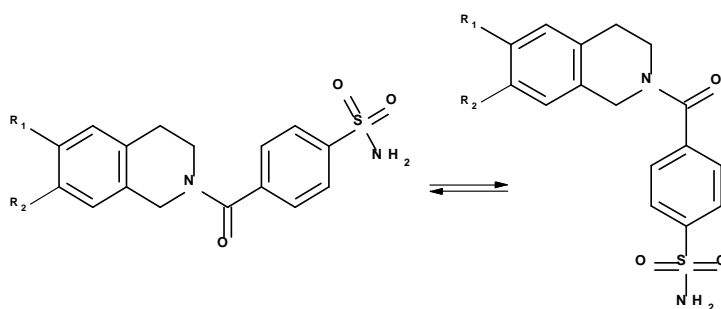
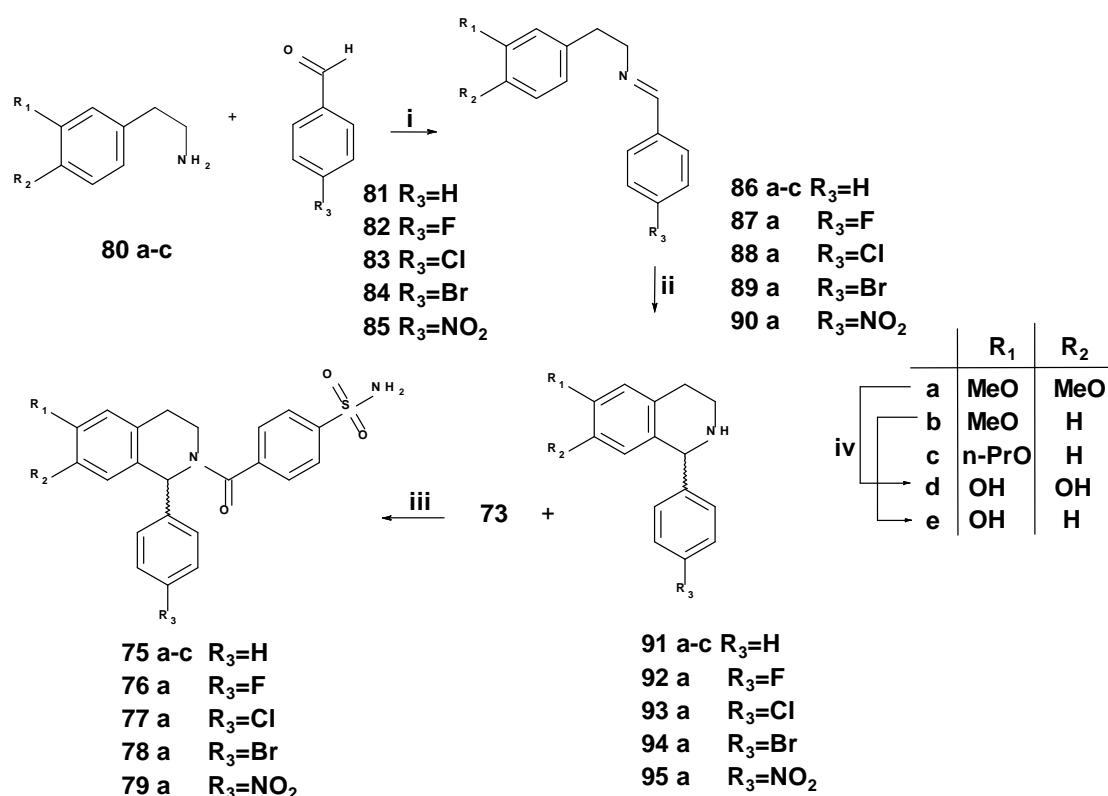


Figure 21. the Couple of rotamers of the compound **70a-e**, observed by $^1\text{H-NMR}$ analysis.

In the scheme 4 we report the synthetic procedure to obtain the racemic mixture of 4-(1-aryl-3,4-dihydro-1*H*-isochinolin-2-carbonyl)benzenesulfonamides (**75a-e**, **76a,d**, **77a,d**, **78a,d** and **79a,d**). We used the Pictet-Spengler approach for the synthesis of tetrahydroisoquinolines.^[78] To improve the yield and reduce reaction time the cyclization was promoted by microwave irradiation. The procedure is similar to that used for derivatives **13-15**, **16-18** and **23-31** but in this case we conducted the reaction for 10 min, at 90°C, 150W, 250Psi.



Scheme 5. Reagents and conditions: i) MW: 10 min, 90°C, 150 W, 250 Psi); ii) TFA, MW: 10 min, 90°C, 150 W, 250 Psi; iii) 4-(aminosulfonyl)benzoic acid, HBTU, TEA, DCM, rt, overnight; iv) BBr₃(1 M in DCM), DCM, rt, overnight.

By reaction of the commercially available phenylethylamine derivatives (**80a-c**) with suitable benzaldehyde derivatives (**81-85**) we obtained the corresponding imine **86a-c**, **87a**, **88a**, **89a**, **90a**, in solvent free condition. In turn, intermediates **86a-c**, **87a**, **88a**, **89a**, **90a** were heated with trifluoroacetic acid (TFA) to provide the desired isoquinolines **91a-c**, **92a**, **93a**, **94a**, **95a** as racemic mixtures. By a coupling reaction in the presence of HBTU and TEA the isoquinolines **91a-c**, **92a**, **93a**, **94a**, **95a** reacted with the 4-(aminosulfonyl)benzoic acid (**73**) to give the desired *N*-substituted isoquinolines **75a-c**, **76a**, **77a**, **78a** and **79a**. Finally, the 6,7-dimethoxy and 6-methoxy derivatives **75a,b**, **76a**, **77a**, **78a** and **79a** were further transformed into the corresponding hydroxyl analogues **75d,e**, **76d**, **77d**, **78d** and **79d** by treatment with BBr₃ in the presence of anhydrous DCM. For a comparative purpose the benzamide **50a** (R₁=R₂=OMe) has been converted into the hydroxyl analogue **50b** (R₁=R₂=OH).

2.2.2 Carbonic anhydrase inhibition assays against hCA isoforms and Structure-Activity Relationships (SARs) considerations

The CA inhibitory effects of the new arylsulfonamides **50b**, **70a-e**, **71c-e**, **75a-e**, **76a,d**, **77a,d**, **78a,d**, **79a,d** were measured toward human CA I, CA II, CA VII, CA IX and CA XIV isoforms. Analogously to previous tested compounds, the inhibitory constants were obtained using a Durrum-Gibson stop-flow spectrophotometer.^[87, 88]

The K_i values are summarized in Table 4 and compared with K_i values of dihydroxyanalogue **50b** and two well-known CA inhibitors **AZM (1)** and **TPM (7)** as reference compounds.

The first analogue *N*-[2-(3,4-dihydroxyphenyl)ethyl]-4-sulfamoylbenzamide (**50b**) displayed lower inhibitory effects than those of parent compound **50a** towards all screened isoforms with exception of hCA VII. In particular, the compound **50b** was an excellent hCA VII inhibitor with K_i value of 2.4 nM which was similar to that of reference compound **1** (K_i value of 2.5 nM). The CA inhibitory screening CA inhibitory shows that the isoquinoline derivatives **70a-e** display K_i values of inhibition in the range 2.8 to 186 nM against the hCA I, hCA II and hCA VII isoforms. The one notable exception to this expected behaviour was that weak inhibition at hCA VII isoform for compounds **70a** and **70b**, which exhibited K_i s > 800 nM. Comparing the results of these data with K_i s measured for unsubstituted and monosubstituted derivatives **70c-e**, which displayed excellent inhibition at all studied isoforms with no exception for hCA VII, we could postulate that the presence of two substituents on benzene-fused ring of 1,2,3,4-tetrahydroisoquinoline nucleus determines an impairment of recognition within catalytic site of hCA VII for compound **70a** and **70b**. Moreover, the 4-[(6-methoxy-3,4-dihydroquinolin-1(2H)-yl)carbonyl]benzenesulfonamide (**71c**) proved to be an unexpected inactive inhibitor (K_i value > 50000 nM at hCA VII) while the isoquinoline analogue 4-[(6-methoxy-3,4-dihydroisoquinolin-2(1H)-yl)carbonyl]benzenesulfonamide (**70c**) showed a good inhibitory activity (K_i = 3.1 nM). On the contrary the quinoline derivatives **71d** (R_1 = OH, R_2 = H) and **71e** (R_1 = R_2 = H) proved to be potent hCA VII inhibitors and showed similar efficacy of isoquinoline derivatives **70d** and **70e**. The results

that we obtained toward the hCA IX and hCA XIV isoforms are interesting. Infact the new arylsulfonamides **70a-b**, **70e** and **71c** have low nanomolar inhibitors (K_i s <10 nM) if we compared with the reference compounds **1** and **7**.

Finally the derivatives **70a-e**, **71c-e** showed no-selectivity over cytosolic hCA I and/or hCA II isoforms.^[106]

Table 4. Inhibition of hCA I, hCA II, hCA VII, hCA IX and hCA XIV isoforms by 1-aryl-6,7-dimethoxy-1,2,3,4-tetrahydroisoquinolines-2-sulfonamides (**70a-e**, **71c-e**), acetazolamide and topiramate.

Compound	K_i(nM)^a						
	R1	R2	hCA I	hCA II	hCA VII	hCA IX	hCA XIV
50a	OMe	OMe	8.7	2.7	5.8	3.8	4.3
50b	OH	OH	31	11.2	2.4	17	58
70a	OMe	OMe	39.9	5.89	878	6.09	7.2
70b	OH	OH	8.52	4.67	819	5.01	5.8
70c	OMe	H	29	9.5	3.1	27	65
70d	OH	H	186	10.4	2.8	28	61
70e	H	H	76.2	7.7	9.2	7.5	9.6
71c	OMe	H	18.5	5.69	n.d.c	6.46	7.88
71d	OH	H	58	15.1	4.0	42	64
71e	H	H	78.6	6.8	8.5	9.4	39.0
AZM (1)^b	-	-	250	12	2.5	25	41.2
TPM (7)^b	-	-	250	10	0.9	58	1460

^a Errors in the range of $\pm 10\%$ of the reported value, from 3 different assays. Recombinant full length hCA I, II, VII and XIV and catalytic domain of hCA IX were used.

^b Data are taken from Ref. [77]

^c n.d. = not detected ($IC_{50} > 50000$ nM).

Regarding the series of derivatives **75a-e**, **76a,d**, **77a,d**, **78a,d**, **79a,d** (Table 5) we can observe that the introduction of a methoxy-groups at C-6 position and phenyl ring at C-1 was well tolerated. In

more details, we can see that the compounds **75a-e**, **76a,d**, **77a,d**, **78a,d** and **79a,d** showed inhibition activity in the range of the subnanomolar concentration toward the hCA VII isoform.

Table 5. Inhibition of hCA I, hCA II, hCA VII, hCA IX and hCA XIV isoforms by (*R,S*)-4-(1-aryl-3,4-dihydro-1H-isochinolin-2-carbonyl)benzenesulfonamides (**75a-e**, **76a,d**, **77a,d**, **78a,d** and **79a,d**) as racemic mixture, acetazolamide and topiramate.

$K_i(\text{nM})^a$								
Compound	R ₁	R ₂	R ₃	hCA I	hCA II	hCA VII	hCA IX	hCA XIV
75a	OMe	OMe	H	16.4	6.9	7.3	4.9	4.3
75b	OMe	H	H	39.1	5.3	1.4	39.2	3.2
75c	n-PrO	H	H	850	33.2	84.4	44.5	25.6
75d	OH	OH	H	15.2	3.5	0.20	36.9	3.3
75e	OH	H	H	6.2	4.5	0.35	50.6	2.9
76a	OMe	OMe	F	6.9	0.84	0.53	9.1	374
76d	OH	OH	F	2.2	0.21	0.51	8.2	346
77a	OMe	OMe	Cl	10.9	5.5	0.77	91.4	325
77d	OH	OH	Cl	3.5	0.29	0.40	9.0	2915
78a	OMe	OMe	Br	38.9	16.9	3.8	90.9	4010
78d	OH	OH	Br	3.4	0.28	0.33	81.5	3930
79a	OMe	OMe	NO ₂	45.5	0.63	0.59	86.2	315
79d	OH	OH	NO ₂	4.7	0.27	0.40	9.3	281
AZM (1)^b	-	-	-	250	12	2.5	25	41.2
TPM (7)^b	-	-	-	250	10	0.9	58	1460

^a Errors in the range of $\pm 10\%$ of the reported value, from 3 different assays. Recombinant full length hCA I, II, VII and XIV and catalytic domain of hCA IX were used.

^b Data are taken from Ref. [77]

The introduction of a fluorine atom at para position of C-1 phenyl ring resulted in a remarkable inhibition of hCA II and hCA VII isoforms for compound **76a**; whereas this modification led to a loss of activity toward hCA XIV. Then, the replacement of fluorine atom with chlorine or bromine

atoms induced a remarkable reduction of potency for hCA XIV isoform for compounds **77a** and **78a** compared with fluorine analogue **76a**. It can be observed that the degree of CA inhibitory potency was the following 4-F>4-Cl>4-Br, thus suggesting that the increasing size of the halogen atom was detrimental for inhibition of all studied isoforms;

Finally, we examined the impact on CA inhibition of the removal of methyl group of 6/7 methoxysubstituents on isoquinoline nucleus. The monohydroxy-derivative **75e** and dihydroxy-derivative **75d** displayed a very similar inhibitory potency against studied hCA isoforms. Specifically, they showed remarkable potency as hCA VII inhibitors (K_i values of 0.20 and 0.35 nM, respectively for compound **75d** and **75e**). Interestingly, the 4-halophenyl derivatives **76d**, **77d** and **78d** proved to be very active inhibitors displaying K_i values ranging from 0.21 to 0.51 nM concentration towards hCA II and hCA VII isoforms. By analysing the hCA VII K_i values shown by hydroxyl compounds **75d,e**, **76d**, **77d** and **78d** we found a flat influence of the steric and electronic effects of the para-phenyl substituent, thus suggesting that this substituent does not establish crucial contacts within catalytic site of hCA VII. Moreover, compounds **76d**, **77d** and **78d** showed high inhibitory potency for hCA I and hCA IX. The replacement of chlorine atom of compound **77d** (K_i value of 9.0 nM) with bromine atom gave about 10-fold reduction of potency (i.e. compound **78d**, K_i value of 81.5 nM) exclusively for hCA IX inhibition. On the contrary, the presence of halogen atoms gave up to 1200-fold drop of potency against hCA XIV (i.e. compound **78d** vs compound **75d**). These data might suggest that the increase in atomic radius impair the binding recognition within catalytic site of hCA XIV.

2.2.3 Enantiomeric separation and CA effects of each enantiomer

For selected (*R,S*)-4-(1-aryl-3,4-dihydro-1H-isochinolin-2-carbonyl)benzenesulfonamides we also studied the impact of the chirality on the CA inhibition performing the enantiomeric separation of some compounds by means of HPLC. Moreover the individual enantiomer has been tested against the hCA I, hCA II, hCA VII, hCA IX and hCA XIV isoforms (Table 5). The complete HPLC resolution of four selected sulfonamides **75a**, **75b**, **75d** and **75e** was achieved on polysaccharide-based chiral stationary phases (CSPs) using normal-phase eluents.

Typical chromatograms of the HPLC enantio-separations on an analytical scale are shown in Figure 22. The optimized analytical enantioselective conditions were successfully scaled up to a multi-milligram level using semi-preparative 250 mm x 10 mm I.D. columns. Both enantiomers of each compound were isolated with high enantiomeric purity (enantiomeric excess > 99 %). The enantiomeric nature of the samples obtained on mg-scale was demonstrated by circular dichroism (CD) analysis (Figure 23).

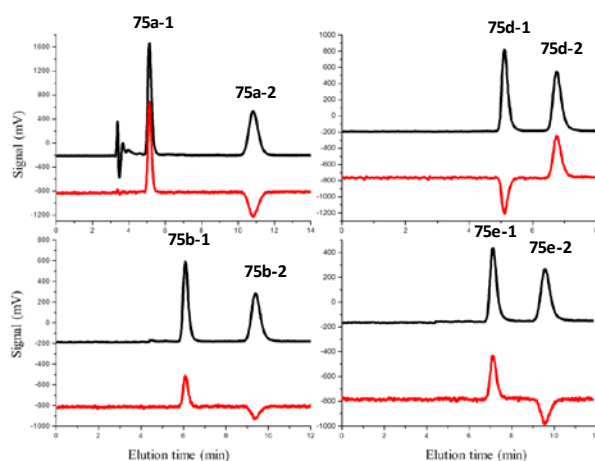


Figure 22. Analytical HPLC resolution of **75a**, **75b**, **75d** and **75e**. **Condition:** Column: Chiralpak AS-H 250 mm x 4.6 mm i.d. (**75a,d,e**) and Chiralpak IA 250 mm x 4.6 mm i.d. (**75b**); mobile phase: *n*-hexane/ethanol/TFA 20/100/0.1 (**75a,d,e**) and *n*-hexane/ethanol/TFA 40/60/0.1 (**75b**); flow rate: 1 mL/min; temperature: 25 (**75b**) and 40 °C (**75a,d,e**); detector: UV (black line) and CD (red line) at 280 nm. The letters a and b denote the enantiomer elution order.

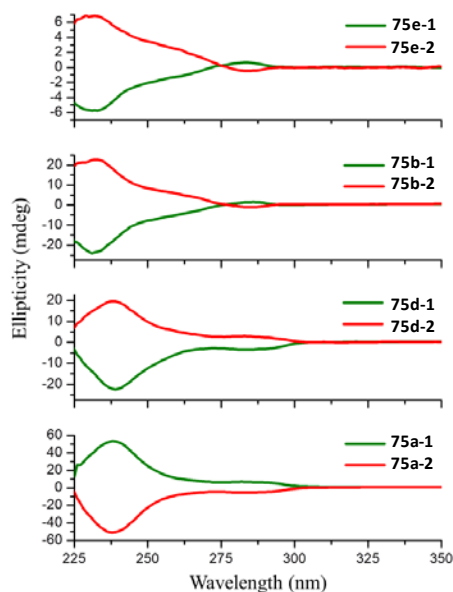


Figure 23. CD spectra of the enantiomers of **75a**, **75b**, **75d** and **75e** in dichloromethane.

The individual enantiomers has been tested against the hCA I, hCA II, hCA VII, hCA IX and hCA XIV isoforms (Table 6). Therefore, for each single enantiomer of four selected sulfonamides we screened the inhibitory effects towards hCA isoforms. By analysing the K_i values summarized in Table 6 we can observe that there is not significant influence of stereochemistry at C-1 on the CA inhibition of each hCA isoform. This evidence suggests that the two enantiomers can assume binding poses which are still effective for CA inhibition. Moreover, we found that the lack of stereoselectivity in CA inhibition is a similar behaviour for all studied isoforms. As result we can hypothesize that the arylsulfonamide fragment occupies the same area of catalytic pocket of all studied isoforms. These hypotheses were successively corroborated by means of structural data (*vide infra*).

Table 6. Inhibition of hCA I, hCA II, hCA VII, hCA IX and hCA XIV isoforms by pair of enantiomers of compounds **75a**, **75b**, **75d** and **75e**.

<i>Compound</i>	<i>K_i(nM)^a</i>						
	R ₁	R ₂	hCA I	hCA II	hCA VII	hCA IX	hCA XIV
75a-1	OMe	OMe	16.6	4.9	9.2	5.0	4.3
75a-2			16.0	8.9	5.4	4.8	4.3
75b-1	OMe	H	15.6	4.8	0.77	25.3	2.4
75b-2			77.8	6.0	4.1	58.7	6.1
75d-1	OH	OH	9.3	3.3	0.21	32.7	3.2
75d-2			9.3	3.6	0.19	39.2	3.4
75e-1	OH	H	7.5	5.0	0.80	73.2	6.3
75e-2			5.6	3.2	0.49	39.8	1.7

^a Errors in the range of $\pm 10\%$ of the reported value, from 3 different assays. Recombinant full length hCA I, II, VII and XIV and catalytic domain of hCA IX were used.

2.2.4 X-ray and docking studies

To establish how the series of new heterocyclic compounds interact with the catalytic pocket of the hCA II isoform we conducted the X-ray studies of some of the interesting compounds.

The co-crystal structures were obtained for the cytosolic dominant isoform hCA II in complex with five carbonylbenzenesulfonamides **70a**, **70b**, **70e**, **71c**, and **71e**, which displayed very low K_i values ranging from 4.67 to 7.7 nM.

The structures of hCA II complexes were solved using the difference Fourier technique, using hCA II structure (Protein Data Bank entry 3PO6)^[107] as the initial model.

In the Table 7 are summarized the data collection and refinement statistics for these five crystal structures, which were deposited into the PDB (see Table).

Table 7. Data collection statistics and refinement statistics.

hCA II in complex with					
	70a	70b	70e	71c	71e
Crystal parameters and diffraction data statistics					
space group	$P2_1$	$P2_1$	$P2_1$	$P2_1$	$P2_1$
unit cell parameters					
a, b, c (Å)	42.2 41.3 72.4	42.1 41.3 72.1	42.1 41.2 72.2	42.4 41.45 72.3	42.2 41.7 72.4
α, β, γ (°)	90 104.5 90	90 104.4 90	90 104.3 90	90 104.4 90	90 104.6 90
wavelength (Å)	0.91841	0.97565	0.97565	1.54179	0.97565
resolution range (Å)	50.0-1.47 (1.56-1.47)	50.0-1.35 (1.43-1.35)	50.0-1.27 (1.35-1.27)	41.5-2.0 (2.05-2.00)	50.0-1.45 (1.54-1.45)
No. of unique reflections	69904	92993(14462)	99304(12514)	14005(653)	43348(6886)
multiplicity	1.3(1.3)	2.1(2.1)	2.2(2.1)	3.8(3.1)	3.7(3.6)
completeness (%)	86.6(81.5)	89.9(86.4)	79.8(62.2)	88.0(90.3)	99.7(99.1)
R_{merge}^a (%)	10.9(44.0)	3.8(44.8)	3.8(28.7)	6.4(25.9)	7.9(56.0)
average $I/\sigma(I)$	6.4(2.2)	14.1(1.9)	13.7(3.0)	7.9(2.8)	11.6(2.4)
Wilson B (Å ²)	16.3	19.1	9.2	23.5	18.4
Refinement statistics					
Resolution range	39.93-1.47 (1.51-1.47)	39.80-1.35 (1.39-1.35)	40.81-1.27 (1.30-1.27)	41.33-2.00 (2.06-2.00)	40.90-1.45 (1.49-1.45)
No. of reflections in working set	35900 (2595)	47453 (3560)	53546 (2857)	13036 (1009)	39013 (2854)
No. of reflections in test set	1995 (137)	2637 (189)	2975 (150)	732 (63)	2168 (150)
R^b (%)	18.8(26.9)	13.4(20.2)	13.7(17.0)	17.2(20.1)	14.9(18.4)
R_{free}^c (%)	21.3(31.4)	17.0(26.0)	17.0(22.4)	24.4(23.7)	19.1(24.5)
RMSD bond length (Å)	0.019	0.012	0.013	0.013	0.017
Mean ADP protein/inhibitor (Å ²)	11.7	16.1	14.2	13.4	13.8
PDB code	4Z1N	4Z1K	4Z1J	4Z1E	4Z0Q

^a $R_{\text{merge}} = \frac{\sum_{\text{hkl}} \sum_i |I_i(\text{hkl}) - \langle I(\text{hkl}) \rangle|}{\sum_{\text{hkl}} \sum_i I_i(\text{hkl})}$, where the $I_i(\text{hkl})$ is an individual intensity of the i th observation of reflection hkl and $\langle I(\text{hkl}) \rangle$ is the average intensity of reflection hkl with summation over all data.

^b $R = \frac{||F_o| - |F_c||}{|F_o|}$, where F_o and F_c are the observed and calculated structure factors, respectively.

^c R_{free} is equivalent to R value but is calculated for 5 % of the reflections chosen at random and omitted from the refinement process.^[108]

In Figure 24A we displayed the crystal structures of hCA II in complex with inhibitor **70a** (orange) and in Fig. 24B we compared the inhibitors **70b** (yellow) and **70e** (purple) within hCA II cavity.

The structures of hCA II in complex with 4-(3,4-dihydroisoquinolin-2(1H)-ylcarbonyl)benzenesulfonamides (**70a**, **70b** and **70e**, Figure 24) have been determined at resolution 1.27-1.47 Å and there is no evidence of alternative conformations for any of the inhibitors as observed for the parent compound **50a** (see Figure 19B).

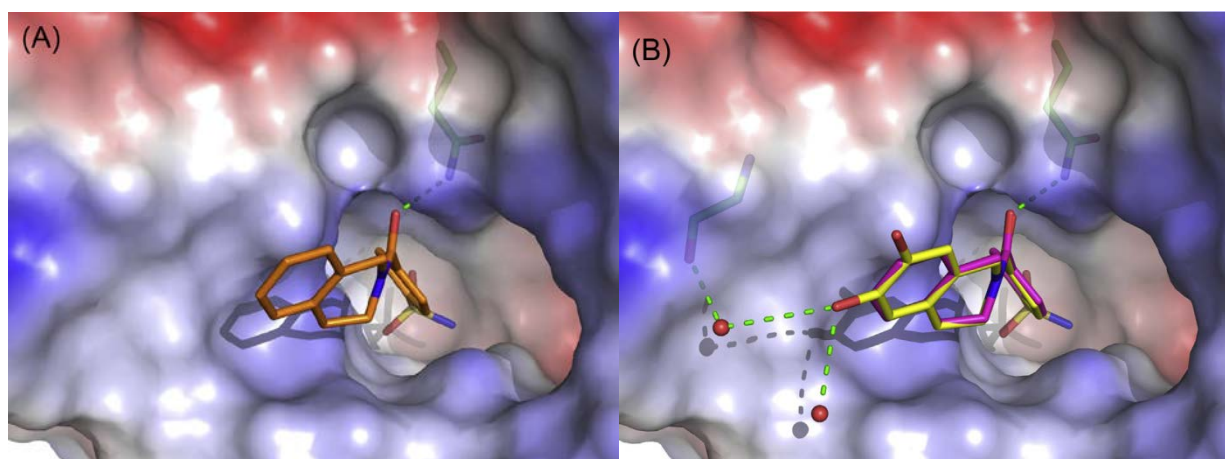


Figure 24. Active site of hCA II colored by electrostatic potential, the inhibitors are depicted in stick representation. (A) hCA II in complex with inhibitor **70a** (orange). (B) comparison of binding pose of the two inhibitors **70b** (yellow) and **70e** (purple).

In detail, the benzene fused ring of isoquinoline moiety of the three inhibitors **70a**, **70b**, and **70e** are nearly superimposable. These structural results are consistent with the observation that the inhibitory K_i values against hCA II are very similar (see Table 4).

In the cocrystal structures of the compounds **70b** and **70e**, the hydrogen bond interaction between carbonyl oxygen and Gln92 are detectable. Moreover, between **70b** or **70e** compounds and hCA II are Van der Waals interactions with each inhibitor and a series of residues: Asn67, Ile91, Gln92, His94, His119, Val121, Phe131, Val 35, Val143, Leu-Thr-Thr-Pro-Pro 198e202, Val204 and Trp 209. Furthermore, there is an additional hydrogen bond (3.2 Å) formed between phenolic oxygen atom of inhibitor **70b** and water molecules (red spheres) in the first hydration shell of hCA II, no other interaction of the hydroxyl or methoxy analogues has been found.

High resolution cocrystal structure of unsubstituted 4-(3,4-dihydroquinolin-1(2H)-ylcarbonyl)benzenesulfonamide (**71e**) (1.45 Å) shows that the inhibitor (K_i value of 6.8 nM) assumes three alternative conformations (Figure 25A) and in the Figure 25B reports the crystal structure of the 4-[(6-methoxy-3,4-dihydroquinolin-1(2H)-yl)carbonyl]benzenesulfonamide (**71c**) (grey) bound to hCA II determined at resolution 2 Å.

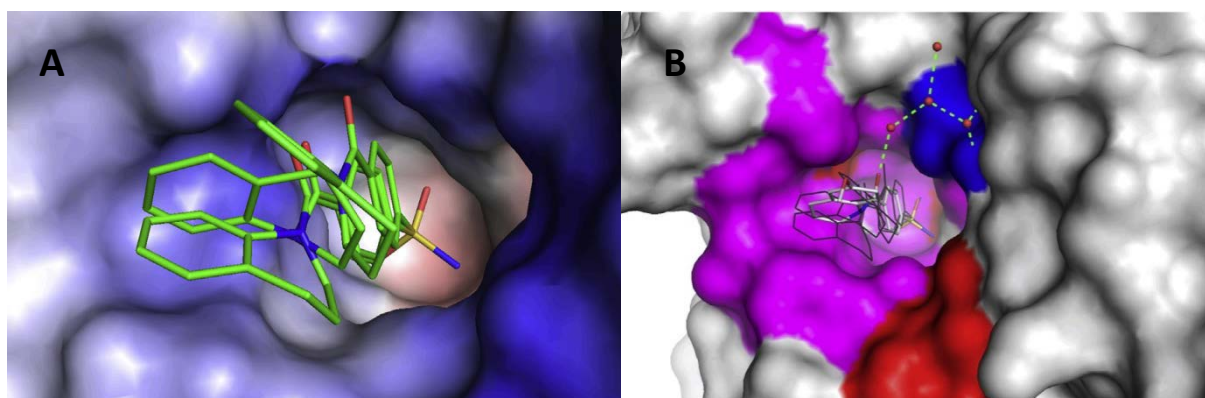


Figure 25. **A** Binding of **71e** into the active site of hCA II. Surface of hCA II is colored by electrostatic potential (blue for positive, red for negative), inhibitor in stick representation has carbon atoms of inhibitor colored green while other atoms are colored according to standard color coding: oxygen red; nitrogen blue; sulphur yellow. **B** Active site of hCA II with inhibitors **71c** and **71e**. Surface of hCA II is colored red for residues interacting with **71e** only; blue are residues interacting only with **71c** inhibitor and residues interacting with both inhibitors are colored magenta; the inhibitor **71e** is depicted in line, inhibitor **71c** is in stick representation (carbon atom are colored black and grey for **71e** and **71c**, respectively).

As expected the inhibitor **71e** established the crucial interactions with the Zinc ion within the catalytic pocket; moreover **71e** engaged hydrogen bond interaction between the side-chain of Gln192 and carbonyl oxygen linked to the nitrogen atom of quinoline moiety.

The crystallographic analysis furnishes suggestions how the introduction of a methoxy group on benzene fused ring could affect the inhibitor binding mode. Interestingly, inhibitor **71c** (K_i value of 5.69 nM) acquires a single binding mode within the active site of hCA II and adopts an orientation for which the binding of sulfonamide anchor is again the “canonical one”.^[77] Although compound **71c** seems to lose the interaction with residue Gln92, the carbonyl oxygen of inhibitor makes hydrogen bond to water molecule from the first hydration shell for which this water molecule is bound to other water molecules interacting to protein atoms. Considering that **71c** and **71e** show very similar K_i values (5.69 nM and 6.8 nM, respectively) we can conclude that this different binding mode does not affect the affinity toward hCA II.

If we compared the binding modes of the inhibitors **71c** and **71e** (Figure 25B), it emerged that the two sulfonamide moieties show essentially overlapping orientation, whereas the two inhibitors exhibited a different rotated position of quinoline ring in the top area of the catalytic site. The reason for different quinoline moiety placement could be the spatial hindrance of methoxy group of **71c** within the active site of hCA II. We can hypothesize that there are possible clashes with

Pro202 and/or flexible N-terminus. Figure 25B also compares the connections with the protein observed for the three alternative binding poses of inhibitor **71e** (depicted in black line) with the single pose of methoxy analogue **71c** (in grey stick presentation). The first group assembles the residues interacting with **71c** only (Asn67 and Gln92, colored in blue); the second group concerns the residues interacting with **71e** only (Trp5, His64, His119 and Leu141, colored in red); the third group collects all residues that interact with both inhibitors (Gln92, His94, Val121, Phe131, Val135, Val143, Leu-Thr-Thr-Pro-Pro 198e202, Val204 and Trp209, colored in magenta).

Therefore, the X-ray co-crystal structures of the compounds **69**, **24-25**, **50a**, **70a**, **70b**, **70e**, **71c**, and **71e** validated our hypotheses about their mode of interaction with hCA II isoform.

These results were supported by docking studies with the superposition of the docking poses of the three inhibitors **70b**, **70e**, and **71c** into the hCA VII (Figure 26, panel A) furnished some suggestions about the inhibitory effects toward this specific isoform. It may be observed that the three inhibitors are anchored to the active site through the coordination of Zinc ion by means of one nitrogen atom of the three superimposable sulfonamide groups, whereas the quinoline/isoquinoline nucleus for each molecule adopts a very different orientation. The panel B of Figure 26 displays the crucial interactions with Zinc ion within catalytic site for the active hCA VII inhibitor **70e**, for which we measured binding energy ($162.073 \text{ kcal mol}^{-1}$) using Discovery Studio Version 2.5. We found that the heterocyclic ring of the compound **70e** (blue) lies the hydrophobic cleft (colored area in magenta) defined by residues Phe131, Ala135, Leu198, Pro202. It is interesting to note that compound **70e** assumes a disposition that is similar to that has been observed in its complex with hCA II isoform. This behavior could explain the very similar K_i values measured for the two compared isoforms (7.7 and 9.2 nM, respectively). Moreover, we can speculate that the reduction of hCA VII inhibitory effects observed for compounds **70b** and **71c** could be due to their alternative orientations into hCA VII catalytic site when compared with their binding poses observed into their complexes with hCA II. As shown in Figure 26 the heterocyclic ring of the low active inhibitor **70b** (yellow) seems to occupy the middle area of catalytic channel making weaker interactions with the hydrophobic cleft thus furnishing a plausible explanation of a K_i value of 819 nM. In the case of compound **71c**, colored in pink, the lack of inhibitory effects might be related to its inability to establish favorable interactions with the before mentioned hydrophobic cleft.

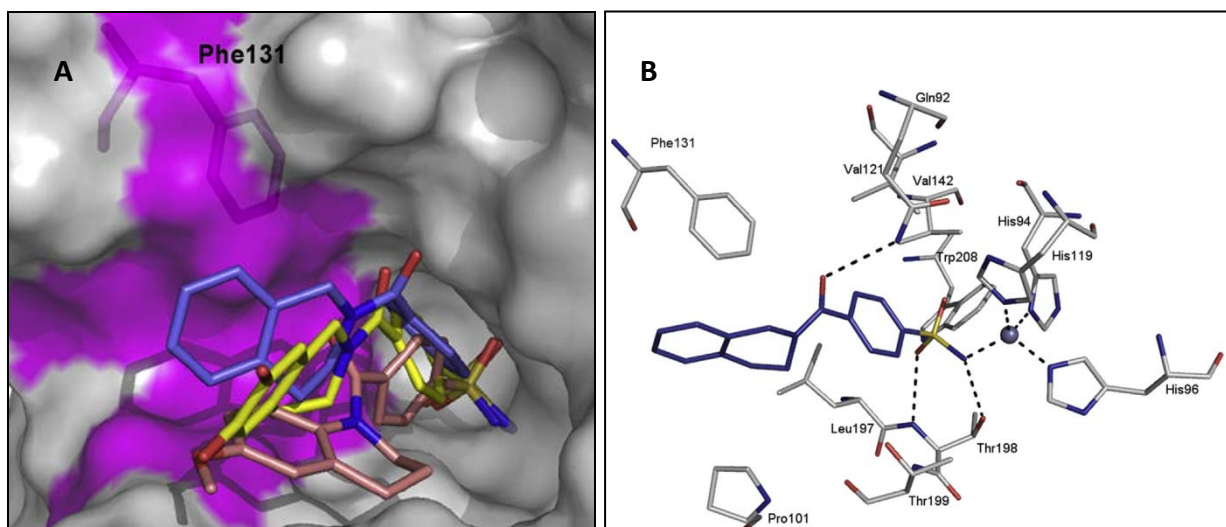


Figure 26. **A** The superposition of the docking poses of the compounds **70b** (yellow), **70e** (blue), and **71c** (pink) into hCA VII; the hCA VII hydrophobic cleft is defined by residues Phe131 and Ala135, Pro202, Leu204 (magenta). **B** Interactions of ligand **70e** with hCA VII; the inhibitor in stick representation has carbon atoms colored in blue marine, other atoms are colored according to standard color coding: oxygen red; nitrogen blue; sulfur yellow. The residues involved in the interactions are also shown as sticks with carbon atoms in light grey. Polar interactions are represented by black dotted lines. Zinc ion is represented by grey sphere.

Thereby, it is also reasonable that the inhibitory effects are especially related to the distance between heterocyclic ring of each inhibitor and the crucial residue Phe131 (highlighted in hydrophobic surface colored in magenta).^[109] On the basis of these findings we hypothesize that for these compounds the residue Phe131 could exert a fine-tuned control of their recognition process into catalytic site of hCA VII.^[106]

To gain further information about the protein/inhibitor recognition of other synthesized inhibitors, we solved the crystal structure of the adduct which hCA II forms with inhibitor **75d**. In particular, the two **75d** enantiomers, namely **75d-1** and **75d-2**, were separated (cfr. HPLC enantiomeric resolution section) and singularly used for soaking experiments. Data collection and refinement of both adducts were performed as described in Table 8.

Table 8 X-ray diffraction data collection and refinement statistics.

	hCA II/75d-1	hCA II/75d-2
Cell parameter		
Space group	P2 ₁	P2 ₁
Unit cell parameters (Å, °)	a= 42.3	a= 42.3
	b= 41.3	b= 41.4
	c= 71.8	c= 72.0
	β= 104.3	β= 104.4
Data collection statistics		
Resolution limits (Å)	50.0-1.70	50.0-1.75
Temperature (K)	100	100
Total reflections	115858	100903
Unique reflections	26226	23683
Completeness (%)	97.9 (91.7)	96.7 (86.8)
R-merge*	0.063 (0.435)	0.090 (0.360)
Mean I/sigma(I)	17.8 (2.7)	13.1 (4.0)
Refinement statistics		
Resolution limits (Å)	50.0-1.70	50.0-1.75
R-factor** (%)	16.2	16.2
R-free** (%)	19.2	19.2
r.m.s.d. from ideal geometry:		
Bond lengths (Å)	0.013	0.013
Bond angles (°)	1.7	1.7
Number of protein atoms	2093	2093
Number of inhibitor atoms	17	17
Number of water molecules	224	224
Average B factor (Å ²)	17.46	17.46

*R-merge = $\sum hkl \sum i |I_i(hkl) - \langle I(hkl) \rangle| / \sum hkl \sum i I_i(hkl)$, where $I_i(hkl)$ is the intensity of an observation and $\langle I(hkl) \rangle$ is the mean value for its unique reflection; summations are over all reflections; **Rfactor = $\sum |F_o - F_c| / \sum F_o$; Rfree calculated with 5% of data withheld from refinement. Values in parentheses are referred to the highest resolution shell (1.76-1.70 Å for hCA II/75d-1 and 1.81-1.75 Å for hCA II/75d-2).

In both complexes, inspection of the initial $F_o - F_c$ electron density maps immediately revealed the binding of each inhibitor (**75d-1** and **75d-2**) in the active site. Each inhibitor binding does not alter hCA II three-dimensional structure. Indeed, the r.m.s.d. values calculated by superposition of all the $C\alpha$ atoms of the hCA II/**75d-1** and hCA II/**75d-2** adducts with those of the native protein were 0.26 Å and 0.25 Å, respectively.

Active site analysis of the two structures showed that the sulfonamide moiety of the two inhibitors maintains a binding mode to the protein similar to that observed for other CAIs containing the same group.^[110] Indeed, the deprotonated nitrogen atom displaces the hydroxyl ion/water molecule present in the native enzyme and coordinates the zinc ion with a tetrahedral geometry, while additional hydrogen bond interactions with residue Thr199 further contribute to stabilize the binding (Figure 27A and 27B).

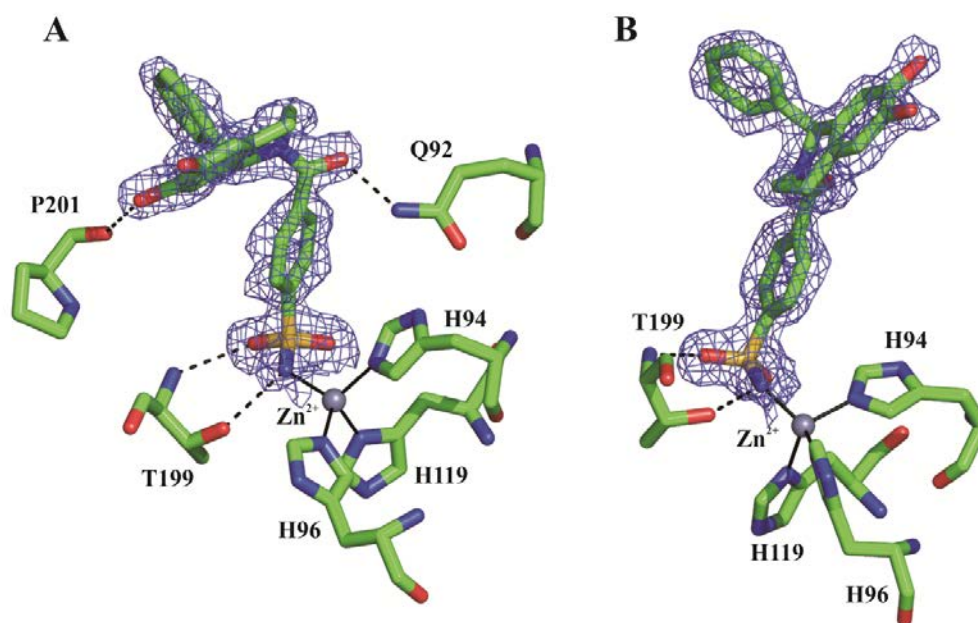


Figure 27. Active site region of the hCA II/(*R*)-**75d-1** (A), hCA II/(*S*)-**75d-2** (B) adducts showing the σ_A -weighted $|2F_o - F_c|$ OMIT map (contoured at 1.0σ) relative to the inhibitor molecule. The zinc ion coordination and polar interactions are also reported.

The orientation of the organic scaffold of the two inhibitors is instead rather peculiar. Indeed, in both cases, the phenyl-substituent at the C-1 position is located in the hydrophobic region of the active site, in a small pocket delimited by residues Phe131, Val135, Leu198 and Pro202, whereas

the tetrahydroisoquinoline ring is oriented toward a poorly explored area of the active site, located at the border between the hydrophobic and hydrophilic regions (Figure 28).^[110]

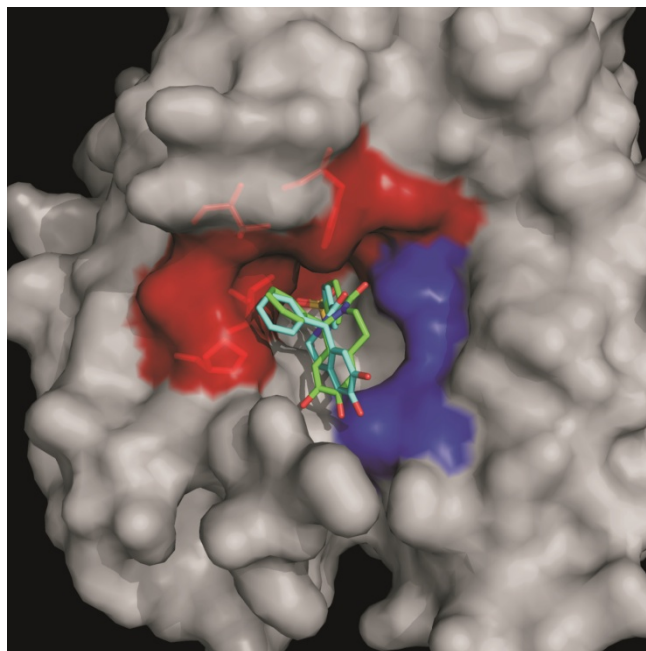


Figure 28. Solvent accessible surface of hCA II/inhibitor adducts. The hydrophobic region of the active site is shown in red, whereas the hydrophilic one in blue. Residues delimiting the small pocket interacting with the C-1 phenyl substituent of both inhibitors (Phe131, Val135, Leu198 and Pro202) are shown in stick representation.

By the superposition of the hCA II/**75d-1** and hCA II/**75d-2** structures, it is evident that poor differences are present in the orientation of the organic scaffold of the two inhibitors, due to the diverse chirality of the C-1 atom (Figure 26). As a consequence **75d-1** establishes with the enzyme two hydrogen bonds, involving both the carbonyl oxygen and one of the two hydroxyl groups (Figure 27A), which instead are not present in the hCA II/**75d-2** structure (Figure 27B). Nevertheless, the two inhibitors retain the same affinity for the enzyme (see Table 5), thus indicating that the influence of these two polar interactions in the binding is negligible with respect to the contribution of the sulfonamide binding and of high number of van der Waals contacts established by the bulky organic scaffold. Interestingly, the superposition of both hCA II/**75d-1** and hCA II/**75d-2** structures with that of the lead compound **69** in complex with the same enzyme^[111] reveals that the introduction of the C-1 phenyl substituent on the tetrahydroisoquinoline ring causes a dramatic rearrangement of the latter within the active site

cavity. Indeed, such ring in the hCA II/**69** structure is located in the small hydrophobic pocket occupied by the phenyl ring in hCA II/**75d-1** and hCA II/**75d-2** adducts (see Figure 29).

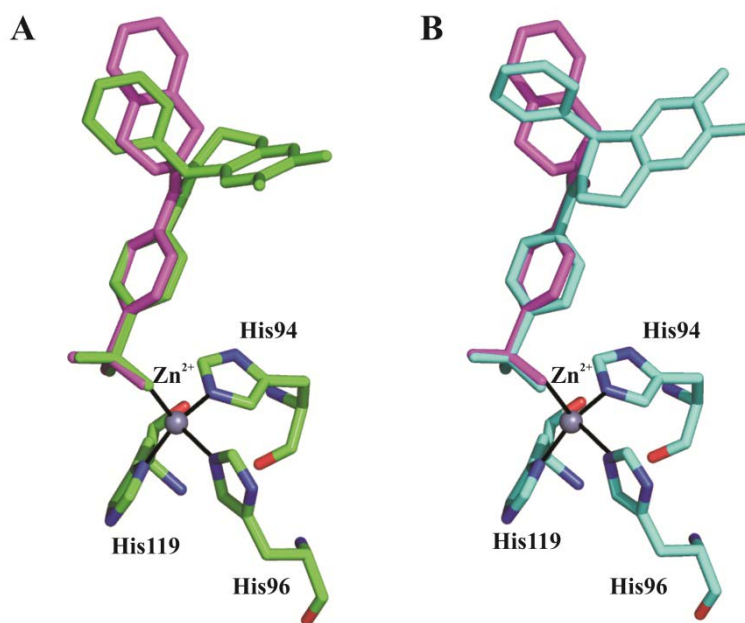


Figure 29. Structural superposition between **75d-1** and **69** (A) and **75d-2** and **69** (B) bound to the hCA II active site. **75d-1**, **75d-2** and **69** are colored in green, cyan and magenta respectively.

These data suggest that the introduction of suitable substituents on the tetrahydroisoquinoline ring of compound **69** is a proper strategy to modulate the interactions of these inhibitors with different regions of the active site.

Conclusion

The research project of this PhD dissertation has been focused on the development of a new series of benzenesulfonamides as carbonic anhydrase inhibitors. As result, some of these synthesized compounds showed significant and relevant CA inhibitory effects. In particular, these novel inhibitors could target the human carbonic anhydrase VII (hCA VII) that is involved in several neurological diseases.

Starting from previously reported “lead compounds” as template, we have made several structural modifications, preserving the isoquinoline and/or quinoline nucleus. As result, we obtained relevant structure-activity relationships (SARs) information in correlation of the binding recognition of these inhibitors within the catalytic pocket and the information on the shape of the pocket.

The sulfonamide inhibitors have been obtained using both classical synthetic and microwave-assisted methods, thus improving the yield, reducing reaction times and solvent amount. All compounds were carefully characterized through spectroscopic measurements such as *NMR*.

The analysis of X-ray data of co-crystal complexes of protein/inhibitors furnished information about the binding mode of the most active ligands. We confirmed that the conical shape of the pocket gives the possibility of the compounds to fluctuate within the pocket and establish interactions with the different areas. The main result can be summarized follow.

Among the series of isoquinolinesulfonamides, **I**, we identify that several of these compounds proved to be very efficient inhibitors exhibiting good selectivity towards the hCA VII isozyme ($K_i < 10$ nM). By means of docking studies we found that the isoquinoline moiety established the numerous van der Waals interactions involving residues in both of the hydrophilic and hydrophobic areas of the hCA II (Gln92, Val121 and Phe131). Moreover, the presence of the substituent in the C-1 of the isoquinoline nucleus oriented the molecules within the catalytic site thus making other interactions with residues in the pocket, such as the methyl substituent of the compound **16** interacts with Leu198.

Furthermore, in the series of the 1,2,3,4-tetrahydroisoquinoline and 1,2,3,4-tetrahydroquinoline (**II** and **III**) we have added the carbonyl-benzenesulfonamide moiety that binds the nitrogen atom in the iso/quinoline nucleus. Remarkably, these compounds showed inhibitory activity in the nanomolar concentration neglecting the selectivity over off-target isoforms.

Finally, the series of (*R,S*)-1-aryl-1,2,3,4-tetrahydroisoquinolines (**IV**) combined the features displayed in previous active inhibitors, we have been kept the 1,2,3,4-tetrahydroisoquinoline skeleton with the nitrogen atom bound with the carbonylbenzenesulfonamide group; and we added a bulky substituent in the C-1 of the isoquinoline nucleus. The biochemical assays have confirmed the substituent in the C-1 and the isoquinoline nucleus, resulted a remarkable potency as hCA VII inhibitors at *subnanomolar* concentration.

Comparing structure analysis and biochemical assay of the couple of enantiomers of the compound **75d** we can observe that two inhibitors assume different orientation which does not affect inhibitory potency.

Overall, the results obtained in this PhD project, could contribute to suggest new ideas to plan the design of new human Carbonic Anhydrase inhibitors improving the potency/selectivity aspects.

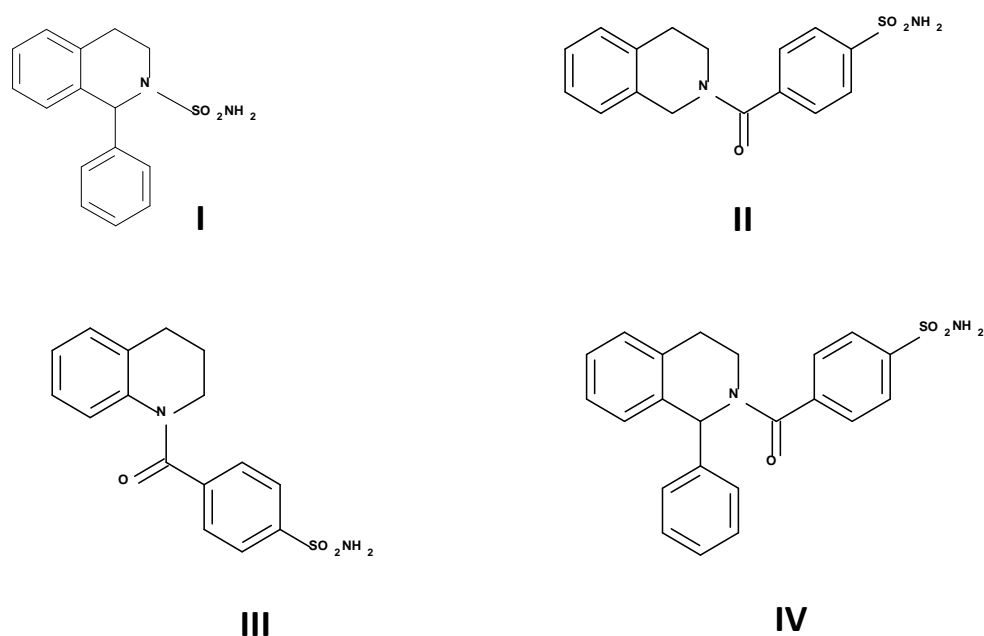


Figure 30. General structures of the designed compounds.

Chapter 3

Experimental section

3.1 Chemistry

All starting materials and reagents were purchased from Sigma Aldrich Milan (Italy) and used without further purification. Microwave-assisted reactions were carried out in a Focused Microwave TM Synthesis System, Model Discover (CEM). Melting points were determined on a Buchi B-545 apparatus and are uncorrected. By combustion analysis (C, H, N) carried out on a Carlo Erba Model 1106 Elemental Analyzer we determined the purity of synthesized compounds; the results were within $\pm 0.4\%$ of the theoretical values. Merck silica gel 60 F254 plates were used for analytical TLC. R_f values were determined on TLC plates using a mixture of DCM/MeOH (94:6) as eluent. Flash Chromatography (FC) was performed on a Biotage SP1 EXP. ^1H NMR and ^{13}C spectra were measured in $\text{DMSO-}d_6$ with a Varian Gemini 300 spectrometer; chemical shifts are expressed in δ (ppm) and coupling constants (J) in Hz. All exchangeable protons were confirmed by addition of deuterium oxide (D_2O). GC-MS spectra for compounds **70c** and **71d** were recorded on a Shimadzu QP500 EI 151 mass spectrometer.

Sulfonamide derivatives **13-15**,^[78] **16-18**,^[79] **19** and **20**,^[1] **21** and **22**,^[77] and **23-31**^[80] were synthesized (Scheme 3) and purified by following previously reported procedures, and the spectral data are in accordance with the literature.^[10]

General procedure for the synthesis of *N*-[2-(3,4-dihydroxyphenyl)ethyl]-4-sulfamoylbenzamide (50b), 4-(3,4-dihydroisoquinolin-2(1*H*)-ylcarbonyl)benzenesulfonamides (70a-e), 4-(3,4-dihydroquinolin-1(2*H*)-ylcarbonyl)benzenesulfonamides (71c-e).

A mixture of 4-(aminosulfonyl)benzoic acid (**73**) (2 mmol, 402 mg), *N,N,N',N'*-tetramethyl-*O*-(1*H*-benzotriazol-1-yl)uranium hexafluorophosphate (HBTU) (2 mmol, 758 mg) in dimethylformamide (2 mL) was stirred at room temperature for 1 h. Then, a solution of the appropriate 1,2,3,4-tetrahydroisoquinoline (**72a,c,e**) or 1,2,3,4-tetrahydroquinoline (**74c,e**) (2 mmol) in TEA (2 mmol, 278 mL) was added dropwise. The reaction mixture was left overnight and then quenched with water (10 mL) and extracted with EtOAc (3 X 5 mL). The organic phase was dried with Na₂SO₄ and the solvent was removed *in vacuo*. The residue was purified by flash chromatography (DCM/MeOH 96:4), crystallized by treatment with diethyl ether and ethanol giving the desired final compounds **70a,c,e** and **71c-e** as white crystals. As starting reagent the benzamide **50a** was re-synthesized following a previously reported procedure and the spectral data were in accordance with literature.^[1] The methoxy derivatives **50a**, **70a,c** and **71c** (1 mmol) were dissolved in methylene chloride (DCM) (5 mL), treated with BBr₃ (1 M in DCM) (6 mmol, 6 mL) under nitrogen atmosphere and stirred overnight. After completion of the reaction, MeOH (7 mL) was carefully added at 0°C and the solvents removed under reduced pressure. The residue was dissolved in EtOAc (10 mL) and washed with H₂O (3 X 10 mL). The organic phase was dried (Na₂SO₄) and concentrated *in vacuo*. The crude products were crystallized from diethyl ether to give the desired hydroxy-derivatives **50b**, **70b,d** and **71d**.

***N*-[2-(3,4-Dihydroxyphenyl)ethyl]-4-sulfamoylbenzamide (50b).**

Yield 63%; mp 204-205 °C; *R*_f = 0.10; ¹H NMR (DMSO-*d*₆): δ 2.63 (t, *J* = 7.8, 2H, CH₂), 3.38 (t, 2H, CH₂), 6.43-6.62 (m, 3H, ArH), 7.44 (bs, 2H, NH₂), 7.85 (d, *J* = 8.5, 2H, ArH), 7.93 (d, *J* = 8.5, 2H, ArH), 8.62 (s, 1H, OH); 8.65 (bs, 1H, NH); 8.73 (s, 1H, OH); Anal. C₁₅H₁₆N₂O₅S.

4-[(6,7-Dimethoxy-3,4-dihydroisoquinolin-2(1*H*)-yl)carbonyl]benzenesulfonamide (70a).

Yield 16%; mp 210-212 °C; *R*_f = 0.50; ¹H NMR (DMSO-*d*₆): the compound exists as a pair of rotamers at room temperature. δ 2.75 (mc, 2H, major rotamer, CH₂), 2.80 (mc, 2H, minor rotamer, CH₂), 3.48 (mc, 2H, major rotamer, CH₂), 3.72 (s, 3H, OCH₃), 3.74 (s, 3H, OCH₃), 3.84 (mc, 2H, minor rotamer, CH₂), 4.45 (mc, 2H, minor rotamer, CH₂), 4.71 (mc, 2H, major rotamer, CH₂), 6.65 (s, 1H,

minor rotamer, ArH), 6.75 (s, 1H, major rotamer, ArH), 6.75 (s, 1H, minor rotamer, ArH), 6.88 (s, 1H, major rotamer, ArH), 7.50 (bs, 2H, NH₂), 7.65 (d, *J* = 6.1, 2H, ArH), 7.90 (d, *J* = 8.3, 2H, ArH); ¹³C NMR (DMSO) (ppm): δ 27.3, 28.4, 40.3, 43.9, 44.9, 48.8, 55.7, 55.7, 100.1, 109.7, 110.2, 112.1, 124.6, 126.0, 127.5, 127.7, 128.2, 139.6, 144.9, 147.6, 168.1, 168.5. Anal. C₁₈H₂₀N₂O₅S.

4-[(6-Methoxy-3,4-dihydroisoquinolin-2(1H)-yl)carbonyl]benzenesulfonamide (70c).

Yield 74%; mp 181-182 °C; *R*_f = 0.46; ¹H NMR (DMSO-*d*₆): the compound exists as a pair of rotamers at room temperature. δ 2.79 (mc, 2H, major rotamer, CH₂), 2.85 (mc, 2H, minor rotamer, CH₂), 3.46 (mc, 2H, major rotamer, CH₂), 3.70 (s, 3H, OCH₃), 3.81 (mc, 2H, minor rotamer, CH₂), 4.42 (mc, 2H, minor rotamer, CH₂), 4.69 (mc, 2H, major rotamer, CH₂), 6.74-7.18 (m, 3H, ArH), 7.47 (bs, 2H, NH₂), 7.63 (d, *J* = 7.7, 2H, ArH), 7.87 (d, *J* = 8.2, 2H, ArH); GC-MS (EI) *m/z* (%): 346 (M⁺, 0), 222 (4.3), 194 (0.5), 177 (35), 176 (18), 164 (0.5), 150 (15), 149 (100), 121 (6.2), 105 (7.8); Anal. C₁₇H₁₈N₂O₄S.

4-(3,4-Dihydroisoquinolin-2(1H)-ylcarbonyl)benzenesulfonamide (70e).

Yield 20%; mp 215-217 °C; *R*_f = 0.51; ¹H NMR (DMSO-*d*₆): the compound exists as a pair of rotamers at room temperature. δ 2.90 (mc, 2H, major rotamer, CH₂), 2.95 (mc, 2H, minor rotamer, CH₂), 3.57 (mc, 2H, major rotamer, CH₂), 3.92 (mc, 2H, minor rotamer, CH₂), 4.57 (mc, 2H, minor rotamer, CH₂), 4.84 (mc, 2H, major rotamer, CH₂), 7.07-7.32 (mc, 4H, ArH), 7.53 (bs, 2H, NH₂), 7.70 (d, *J* = 6.4, 2H, ArH), 7.95 (d, *J* = 8.3, 2H, ArH); ¹³C NMR (DMSO) (ppm): d 27.6, 28.7, 40.1, 44.1, 44.6, 48.8, 125.9, 127.3, 128.6, 132.8, 134.1, 135.4, 139.3, 144.8, 168.0, 168.4. Anal. C₁₆H₁₆N₂O₃S.

4-[(6-Methoxy-3,4-dihydroquinolin-1(2H)-yl)carbonyl]benzenesulfonamide (71c).

Yield 69%; mp 176-177 °C; *R*_f = 0.52; ¹H NMR (DMSO-*d*₆): δ 1.94 (t, 2H, CH₂), 2.80 (t, 2H, CH₂), 3.69 (s, 3H, OCH₃), 3.72 (s, 2H, CH₂), 6.81 (mc, 1H, ArH), 7.46 (bs, 2H, NH₂), 7.50 (d, *J* = 7.7, 2H, ArH), 7.76 (d, *J* = 8.2, 2H, ArH); Anal. C₁₇H₁₈N₂O₄S.

4-(3,4-Dihydroquinolin-1(2H)-ylcarbonyl)benzenesulfonamide (71e).

Yield 16%; mp 225-227 °C; *R*_f = 0.61; ¹H NMR (DMSO-*d*₆): δ 1.94 (q, 2H, CH₂), 2.81 (t, 2H, CH₂), 3.73 (t, 2H, CH₂), 6.87-7.21 (m, 4H, ArH), 7.44 (bs, 2H, NH₂), 7.50 (d, *J* = 8.3, 2H, ArH), 7.74 (d, *J* = 8.3, 2H, ArH); Anal. C₁₆H₁₆N₂O₃S.

4-[(6,7-Dihydroxy-3,4-dihydroisoquinolin-2(1H)-yl)carbonyl] benzenesulfonamide (70b).

Yield 60%; mp 240-243 °C; $R_f=0.52$; $^1\text{H NMR}$ (DMSO- d_6): the compound exists as a pair of rotamers at room temperature. δ 2.64 (mc, 2H, major rotamer, CH₂), 2.69 (mc, 2H, minor rotamer, CH₂), 3.43 (mc, 2H, major rotamer, CH₂), 3.79 (mc, 2H, minor rotamer, CH₂), 4.31 (mc, 2H, minor rotamer, CH₂), 4.59 (mc, 2H, major rotamer, CH₂), 6.52 (mc, 1H, ArH), 6.59 (mc, 1H, ArH), 7.49 (bs, 2H, NH₂), 7.63 (d, $J=7.7$, 2H, ArH), 7.89 (d, $J=8.3$, 2H, ArH), 8.83 (s, 2H, OH); Anal. C₁₆H₁₆N₂O₅S.

4-[(6-Hydroxy-3,4-dihydroisoquinolin-2(1H)-yl)carbonyl] benzenesulfonamide (70d).

Yield 92%; mp 222-223 °C; $R_f = 0.24$; $^1\text{H NMR}$ (DMSO- d_6): the compound exists as a pair of rotamers at room temperature. δ 2.74 (mc, 2H, major rotamer, CH₂), 2.80 (mc, 2H, minor rotamer, CH₂), 3.47 (mc, 2H, major rotamer, CH₂), 3.82 (mc, 2H, minor rotamer, CH₂), 4.40 (mc, 2H, minor rotamer, CH₂), 4.67 (mc, 2H, major rotamer, CH₂), 6.57-7.08 (m, 3H, ArH), 7.49 (bs, 2H, NH₂), 7.65 (d, $J=8.2$, 2H, ArH), 7.90 (d, $J=8.2$, 2H, ArH), 9.29 (s, 1H, OH); Anal. C₁₆H₁₆N₂O₄S.

4-[(6-Hydroxy-3,4-dihydroquinolin-1(2H)-yl)carbonyl]benzenesulfonamide (71d).

Yield 44%; mp 229-230 °C; $R_f = 0.26$; $^1\text{H NMR}$ (DMSO- d_6): δ 1.92 (t, 2H, CH₂), 2.73 (t, 2H, CH₂), 3.69 (d, 2H, CH₂), 6.59 (m, 3H, ArH), 7.45 (bs, 2H, NH₂), 7.46 (mc, 2H, ArH), 7.75 (d, 2H, ArH), 9.30 (s, 1H, OH); 332 (M⁺, 0), 222 (3.5), 194 (0.5), 177 (32), 176 (16), 164 (0.5), 150 (14), 149 (100), 121 (5.8), 105 (7.7); Anal. C₁₆H₁₆N₂O₄S.

General procedure for the synthesis of (R,S)-1-aryl-1,2,3,4-tetrahydroisoquinolines (91a-c, 92a, 93a, 94a, 95a)

Following a previously reported procedure, the appropriate benzaldehyde (**81-85**) (1.2 mmol) and suitable phenylethylamine (**80a-c**) (1.0 mmol,) were placed in a cylindrical quartz tube (\varnothing 2 cm), then stirred and irradiated in a microwave oven at 150W for 10 min at 90 °C. After cooling to room temperature, trifluoroacetic acid (3,3 ml) was added to crude intermediates **86a-c**, **87a**, **88a**, **89a**, **90a** obtained in the previous step and the mixture was irradiated at 150W for 10 min at 90 °C. The reaction was basified (pH \approx 9) with sodium hydroxide, 10 N. The mixture was quenched by addition of H₂O (5 mL) and extracted with EtOAc (3 x 5 mL). The organic layer was dried over Na₂SO₄ and concentrated until dryness under reduced pressure. The crude product was collected by filtration and purified by crystallization with Et₂O and EtOH to afford compounds **91a-c**, **92a**, **93a**, **94a**, **95a**.

Analytical data for compounds **91a-c**, **92a**, **93a**, **94a**, **95a** are in accordance with literature.^[78, 79, 112]

1-Phenyl-6-propoxy-1,2,3-tetrahydroisoquinoline (91c).

Yield 58%; mp 138-140 °C; ¹HNMR (DMSO-*d*₆): δ 0.93 (t, 3H, CH₃, *J* = 7.0, *J* = 7.6), 1.66 (m, 2H, CH₂), 3.64-3.06 (m, 4H, CH₂), 3.84 (t, 2H, CH₂, *J* = 6.4, *J* = 6.5), 4.88 (s, 1H, CH), 6.47 (d, *J* = 8.2, 1H, ArH), 6.55 (d, *J* = 8.2, 1H, ArH), 6.64 (s, 1H, ArH), 7.21-7.28 (m, 5H, ArH); Anal. Calcd for C₁₈H₂₁NO: C 80.86% H 7.92% N 5.24%; Found: C 80.96; H 7.83; N 5.16.

General procedure for the synthesis of 6/7-alkoxy-substituted (*R,S*)-4-(1-aryl-3,4-dihydro-1*H*-isoquinoline-2-carbonyl)benzenesulfonamides (75a-e, 76a-b, 77a-b, 78a-b, 79a-b)

To obtain the compounds **75a-c**, **76a**, **77a**, **78a**, **79a** and **75d,e**, **76b**, **77b**, **78b**, **79b** we used the synthetic procedure employed for the compounds (**50b**), (**70a-e**) and (**71c-e**) with slight modifications.

4-(6,7-Dimethoxy-1-phenyl-1,2,3,4-tetrahydroisoquinoline-2-carbonyl)benzenesulfonamide (75a)

Yield 66%; mp 248-250 °C; *R*_f = 0.41 ¹HNMR (DMSO-*d*₆): δ 2.63-3.25 (m, 4H, CH₂), 3.63 (s, 3H, OCH₃), 3.74 (s, 3H, OCH₃), 6.72 (s, 1H, CH), 6.78 (s, 1H, ArH), 6.80 (s, 1H, ArH), 7.22-7.34 (m, 5H, ArH), 7.46 (s, 2H, NH₂), 7.55 (d, *J* = 8.2, 2H, ArH), 7.85 (d, *J* = 8.2, 2H, ArH); Anal. Calcd for C₂₄H₂₄N₂O₅S: C 63.70%, H 5.35%, N 6.19%; Found: C 63.52, H 5.21, N 6.02.

4-(6-Methoxy-1-phenyl-1,2,3,4-tetrahydroisoquinolin-2-carbonyl)benzenesulfonamide (75b)

Yield 31%; mp 239-241 °C; *R*_f = 0.36; ¹HNMR (DMSO-*d*₆): δ 2.71-3.38 (m, 4H, CH₂), 3.74 (s, 3H, OCH₃), 6.76 (s, 1H, CH), 6.81 (m, 2H, ArH), 7.05 (m, 1H, ArH), 7.24-7.33 (m, 5H, ArH), 7.46 (s, 2H, NH₂), 7.58 (d, *J* = 8.2, 2H, ArH); 7.87 (d, *J* = 8.2, 2H, ArH); Anal. Calcd for (C₂₃H₂₂N₂O₄S): C 65.38%, H 5.25%, N 6.63%; Found: C 65.01, H 5.06, N 6.23.

4-(1-Phenyl-6-propoxy-1,2,3,4-tetrahydroisoquinoline-2-carbonyl)benzenesulfonamide (75c)

Yield 61%; m. 231-233 °C; *R*_f = 0.41; ¹HNMR (DMSO-*d*₆) δ 0.96 (t, 3H, *J* = 7.0, CH₃), 1.70-1.75 (m, 2H, CH₂), 2.69-2.94 (m, 4H, CH₂), 3.91 (t, 2H, *J* = 6.5, OCH₂), 6.76 (s, 1H, CH), 6.81 (m, 1H, ArH), 7.04-7.07 (m, 2H, ArH), 7.25-7.34 (m, 5H, ArH), 7.47 (s, 1H, NH₂), 7.59 (d, *J* = 8.0, 2H, ArH), 7.86 7.88 (d, *J* = 8.0, 2H, CH₂); Anal. Calcd for C₂₅H₂₆N₂O₄S: C 66.64%, H 5.82%, N 6.22%; Found: C 66.60, H 5.80, N 6.20.

6,7-Dimethoxy-4-[1-(4-fluorophenyl)-1,2,3,4-tetrahydro-1H-isoquinoline-2-carbonyl]benzenesulfonamide (76a)

Yield 41%; mp 220-222 °C; $R_f = 0.47$; $^1\text{H-NMR}$ (DMSO- d_6) δ 2.63-3.40 (m, 4H, CH₂), 3.63 (s, 3H, OCH₃), 3.75 (s, 3H, OCH₃), 6.72 (s, 1H, CH), 6.78 (s, 1H, ArH), 6.81 (s, 1H, ArH), 7.14-7.27 (m, 4H, ArH), 7.46 (bs, 2H, NH₂), 7.57 (d, $J = 8.6$, 2H, ArH), 7.87 (d, $J = 8.6$, 2H, ArH); Anal. Calcd for C₂₄H₂₃FN₂O₅S: C 61.27%, H 4.93%, N 5.95%; Found: C 61.37, H 4.80, N 5.80.

4-[1-(4-Chlorophenyl)-6,7-dimethoxy-1,2,3,4-tetrahydro-1H-isoquinoline-2-carbonyl]benzenesulfonamide (77a)

Yield 50%; mp 204-205 °C; $R_f = 0.40$; $^1\text{H-NMR}$ (DMSO- d_6) δ 2.64-3.23 (m, 4H, CH₂), 3.64 (s, 3H, OCH₃), 3.75 (s, 3H, OCH₃), 6.73 (s, 1H, CH), 6.77 (s, 1H, ArH), 6.81 (s, 1H, ArH), 7.28 (d, $J = 8.2$, 2H, ArH), 7.45 (bs, 2H, NH₂), 7.57 (d, $J = 8.2$, 2H, ArH), 7.87 (d, $J = 8.2$, 2H, ArH); Anal. Calcd for C₂₄H₂₃ClN₂O₅S: C 59.20%, H 4.76%, N 5.75%; Found: C 59.30, H 4.66, N 5.85.

4-[1-(4-Bromophenyl)-6,7-dimethoxy-1,2,3,4-tetrahydro-1H-isoquinoline-2-carbonyl]benzenesulfonamide (78a)

Yield 51%; mp 191-192 °C; $R_f = 0.41$; $^1\text{H-NMR}$ (DMSO- d_6) δ 2.63-3.38 (m, 4H, CH₂), 3.64 (s, 3H, OCH₃), 3.75 (s, 3H, OCH₃), 6.74 (m, 2H, ArH), 6.81 (s, 1H, CH), 7.19 (d, $J = 8.2$, 2H, ArH), 7.46 (bs, 2H, NH₂), 7.53-7.58 (m, 4H, ArH), 7.88 (d, $J = 7.6$, 2H, ArH); Anal. Calcd for C₂₄H₂₃BrN₂O₅S: C 54.24%, H 4.36%, N 5.27%; Found: C 54.34, H 4.46, N 5.20.

4-[6,7-dimethoxy-1-(3-nitrophenyl)-1,2,3,4-tetrahydro-1H-isoquinoline-2-carbonyl]benzenesulfonamide (79a)

Yield: 30%; mp 209-211 °C; $R_f = 0.47$; $^1\text{H-NMR}$ (DMSO- d_6): δ 2.73 (m, 1H, CH₂), 2.87 (m, 1H, CH₂), 3.24 (m, 2H, CH₂), 3.64 (s, 3H, OCH₃), 3.76 (s, 3H, OCH₃), 6.82 (s, 1H, CH), 6.85 (s, 1H, ArH), 6.88 (s, 1H, ArH), 7.47 (s, 2H, SO₂NH₂), 7.60 (d, $J = 7.6$, 2H, ArH), 7.68-7.70 (m, 2H, ArH), 7.88 (d, $J = 8.2$, 2H, ArH), 8.07 (s, 1H, ArH), 8.15-8.17 (m, 2H, ArH); Anal. Calcd for C₂₄H₂₃N₃O₇S: C 57.94%, H 4.66%, N 8.45%; Found: C 57.98, H 4.70, N 8.49.

4-(6,7-Dihydroxy-1-phenyl-1,2,3,4-tetrahydroisoquinoline-2-carbonyl)benzenesulfonamide (75d)

Yield 83%; mp 239-240 °C; $R_f = 0.10$; $^1\text{H-NMR}$ (DMSO- d_6): δ 2.71-3.28 (m, 4H, CH₂), 6.41 (s, 1H, CH), 6.57 (s, 1H, ArH), 6.60 (s, 1H, ArH), 7.24-7.33 (m, 5H, ArH), 7.46 (s, 2H, NH₂), 7.54 (d, $J = 8.2$, 2H, ArH), 7.85 (d, $J = 8.2$, 2H, ArH), 8.86 (s, 1H, OH), 8.95 (s, 1H, OH); Anal. Calcd for C₂₂H₂₀N₂O₅S: C 62.25%, H 4.75%, N 6.60%; Found: C 62.01, H 4.45, N 6.52.

4-(6-Hydroxy-1-phenyl-1,2,3,4-tetrahydroisoquinolin-2-carbonyl)benzenesulfonamide (75e)

Yield 86%; mp 282-284 °C; $R_f = 0.23$; $^1\text{H NMR}$ (DMSO- d_6): δ 2.62-3.39 (m, 4H, CH₂), 6.62 (s, 1H, ArH), 6.72 (s, 1H, CH), 6.93 (m, 1H, ArH), 7.22 (d, 1H, ArH), 7.25-7.34 (m, 5H, ArH), 7.46 (s, 2H, NH₂), 7.58 (d, $J = 8.2$, 2H, ArH), 7.87 (d, $J = 8.2$, 2H, ArH), 9.42 (bs, 1H, OH); Anal. Calcd for C₂₂H₂₀N₂O₄S: C 64.69%, H 4.94%, N 6.86%; Found: C 64.49, H 4.65, N 6.75.

6,7-Dihydroxy-4-[1-(4-fluorophenyl)-1,2,3,4-tetrahydro-1H-isoquinoline-2-carbonyl]benzenesulfonamide (76b)

Yield 31%; mp 240-243 °C; $R_f = 0.11$; $^1\text{H NMR}$ (DMSO- d_6) δ 2.57-3.23 (m, 4H, CH₂), 3.64 (s, 3H, OCH₃), 3.76 (s, 3H, OCH₃), 6.82 (s, 1H, CH), 6.85 (s, 1H, ArH), 6.88 (s, 1H, ArH), 7.47 (bs, 2H, NH₂), 7.58-7.70 (m, 4H, ArH), 7.88 (d, $J = 8.2$, 2H, ArH), 8.07 (s, 1H, ArH); 8.16 (m, 1H, ArH); Anal. Calcd for C₂₄H₂₃N₃O₇S: C 57.94%, H 4.66%, N 8.45%; Found: C 57.84, H 4.76, N 8.55.

4-[1-(4-Chlorophenyl)-6,7-dihydroxy-1,2,3,4-tetrahydro-1H-isoquinoline-2-carbonyl]benzenesulfonamide (77b)

Yield 67%; mp 185-186 °C; $R_f = 0.12$; $^1\text{H NMR}$ (DMSO- d_6) δ 2.42-3.23 (m, 4H, CH₂), 6.42 (s, 1H, CH), 6.57-6.58 (m, 2H, ArH), 7.27 (d, $J = 8.2$, 2H, ArH), 7.40 (d, $J = 8.2$, 2H, ArH), 7.46 (bs, 2H, NH₂) 7.55 (d, $J = 8.2$, 2H, ArH), 7.85 (d, $J = 8.2$, 2H, ArH), 8.88 (bs, 1H, OH), 8.98 (bs, 1H, OH); Anal. Calcd for C₂₂H₁₉ClN₂O₅S: C 57.58%, H 4.17%, N 6.10%; Found: C 57.68, H 4.10, N 6.20.

4-[1-(4-Bromophenyl)-6,7-dihydroxy-1,2,3,4-tetrahydro-1H-isoquinoline-2-carbonyl]benzenesulfonamide (78b)

Yield 42%; mp 189-191 °C; $R_f = 0.13$; $^1\text{H NMR}$ (DMSO- d_6) δ 2.07 (m, 4H, CH₂), 6.41 (s, 1H, CH), 6.57 (s, 2H, ArH), 7.20 (d, $J = 8.3$, 2H, ArH), 7.46 (bs, 2H, NH₂), 7.52-7.56 (m, 4H, ArH), 7.85 (d, $J = 8.3$, 2H, ArH), 9.00 (bs, 2H, OH); Anal. Calcd for C₂₂H₁₉BrN₂O₅S: C 52.49%, H 3.80%, N 5.57%; Found: C 52.52, H 3.84, N 5.60.

4-[6,7-dihydroxy-1-(3-nitrophenyl)-1,2,3,4-tetrahydro-1H-isoquinoline-2-carbonyl]benzenesulfonamide (79b)

Yield: 40%; mp 232-234 °C; $R_f = 0.33$; $^1\text{H NMR}$ (DMSO- d_6): δ 2.56-2.87 (m, 3H, CH₂CH₂), 3.15 (m, 1H, CH₂), 6.48 (s, 1H, CH), 6.61 (s, 1H, ArH), 6.72 (s, 1H, ArH), 7.46 (bs, 2H, NH₂), 7.58 (d, $J = 7.6$, 2H, ArH), 7.68-7.74 (m, 2H, ArH), 7.87 (d, $J = 8.2$, 2H, ArH), 8.06 (s, 1H, ArH), 8.16 (d, 2H, ArH), 8.97 (bs, 2H OH); Anal. Calcd for C₂₂H₁₉N₃O₇S: C 56.29%, H 4.08%, N 8.95%; Found: C 56.25, H 4.04, N 8.91.

3.2 CA inhibition assay

An Applied Photophysics stopped-flow instrument has been used for assaying the CA catalysed CO₂ hydration activity. Phenol red (at a concentration of 0.2 mM) has been used as indicator, working at the absorbance maximum of 557 nm, with 10e20 mM Hepes (pH 7.5) or Tris (pH 8.3) as buffers, and 20 mM Na₂SO₄ or 20 mM NaClO₄ (for maintaining constant the ionic strength), following the initial rates of the CA-catalyzed CO₂ hydration reaction for a period of 10-100 s. The CO₂ concentrations ranged from 1.7 to 17 mM for the determination of the kinetic parameters and inhibition constants. For each inhibitor at least six traces of the initial 5-10% of the reaction have been used for determining the initial velocity. The uncatalyzed rates were determined in the same manner and subtracted from the total observed rates. Stock solutions of inhibitor (10 mM) were prepared in distilled-deionized water and dilutions up to 0.01 nM were done thereafter with distilled-deionized water. Inhibitor and enzyme solutions were preincubated together for 15 min at room temperature prior to assay, in order to allow for the formation of the E-I complex. The inhibition constants were obtained by non-linear least-squares methods using PRISM 3, as reported earlier, and represent the mean from at least three different determinations. CA isoforms were recombinant ones obtained as reported earlier by this group.^[113-116]

3.3 Anticonvulsant activity in DBA/2 mice

All experiments were performed with DBA/2 mice, which are genetically susceptible to sound-induced seizures.^[117] DBA/2 mice (8–12 g; 22–25 days old) were purchased from Harlan Italy (Corezzano, Italy). Groups of 10 mice of either sex were exposed to auditory stimulation for 30 min following administration of either the vehicle or each dose of reference compound TPM (**7**) or the racemic mixture of tested compounds **13-31**. The compound was administered intraperitoneally

(0.1 mL per 10g mouse body weight) as a freshly prepared solution in 50% dimethyl sulfoxide (DMSO) and 50% sterile saline (0.9% NaCl). Individual mice were placed under a hemispheric Perspex dome (diameter 58 cm), and 60 s was allowed for habituation and assessment of locomotor activity. Auditory stimulation (12–16 kHz, 109 dB) was applied for 60 s or until tonic extension occurred and induced a sequential seizure response in control DBA/2 mice, consisting of an early wild running phase, followed by generalized myoclonus and tonic flexion and extension sometimes followed by respiratory arrest. The control and drug-treated mice were scored for latency to and incidence of the different phases of the seizures. Procedures involving animals and their care were conducted in conformity with international and national law and policies (EU Directive 2010/63/EU for animal experiments and the Basel declaration including the 3R concept). The experimental protocols and procedures described in this paper were approved by the local ethical committee of the University of Catanzaro. All efforts were made to minimize animal suffering and to minimize the number of animals used. All studies involving animals are reported in accordance with the arrive guidelines for reporting experiments involving animals. Statistical comparisons between groups of control and drug-treated animals were made by using Fisher's exact probability test (incidence of the seizure phases). The ED₅₀ values of each phase of audiogenic seizures was determined for each dose of the compound administered, and dose–response curves were fitted by using a computer program by Litchfield and Wilcoxon's method.

[118]

3.4 Enantiomeric resolution

Enantioselective HPLC analyses were performed by using stainless-steel Chiralpak IA (250 mm x 4.6 mm I.D. and 250 mm x 10 mm I.D.) and Chiralpak AS-H (250 mm x 4.6 mm I.D. and 250 mm x 10 mm I.D.) (Daicel, Chemical Industries, Tokyo, Japan) columns. HPLC-grade solvents were used as supplied by Aldrich (Milan, Italy). The HPLC apparatus consisted of a Perkin Elmer (Norwalk, CT, USA) 200 lc pump equipped with a Rheodyne (Cotati, CA, USA) injector, a 1000- μ l sample loop, a

HPLC Perkin Elmer oven and a Perkin Elmer 290 detector. The signal was acquired and processed by Clarity software (DataApex, Prague, The Czech Republic). HPLC resolutions were carried out by using polysaccharide-based chiral stationary phases (CSPs). The CD spectra of the enantiomers isolated at semipreparative scale, dissolved in dichloromethane (concentration about 0.2 mg/ml) in a quartz cell (0.1 cm-path length) at 25 °C, were measured by using a Jasco (Jasco, Ishikawa-cho, Hachioji City, Tokyo, Japan) Model J-700 spectropolarimeter in the 400-200 nm spectral range. The spectra are average computed over three instrumental scans and the intensities are presented in terms of terms of ellipticity values (mdeg).

3.5 X-ray studies

3.5.1. Co-crystal structures of inhibitors 70a, 70b, 70e, 71c and 71e in complex with hCA II

Co-crystals of human carbonic anhydrase II (purchased from Sigma, catalog No. C6165) with compounds **70a**, **70b**, **70e**, **71c** and **71e** are obtained by vapor-diffusion hanging drop method at 18 °C. Complexes were prepared by adding 2 or 3.5-fold molar excess of inhibitor (dissolved in pure DMSO) to 12-13 mg x mL⁻¹ protein solution in water. 2 mL of complex solution were mixed with 2 mL of precipitant solution containing 1.6 M sodium citrate, 50 mM Tris HCl pH 7.8 and equilibrated over a 1 mL reservoir of precipitant solution. The final DMSO concentration did not exceed 1.5% (v/v). Crystals with dimensions of 0.5 mm x 0.3 mm x 0.2 mm grew within 2 weeks. Before data collection, the crystals were soaked for 5-10s in reservoir solution supplemented with 25% (w/v) sucrose and stored in liquid N₂. Diffraction data for crystallized complexes CAII-**70a,b,e** and **71e** were collected at 100 K at beamline MX14.2 of BESSY, Berlin, Germany ^[119] and these diffraction data were integrated and reduced using XDS program ^[120] and its graphical interface XDSAPP. ^[121] Diffraction data of crystallized complex CAII-**71c** were collected to 2.0 Å resolution at

120 K using an in house diffractometer (Nonius FR 591) connected to 345 mm Mar-Research image plate detector. Diffraction data were integrated and reduced using MOSFLM^[122] and scaled using SCALA^[123] from the CCP4 suite of programs.^[124] Crystal parameters and data collection statistics for both complexes are summarized in Table 7. The structures of hCA II complexes were solved using the difference Fourier technique, using hCA II structure (Protein Data Bank entry 3PO6)^[107] as the initial model. Initial rigid-body refinement and subsequent restrained refinement for both hCA II complexes were performed using the program REFMAC5^[124] with isotropic ADPs. The structures were refined with one inhibitor molecule in the enzyme active site with occupancy 1, however for the compound **71e**, the model of inhibitor molecule was build up in three partially different alternative conformations. Atomic coordinates and geometric library for the inhibitor were generated using the PRODRG server.^[125] The Coot program^[126] was used for inhibitor fitting, model rebuilding, and addition of water molecules. All structures were first refined with isotropic ADPs. After addition of solvent atoms, metal ions (zinc), building inhibitor molecules in the active site, and several alternate conformations for a number of residues, anisotropic ADPs were refined for nearly all atoms for the complexes CAII-**70b,e** and **71e** (with the exception of spatially overlapping atoms in segments with alternate conformations; also oxygen atoms of water molecules with unrealistic ratio of ellipsoid axes were refined with isotropic ADPs) including the inhibitor molecules. For the complexes CAII-4a and 5c the refinement was finished using isotropic ADPs. The quality of the crystallographic model was assessed with MolProbity.^[127] The final refinement statistics are summarized in Table 5. All figures showing structural representations were prepared using PYMOL Molecular Graphics System (Version 1.3r1 Schrodinger, LLC. 2010).

3.5.2. Co-crystal structures of inhibitors (R)-75d and (S)-75d in complex with hCA II

Crystals of hCA II adducts with inhibitors **(R)-75d** and **(S)-75d** were prepared by the soaking technique. In particular, hCA II native crystals were grown at room temperature using the vapor

diffusion hanging drop method. Equal volumes of protein (10 mg/ml in 0.02 M Tris-HCl pH 8.0) and precipitant solutions (1.3 M sodium citrate and 0.1 M Tris-HCl, pH 8.5) were mixed and equilibrated against 1 mL reservoir containing the same precipitant solution. A few native enzyme crystals were then transferred in a 3 μ l drop of freshly prepared precipitant solution, containing 10% (v/v) glycerol and 20 mM inhibitor. These crystals were kept in the soaking solution for about 12 hours. Crystals were frozen in a gaseous nitrogen stream prior to the diffraction experiment. A complete X-ray data set was collected at 100 K by a copper rotating anode generator developed by Rigaku and equipped with a Rigaku Saturn CCD detector. Diffraction data up to 1.70 Å resolution for hCA II/**(R)**-75d and 1.75 Å resolution for hCA II/**(S)**-75d were processed and scaled using program HKL2000 (HKL Research).^[128] Data collection statistics are reported in Table 8. The initial phases of hCA II/inhibitor structures were calculated using the atomic coordinates of the native enzyme with waters removed (PDB entry 1CA2).^[37] Clear electron density for all compounds was observed in the difference map after a single round of refinement. A model for **(R)**-75d and **(S)**-75d was then built and introduced into the atomic coordinates set for further refinement, which proceeded to convergence with alternating cycles of water addition, manual rebuilding with the O program^[129], and energy minimization and B-factor refinement with the CNS program^[130]. Topology files for all compounds were obtained using the PRODRG server.^[131] The final crystallographic R-factor and R-free values were 0.184 and 0.218 for hCA II/**(R)**-75d and 0.184 and 0.218 for hCA II/**(S)**-75d. Refinement statistics are summarized in Table 3. Coordinates and structure factors have been deposited in the Protein Data Bank (accession codes to be released).

3.6 Molecular docking

The crystal structures of hCA VII in complex with the inhibitor acetazolamide was retrieved from the RCSB Protein Data Bank (PDB code 3ML5).^[132] The ligand and water molecules were discarded, and the hydrogen atoms were added to protein with Discovery Studio 2.5.5.^[133] The structures of the ligands were constructed using Discovery Studio 2.5.5 and energy minimized using the Smart Minimizer protocol (1000 steps) which combines the Steepest Descent and the Conjugate Gradient

methods. The ligands minimized in this way were docked in their corresponding proteins by means of Gold Suite 5.0.1.^[134] The region of interest used by Gold program was defined in order to contain the residues within 10 Å from the original position of the ligand in the X-ray structure. A scaffold constraint (penalty = 10.0) was used to restrict the solutions in which the sulfonamide moiety was able to coordinate the metal within the catalytic binding site. GoldScore was chosen as fitness function and the standard default setting were used in all calculations and the ligands were submitted to 100 genetic algorithm runs. The “allow early termination” command was deactivated. Results differing by less than 0.75 Å in ligand-all atom RMSD, were clustered together. The best GOLD-calculated conformation was used both for analysis and representation.

References

1. Gitto, R., et al., *Identification of potent and selective human carbonic anhydrase VII (hCA VII) inhibitors*. ChemMedChem, 2010. **5**(6): p. 823-6.
2. Thiry, A., et al., *Recent developments of carbonic anhydrase inhibitors as potential anticancer drugs*. J Med Chem, 2008. **51**(11): p. 3051-6.
3. Mincione, F., A. Scozzafava, and C.T. Supuran, *The development of topically acting carbonic anhydrase inhibitors as antiglaucoma agents*. Curr Pharm Des, 2008. **14**(7): p. 649-54.
4. De Simone, G. and C.T. Supuran, *Antiobesity carbonic anhydrase inhibitors*. Curr Top Med Chem, 2007. **7**(9): p. 879-84.
5. Thiry, A., et al., *Carbonic anhydrase inhibitors as anticonvulsant agents*. Curr Top Med Chem, 2007. **7**(9): p. 855-64.
6. Truppo, E., et al., *Carbonic anhydrase VII is S-glutathionylated without loss of catalytic activity and affinity for sulfonamide inhibitors*. Bioorg Med Chem Lett, 2012. **22**(4): p. 1560-4.
7. Booterabi, F., et al., *Analysis of a shortened form of human carbonic anhydrase VII expressed in vitro compared to the full-length enzyme*. Biochimie, 2010. **92**(8): p. 1072-80.
8. Thiry, A., et al., *Exploration of the binding mode of indanesulfonamides as selective inhibitors of human carbonic anhydrase type VII by targeting Lys 91*. ChemMedChem, 2007. **2**(9): p. 1273-80.
9. Asiedu, M., et al., *Acetazolamide and midazolam act synergistically to inhibit neuropathic pain*. Pain, 2010. **148**(2): p. 302-8.
10. Bruno, E., et al., *In Vivo Evaluation of Selective Carbonic Anhydrase Inhibitors as Potential Anticonvulsant Agents*. ChemMedChem, 2016. **11**(16): p. 1812-8.
11. Winum, J.Y. and C.T. Supuran, *Recent advances in the discovery of zinc-binding motifs for the development of carbonic anhydrase inhibitors*. J Enzyme Inhib Med Chem, 2015. **30**(2): p. 321-4.
12. Holm, R.H., P. Kennepohl, and E.I. Solomon, *Structural and Functional Aspects of Metal Sites in Biology*. Chem Rev, 1996. **96**(7): p. 2239-2314.
13. Ma, X., H.H. Ezzeldin, and R.B. Diasio, *Histone deacetylase inhibitors: current status and overview of recent clinical trials*. Drugs, 2009. **69**(14): p. 1911-34.
14. Fisher, J.F. and S. Mobashery, *Recent advances in MMP inhibitor design*. Cancer Metastasis Rev, 2006. **25**(1): p. 115-36.
15. Dive, V., et al., *Inhibition of zinc metallopeptidases in cardiovascular disease--from unity to trinity, or duality?* Curr Pharm Des, 2009. **15**(31): p. 3606-21.
16. Masereel, B., et al., *Carbonic anhydrase inhibitors: anticonvulsant sulfonamides incorporating valproyl and other lipophilic moieties*. J Med Chem, 2002. **45**(2): p. 312-20.
17. Supuran, C.T., *Carbonic anhydrase inhibitors as emerging drugs for the treatment of obesity*. Expert Opin Emerg Drugs, 2012. **17**(1): p. 11-5.
18. Day, J.A. and S.M. Cohen, *Investigating the selectivity of metalloenzyme inhibitors*. J Med Chem, 2013. **56**(20): p. 7997-8007.
19. Ondetti, M.A.C., D. W., *Azetidine-2-carboxylic acid derivatives*. 1977.
20. Ferro, S., et al., *Chemical exploration of 4-(4-fluorobenzyl)piperidine fragment for the development of new tyrosinase inhibitors*. Eur J Med Chem, 2016. **125**: p. 992-1001.
21. Meldrum, N.U. and F.J. Roughton, *Carbonic anhydrase. Its preparation and properties*. J Physiol, 1933. **80**(2): p. 113-42.
22. Supuran, C.T., *Structure and function of carbonic anhydrases*. Biochem J, 2016. **473**(14): p. 2023-32.
23. Supuran, C.T., *Carbonic anhydrases: novel therapeutic applications for inhibitors and activators*. Nat Rev Drug Discov, 2008. **7**(2): p. 168-81.
24. Smith, K.S., et al., *Carbonic anhydrase is an ancient enzyme widespread in prokaryotes*. Proc Natl Acad Sci U S A, 1999. **96**(26): p. 15184-9.
25. Xu, Y., et al., *Structure and metal exchange in the cadmium carbonic anhydrase of marine diatoms*. Nature, 2008. **452**(7183): p. 56-61.
26. Capasso, C. and C.T. Supuran, *Bacterial, fungal and protozoan carbonic anhydrases as drug targets*. Expert Opin Ther Targets, 2015. **19**(12): p. 1689-704.

27. Supuran, C.T., *Bacterial carbonic anhydrases as drug targets: toward novel antibiotics?* Front Pharmacol, 2011. **2**: p. 34.
28. Capasso, C. and C.T. Supuran, *An overview of the alpha-, beta- and gamma-carbonic anhydrases from Bacteria: can bacterial carbonic anhydrases shed new light on evolution of bacteria?* J Enzyme Inhib Med Chem, 2015. **30**(2): p. 325-32.
29. Neri, D. and C.T. Supuran, *Interfering with pH regulation in tumours as a therapeutic strategy.* Nat Rev Drug Discov, 2011. **10**(10): p. 767-77.
30. Del Prete, S., et al., *Biochemical characterization of the delta-carbonic anhydrase from the marine diatom Thalassiosira weissflogii, TweCA.* J Enzyme Inhib Med Chem, 2014. **29**(6): p. 906-11.
31. Del Prete, S., et al., *Discovery of a new family of carbonic anhydrases in the malaria pathogen Plasmodium falciparum--the eta-carbonic anhydrases.* Bioorg Med Chem Lett, 2014. **24**(18): p. 4389-96.
32. Tripp, B.C., et al., *A role for iron in an ancient carbonic anhydrase.* J Biol Chem, 2004. **279**(8): p. 6683-7.
33. Capasso, C. and C.T. Supuran, *An Overview of the Selectivity and Efficiency of the Bacterial Carbonic Anhydrase Inhibitors.* Curr Med Chem, 2015. **22**(18): p. 2130-9.
34. Supuran, C.T., *Structure-based drug discovery of carbonic anhydrase inhibitors.* J Enzyme Inhib Med Chem, 2012. **27**(6): p. 759-72.
35. De Simone, G., et al., *The zinc coordination pattern in the eta-carbonic anhydrase from Plasmodium falciparum is different from all other carbonic anhydrase genetic families.* Bioorg Med Chem Lett, 2015. **25**(7): p. 1385-9.
36. Domsic, J.F., et al., *Entrapment of carbon dioxide in the active site of carbonic anhydrase II.* J Biol Chem, 2008. **283**(45): p. 30766-71.
37. Eriksson, A.E., T.A. Jones, and A. Liljas, *Refined structure of human carbonic anhydrase II at 2.0 Å resolution.* Proteins, 1988. **4**(4): p. 274-82.
38. Aggarwal, M., et al., *Structural annotation of human carbonic anhydrases.* J Enzyme Inhib Med Chem, 2013. **28**(2): p. 267-77.
39. Alterio, V., et al., *Multiple binding modes of inhibitors to carbonic anhydrases: how to design specific drugs targeting 15 different isoforms?* Chem Rev, 2012. **112**(8): p. 4421-68.
40. Lindskog, S., *Structure and mechanism of carbonic anhydrase.* Pharmacol Ther, 1997. **74**(1): p. 1-20.
41. Briganti, F., et al., *Carbonic anhydrase activators: X-ray crystallographic and spectroscopic investigations for the interaction of isozymes I and II with histamine.* Biochemistry, 1997. **36**(34): p. 10384-92.
42. Supuran, C.T. and A. Scozzafava, *Carbonic anhydrases as targets for medicinal chemistry.* Bioorg Med Chem, 2007. **15**(13): p. 4336-50.
43. Nair, S.K. and D.W. Christianson, *Structural properties of human carbonic anhydrase II at pH 9.5.* Biochem Biophys Res Commun, 1991. **181**(2): p. 579-84.
44. Sjoblom, B., M. Polentarutti, and K. Djinovic-Carugo, *Structural study of X-ray induced activation of carbonic anhydrase.* Proc Natl Acad Sci U S A, 2009. **106**(26): p. 10609-13.
45. Avvaru, B.S., et al., *A short, strong hydrogen bond in the active site of human carbonic anhydrase II.* Biochemistry, 2010. **49**(2): p. 249-51.
46. Parkkila, S., *An overview of the distribution and function of carbonic anhydrase in mammals.* EXS, 2000(90): p. 79-93.
47. Supuran, C.T. and A. Scozzafava, *Activation of carbonic anhydrase isozymes.* EXS, 2000(90): p. 197-219.
48. Supuran, C.T., A. Scozzafava, and A. Casini, *Carbonic anhydrase inhibitors.* Med Res Rev, 2003. **23**(2): p. 146-89.
49. Kalinin, S., C.T. Supuran, and M. Krasavin, *Multicomponent chemistry in the synthesis of carbonic anhydrase inhibitors.* J Enzyme Inhib Med Chem, 2016: p. 1-15.
50. Stams, T. and D.W. Christianson, *X-ray crystallographic studies of mammalian carbonic anhydrase isozymes.* EXS, 2000(90): p. 159-74.
51. Krebs, H.A., *Inhibition of carbonic anhydrase by sulphonamides.* Biochem J, 1948. **43**(4): p. 525-8.
52. Supuran, C.T., *Carbonic anhydrase inhibitors.* Bioorg Med Chem Lett, 2010. **20**(12): p. 3467-74.

53. Thiry, A., et al., *Targeting tumor-associated carbonic anhydrase IX in cancer therapy*. Trends Pharmacol Sci, 2006. **27**(11): p. 566-73.
54. Pastorekova, S., et al., *Carbonic anhydrases: current state of the art, therapeutic applications and future prospects*. J Enzyme Inhib Med Chem, 2004. **19**(3): p. 199-229.
55. Supuran, C.T. and A. Scozzafava, *Carbonic anhydrase inhibitors: aromatic sulfonamides and disulfonamides act as efficient tumor growth inhibitors*. J Enzyme Inhib, 2000. **15**(6): p. 597-610.
56. Scozzafava, A., et al., *Carbonic anhydrase inhibitors: perfluoroalkyl/aryl-substituted derivatives of aromatic/heterocyclic sulfonamides as topical intraocular pressure-lowering agents with prolonged duration of action*. J Med Chem, 2000. **43**(23): p. 4542-51.
57. Winum, J.Y., et al., *Carbonic anhydrase inhibitors: clash with Ala65 as a means for designing inhibitors with low affinity for the ubiquitous isozyme II, exemplified by the crystal structure of the topiramate sulfamide analogue*. J Med Chem, 2006. **49**(24): p. 7024-31.
58. Saczewski, F., et al., *Carbonic anhydrase inhibitors. Inhibition of the cytosolic human isozymes I and II, and the transmembrane, tumor-associated isozymes IX and XII with substituted aromatic sulfonamides activatable in hypoxic tumors*. Bioorg Med Chem Lett, 2006. **16**(18): p. 4846-51.
59. De Simone, G., et al., *Carbonic anhydrase inhibitors: Hypoxia-activatable sulfonamides incorporating disulfide bonds that target the tumor-associated isoform IX*. J Med Chem, 2006. **49**(18): p. 5544-51.
60. Maresca, A., et al., *Non-zinc mediated inhibition of carbonic anhydrases: coumarins are a new class of suicide inhibitors*. J Am Chem Soc, 2009. **131**(8): p. 3057-62.
61. Maresca, A., et al., *Deciphering the mechanism of carbonic anhydrase inhibition with coumarins and thiocoumarins*. J Med Chem, 2010. **53**(1): p. 335-44.
62. Touisni, N., et al., *Glycosyl coumarin carbonic anhydrase IX and XII inhibitors strongly attenuate the growth of primary breast tumors*. J Med Chem, 2011. **54**(24): p. 8271-7.
63. Bonneau, A., et al., *Metronidazole-coumarin conjugates and 3-cyano-7-hydroxy-coumarin act as isoform-selective carbonic anhydrase inhibitors*. J Enzyme Inhib Med Chem, 2013. **28**(2): p. 397-401.
64. Bhatt, A., et al., *Structure activity relationships of benzenesulfonamide-based inhibitors towards carbonic anhydrase isoform specificity*. Chembiochem, 2016.
65. Supuran, C.T., *Drug interaction considerations in the therapeutic use of carbonic anhydrase inhibitors*. Expert Opin Drug Metab Toxicol, 2016. **12**(4): p. 423-31.
66. Fisher, S.Z., et al., *Neutron diffraction of acetazolamide-bound human carbonic anhydrase II reveals atomic details of drug binding*. J Am Chem Soc, 2012. **134**(36): p. 14726-9.
67. Chandak, N., et al., *Novel sulfonamide bearing coumarin scaffolds as selective inhibitors of tumor associated carbonic anhydrase isoforms IX and XII*. Bioorg Med Chem, 2016. **24**(13): p. 2882-6.
68. Diaz, J.R., et al., *Salts of 5-amino-2-sulfonamide-1,3,4-thiadiazole, a structural and analog of acetazolamide, show interesting carbonic anhydrase inhibitory properties, diuretic, and anticonvulsant action*. J Enzyme Inhib Med Chem, 2016. **31**(6): p. 1102-10.
69. De Luca, L., et al., *Structure-based screening for the discovery of new carbonic anhydrase VII inhibitors*. Eur J Med Chem, 2014. **71**: p. 105-11.
70. Wolber, G. and T. Langer, *LigandScout: 3-D pharmacophores derived from protein-bound ligands and their use as virtual screening filters*. J Chem Inf Model, 2005. **45**(1): p. 160-9.
71. Shank, R.P., et al., *Topiramate: preclinical evaluation of structurally novel anticonvulsant*. Epilepsia, 1994. **35**(2): p. 450-60.
72. Casini, A., et al., *Carbonic anhydrase inhibitors: SAR and X-ray crystallographic study for the interaction of sugar sulfamates/sulfamides with isozymes I, II and IV*. Bioorg Med Chem Lett, 2003. **13**(5): p. 841-5.
73. Scozzafava, A., C.T. Supuran, and F. Carta, *Antiobesity carbonic anhydrase inhibitors: a literature and patent review*. Expert Opin Ther Pat, 2013. **23**(6): p. 725-35.
74. Supuran, C.T.D.F., A.; & De Simone, G., *Carbonic anhydrase inhibitors as emerging drugs for the treatment of obesity* Expert Opin. Emerging Drugs, 2008. **13**: p. 383-392.
75. Fukuoka, K., et al., *Mechanisms of action of the novel sulfonamide anticancer agent E7070 on cell cycle progression in human non-small cell lung cancer cells*. Invest New Drugs, 2001. **19**(3): p. 219-27.

76. Abbate, F., et al., *Carbonic anhydrase inhibitors: E7070, a sulfonamide anticancer agent, potently inhibits cytosolic isozymes I and II, and transmembrane, tumor-associated isozyme IX*. *Bioorg Med Chem Lett*, 2004. **14**(1): p. 217-23.
77. Gitto, R., et al., *Synthesis, structure-activity relationship studies, and X-ray crystallographic analysis of arylsulfonamides as potent carbonic anhydrase inhibitors*. *J Med Chem*, 2012. **55**(8): p. 3891-9.
78. Gitto, R., et al., *Synthesis and evaluation of pharmacological profile of 1-aryl-6,7-dimethoxy-3,4-dihydroisoquinoline-2(1H)-sulfonamides*. *Bioorg Med Chem*, 2009. **17**(10): p. 3659-64.
79. Gitto, R., et al., *Synthesis and biological profile of new 1,2,3,4-tetrahydroisoquinolines as selective carbonic anhydrase inhibitors*. *Bioorg Med Chem*, 2011. **19**(23): p. 7003-7.
80. Gitto, R., et al., *Identification of 3,4-Dihydroisoquinoline-2(1H)-sulfonamides as potent carbonic anhydrase inhibitors: synthesis, biological evaluation, and enzyme–ligand X-ray studies*. *J Med Chem*, 2010. **53**(6): p. 2401-8.
81. Lason, W., M. Chlebicka, and K. Rejdak, *Research advances in basic mechanisms of seizures and antiepileptic drug action*. *Pharmacol Rep*, 2013. **65**(4): p. 787-801.
82. Meldrum, B.S. and M.A. Rogawski, *Molecular targets for antiepileptic drug development*. *Neurotherapeutics*, 2007. **4**(1): p. 18-61.
83. Ruusuvoori, E., et al., *Neuronal carbonic anhydrase VII provides GABAergic excitatory drive to exacerbate febrile seizures*. *EMBO J*, 2013. **32**(16): p. 2275-86.
84. Pictet, A.S., T., *Über die Bildung von Isochinolin-derivaten durch Einwirkung von Methylal auf Phenyl-äthylamin, Phenyl-alanin und Tyrosin*. *Berichte der deutschen chemischen Gesellschaft*, 1911. **44**(3): p. 2030-2036.
85. Wishart, D.E. and J.B. Whaley, *Rhinology in children; resume of and comments on the literature for 1950*. *Laryngoscope*, 1951. **61**(10): p. 957-88.
86. Hahn G., L.H., *Synthese von Tetrahydro-harman-Derivaten unter physiologischen Bedingungen*. *Chemische Berichte*, 1934. **67**(12): p. 2033.
87. Clark, A.M. and D.D. Perrin, *A re-investigation of the question of activators of carbonic anhydrase*. *Biochem J*, 1951. **48**(4): p. 495-503.
88. Kjalifah, R.G., *The Carbon Dioxide Hydration Activity of Carbonic Anhydrase*. *J. Biol. Chem.*, 1971. **246**: p. 2561-2573.
89. Box, K., et al., *High-throughput measurement of pKa values in a mixed-buffer linear pH gradient system*. *Anal Chem*, 2003. **75**(4): p. 883-92.
90. 11.02, A.L.S.V., www.acdlabs.com. Toronto, (Canada),, 2004.
91. Scherrer, R.A. and S.M. Howard, *Use of distribution coefficients in quantitative structure-activity relationships*. *J Med Chem*, 1977. **20**(1): p. 53-8.
92. Pajouhesh, H. and G.R. Lenz, *Medicinal chemical properties of successful central nervous system drugs*. *NeuroRx*, 2005. **2**(4): p. 541-53.
93. Summerfield, S.G., et al., *Central nervous system drug disposition: the relationship between in situ brain permeability and brain free fraction*. *J Pharmacol Exp Ther*, 2007. **322**(1): p. 205-13.
94. Perola, E., *An analysis of the binding efficiencies of drugs and their leads in successful drug discovery programs*. *J Med Chem*, 2010. **53**(7): p. 2986-97.
95. Shityakov, S., et al., *Characterization, in Vivo Evaluation, and Molecular Modeling of Different Propofol-Cyclodextrin Complexes To Assess Their Drug Delivery Potential at the Blood-Brain Barrier Level*. *J Chem Inf Model*, 2016.
96. Hopkins, A.L., et al., *The role of ligand efficiency metrics in drug discovery*. *Nat Rev Drug Discov*, 2014. **13**(2): p. 105-21.
97. Supuran, C.T., *Carbonic anhydrases: again, and again, and again*. *Curr Pharm Des*, 2010. **16**(29): p. 3231-2.
98. Murray, C.W., et al., *Validity of ligand efficiency metrics*. *ACS Med Chem Lett*, 2014. **5**(6): p. 616-8.
99. Alterio, V., et al., *The first example of a significant active site conformational rearrangement in a carbonic anhydrase-inhibitor adduct: the carbonic anhydrase I-topiramate complex*. *Org Biomol Chem*, 2010. **8**(15): p. 3528-33.
100. Alterio, V., et al., *Crystal structure of the catalytic domain of the tumor-associated human carbonic anhydrase IX*. *Proc Natl Acad Sci U S A*, 2009. **106**(38): p. 16233-8.

101. Whittington, D.A., et al., *Expression, assay, and structure of the extracellular domain of murine carbonic anhydrase XIV: implications for selective inhibition of membrane-associated isozymes*. J Biol Chem, 2004. **279**(8): p. 7223-8.
102. Winum, J.Y., et al., *Sulfamates and their therapeutic potential*. Med Res Rev, 2005. **25**(2): p. 186-228.
103. Srivastava, D.K., et al., *Structural analysis of charge discrimination in the binding of inhibitors to human carbonic anhydrases I and II*. J Am Chem Soc, 2007. **129**(17): p. 5528-37.
104. de Koning, C.B., van Otterlo, W.A.L., Michael, J.P., , *Amide rotamers of N-acetyl-1,3-dimethyltetrahydroisoquinolines: synthesis, variable temperature NMR spectroscopy and molecular modeling*. Tetrahedron, 2003. **59**: p. 8337-8345.
105. Lopes, A.B., et al., *Characterization of amide bond conformers for a novel heterocyclic template of N-acylhydrazone derivatives*. Molecules, 2013. **18**(10): p. 11683-704.
106. Buemi, M.R., et al., *Carbonic anhydrase inhibitors: Design, synthesis and structural characterization of new heteroaryl-N-carbonylbenzenesulfonamides targeting druggable human carbonic anhydrase isoforms*. Eur J Med Chem, 2015. **102**: p. 223-32.
107. Mader, P., et al., *Structural basis for the interaction between carbonic anhydrase and 1,2,3,4-tetrahydroisoquinolin-2-ylsulfonamides*. J Med Chem, 2011. **54**(7): p. 2522-6.
108. Brunger, A.T., *Free R value: a novel statistical quantity for assessing the accuracy of crystal structures*. Nature, 1992. **355**(6359): p. 472-5.
109. Bozdag, M., et al., *Structural insights on carbonic anhydrase inhibitory action, isoform selectivity, and potency of sulfonamides and coumarins incorporating arylsulfonylureido groups*. J Med Chem, 2014. **57**(21): p. 9152-67.
110. Alterio, V., et al., *Multiple binding modes of inhibitors to carbonic anhydrases: how to design specific drugs targeting 15 different isoforms?* Chemical reviews, 2012. **112**(8): p. 4421-68.
111. Buemi, M.R., et al., *Carbonic anhydrase inhibitors: Design, synthesis and structural characterization of new heteroaryl-N-carbonylbenzenesulfonamides targeting druggable human carbonic anhydrase isoforms*. European Journal of Medicinal Chemistry, 2015. **102**: p. 223-232.
112. Sherlock, M., N.J. Gittoes, and W. Arlt, *Adrenal crisis causing critical illness related reversible myocardial dysfunction*. Clin Endocrinol (Oxf), 2008. **68**(4): p. 667-9.
113. Nishimori, I., et al., *Carbonic anhydrase inhibitors: inhibition of the transmembrane isozyme XIV with sulfonamides*. Bioorg Med Chem Lett, 2005. **15**(17): p. 3828-33.
114. Nishimori, I., et al., *Carbonic anhydrase inhibitors. The mitochondrial isozyme VB as a new target for sulfonamide and sulfamate inhibitors*. J Med Chem, 2005. **48**(24): p. 7860-6.
115. Innocenti, A., et al., *Carbonic anhydrase inhibitors. Inhibition of transmembrane isozymes XII (cancer-associated) and XIV with anions*. Bioorg Med Chem Lett, 2007. **17**(6): p. 1532-7.
116. Nishimori, I., et al., *Carbonic anhydrase inhibitors: DNA cloning and inhibition studies of the alpha-carbonic anhydrase from Helicobacter pylori, a new target for developing sulfonamide and sulfamate gastric drugs*. J Med Chem, 2006. **49**(6): p. 2117-26.
117. Chapman, A.G., M.J. Croucher, and B.S. Meldrum, *Evaluation of anticonvulsant drugs in DBA/2 mice with sound-induced seizures*. Arzneimittelforschung, 1984. **34**(10): p. 1261-4.
118. Litchfield, J.T., Jr., *A method for rapid graphic solution of time-per cent effect curves*. J Pharmacol Exp Ther, 1949. **97**(4): p. 399-408, 3 tab.
119. Mueller, U., et al., *Facilities for macromolecular crystallography at the Helmholtz-Zentrum Berlin*. J Synchrotron Radiat, 2012. **19**(Pt 3): p. 442-9.
120. Kabsch, W., *Xds*. Acta Crystallogr D Biol Crystallogr, 2010. **66**(Pt 2): p. 125-32.
121. M. Krug, M.S.W., U. Heinemann, U. Mueller, *XDSAPP: a graphical user interface for the convenient processing of diffraction data using XDS*. J. Appl. Crystall., 2012. **45**(568-572).
122. Leslie, A.G., *Integration of macromolecular diffraction data*. Acta Crystallogr D Biol Crystallogr, 1999. **55**(Pt 10): p. 1696-702.
123. P.R. Evans, i.L.S., N. Isaacs, S. Bailey (Eds.), *Proceedings of the CCP4 Study Weekend. Data Collection and Processing*. Daresbury Laboratory, Warrington,, 1993(114-122).
124. *The CCP4 suite: programs for protein crystallography*. Acta Crystallogr. Sect.D, 1994. **50**(760-763).

125. Schuttelkopf, A.W. and D.M. van Aalten, *PRODRG: a tool for high-throughput crystallography of protein-ligand complexes*. Acta Crystallogr D Biol Crystallogr, 2004. **60**(Pt 8): p. 1355-63.
126. Emsley, P. and K. Cowtan, *Coot: model-building tools for molecular graphics*. Acta Crystallogr D Biol Crystallogr, 2004. **60**(Pt 12 Pt 1): p. 2126-32.
127. Lovell, S.C., et al., *Structure validation by Calpha geometry: phi,psi and Cbeta deviation*. Proteins, 2003. **50**(3): p. 437-50.
128. Otwinowski, Z., Minor, W., *Processing of X-ray diffraction data collected in oscillation mode*. Methods Enzymol, 1997. **276**: p. 307-326.
129. Jones, T.A., et al., *Improved methods for building protein models in electron density maps and the location of errors in these models*. Acta crystallographica. Section A, Foundations of crystallography, 1991. **47 (Pt 2)**: p. 110-9.
130. Brunger, A.T., *Version 1.2 of the Crystallography and NMR system*. Nature protocols, 2007. **2**(11): p. 2728-33.
131. Schuttelkopf, A.W. and D.M. van Aalten, *PRODRG: a tool for high-throughput crystallography of protein-ligand complexes*. Acta crystallographica. Section D, Biological crystallography, 2004. **60**(Pt 8): p. 1355-63.
132. Di Fiore, A., et al., *Crystal structure of the C183S/C217S mutant of human CA VII in complex with acetazolamide*. Bioorg Med Chem Lett, 2010. **20**(17): p. 5023-6.
133. Discovery Studio, A., <http://www.accelrys.com>. CA USA, San Diego, 2009.
134. Jones, G., et al., *Development and validation of a genetic algorithm for flexible docking*. J Mol Biol, 1997. **267**(3): p. 727-48.

ANNEX

Several techniques used to obtain a recombinant protein and Isothermal titration calorimetry (ITC)

Supervisor: Prof. Alessio Ciulli

Division of Biological Chemistry & Drug
Discovery, School of Life Sciences



**April 04 – October 07
2016**

During the third year of my PhD, the research activity has been also characterized by the experience done, as visiting graduate student under the supervision of Professor Alessio Ciulli, at the University of Dundee, Division of Biological Chemistry & Drug Discovery, School of Life Sciences, from April to October 2016. Research interests in the Ciulli lab are broadly in understanding and elucidating protein-protein interactions (PPIs) and protein surfaces, in interrogating their ligandability i.e. propensity to bind strongly to small molecules, and in exploiting protein-protein and protein-ligand molecular recognition to develop novel small molecules that modulate biological systems. A present focus is on PPIs and PTM recognition within two protein families of biological and medical relevance within the ubiquitin and chromatin systems: the Cullin RING E3 ubiquitin ligases (CRLs) and a family of proteins containing paired chromatin-reader domains.

1.1 Recombinant protein

To obtain a recombinant protein the procedure consists of several steps. Once the gene of interest is chosen, key decisions include the choice of the expression system and expression vector, transforming the host of choice with such vector, inducing protein expression and, finally, purification and characterization of the recombinant protein.

The choice of the host cell whose protein synthesis machinery will produce the precious protein will initiate the outline of the whole process. Among microorganisms, host systems that are available include bacteria, yeast, filamentous fungi, and unicellular algae.

Escherichia coli is one of the organisms of choice for the production of recombinant proteins. Its use as a cell factory is well established and it has become the most popular expression platform.

The advantages of using *E. coli* as the host organism are well known. First of all, it has unparalleled fast growth kinetics. Indeed, the doubling time during steady-state growth is ~20 min. This means that a culture inoculated with a 1/100 dilution of a saturated starter culture may reach stationary phase in a few hours.^[1] Second, high cell density cultures can be easily achieved.^[2] Finally, transformation with exogenous DNA is fast and easy. Plasmid transformation of *E. coli* can be performed in as little as 5 min.^[3, 4]

The most common expression plasmids in use today are the result of multiple combinations of replicons, promoters, selection markers, multiple cloning sites, and fusion protein/fusion protein removal strategies (Figure 1).

Replicon: is a genetic element present in the plasmids that undergoes replication as autonomous units. There are several, commonly used, vectors, such as the pET series, that possess the pMB1 origin (ColE1-derivative, 15–60 copies per cell),^[5, 6] a mutated version of the pMB1 origin is present in the pUC series (500–700 copies per cell).^[6] They all belong to the same group, meaning that they cannot be propagated together in the same cell as they compete with each other for the replication machinery.^[7, 8] Alternatively, the use of the Duet vectors (Novagen) simplifies dual expression by allowing cloning of two genes in the same plasmid. The Duet plasmids possess two multiple cloning sites, each preceded by a T7 promoter, a *lac* operator and a ribosome binding site.

Promoter: The *lac* is the component key of the promoter. Lactose causes induction of the system and this sugar can be used for protein production. However, induction is difficult in the presence of readily metabolizable carbon sources (such as glucose present in rich media).

The T7 promoter system present in the pET vectors (pMB1 ori, medium copy number, Novagen) is extremely popular for recombinant protein expression. This is not surprising as the target protein can represent 50% of the total cell protein in successful cases.^[9, 10] Thus, the system can be induced by lactose or its non-hydrolyzable analog isopropyl β -D-1-thiogalactopyranoside (IPTG).

Selection marker: To deter the growth of plasmid-free cells, an antibiotic resistance marker is added to the plasmid backbone. Resistance to ampicillin is conferred by the *bla* gene whose product is a periplasmic enzyme that inactivates the β -lactam ring of β -lactam antibiotics. However, as the β -lactamase is continuously secreted, degradation of the antibiotic ensues and in a couple of hours, ampicillin is almost depleted.^[11] Under this situation, cells that do not carry the plasmid are allowed to increase in number during cultivation. To overcome this issue, a combination of different antibiotics including ampicillin, streptomices, and tetracycline, can be used.

Tag removal: Once the protein is obtained and extracted from the cell, it can be useful to cleave the fusion partner off from the recombinant protein. This is because the fusion partner can often interfere with protein activity and structure.^[12, 13] Tags can be eliminated by either enzymatic cleavage or chemical cleavage. For enzymatic cleavage, the expression vectors possess sequences that encode for protease cleavage sites downstream of the gene coding for the tag. Enterokinase, thrombin, factor Xa and the tobacco etch virus (TEV) protease have all been successfully used for the removal of peptide tags and fusion partners. The use of *His-tagged TEV* has become an everyday choice due to its high cleavage specificity and convenient removal following a second Ni-NTA affinity chromatography purification step.

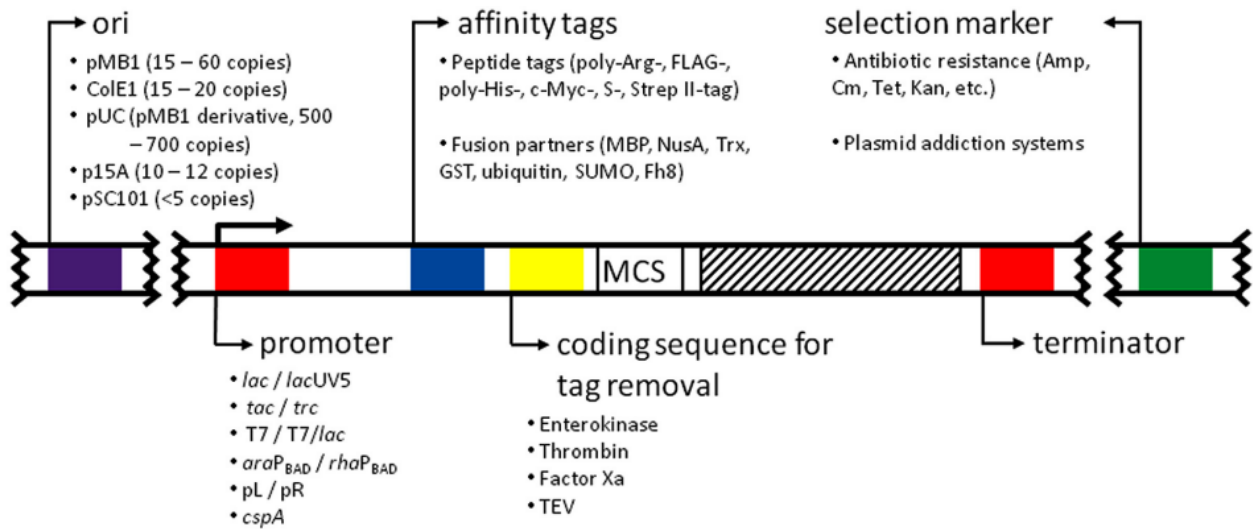


Figure 1: Structure of an expression vector with the major features present in common expression vectors.^[4]

1.1.1 Procedure for protein expression in *Escherichia coli* - BL21(DE3)

There are several reported strains of *E. coli*, and the BL21(DE3) and its derivatives are by far the most used strains for protein expression. In the first step, the transformation of the protein-coding plasmid into BL21(DE3) begins by taking competent cell stock aliquots out of a -80°C freezer and placing them on ice to thaw for about 30 min. After in the thawed competent cells add the chosen plasmids, vortex briefly to mix and let incubate on ice for a least 20 min. Next submit the sample to heat shock at exactly 42°C for 1 min, and swiftly place it on ice. At this point add an aliquot of LB (Luria-Bertani broth), a medium popular with bacteriologists because it permits fast and effective growth yields for many bacterial species. Shake at 37°C for at least 1 h.

In the end the content present in the eppendorf was transferred into an LB agar plate and after the addition of the appropriate antibiotics the plate has been incubated at 37°C for 14 h.

In the second step of the procedure of protein expression, a single bacterial colony was picked from the plate using a sterile inoculation loop and added into a flask with typically 250 to 500 mL

of LB used for the culture, along with an antibiotic. This was incubated in a shaker (190 rpm) at 37°C for about 16 h. After 16 h the OD₆₀₀ of the culture was measured. The abbreviation OD600 is a metric that indicates the absorbance, or optical density, of a sample measured at a wavelength of 600 nm. This method is used to estimate the concentration of bacterial cells in a solution. In this way, we can know the stage of cultured cell population, i.e. whether it is in lag phase, exponential phase, or stationary phase. So, to obtain a good bacteria growth the measurement of the OD it is fundamental. The ideal starting culture OD values are between 0.5 to 1.5. When the cultures were around this value of OD, they were equally divided in different flasks, pre-filled with LB and desired antibiotics, chosen to obtain the desired bacterial growth. These flasks were shaken at 190 rpm at 37°C. When the OD value reached around 0.8 (roughly after 3-4 h from inoculation), we induced protein expression by adding IPTG. This step is called *induction*. We added the same amount of IPTG in each flask, which were incubated shaking at 18°C overnight.

1.1.2 Procedure to purify the protein

In the beginning we must proceed to lysis and sonication of the bacteria. The contents of flasks were transferred in empty bottles and placed in a high-speed centrifuge to separate the cell pastes by centrifugation. Once the supernatant was removed, the pellets remaining at the bottom of the bottles were treated with a lysis buffer, to which lysozyme was added, and stirred for 15 min. After the procedure of homogenization, the suspension becomes turbid and viscous due to release of the bacteria's genomic DNA. In order to eliminate this extreme turbidity, the suspension was sonicated (~5 min) until the turbidity is similar to that of a normal protein solution. Following high-speed centrifugation, the pellet and the supernatant fractions are separated. Generally the protein is found soluble in the supernatant fraction, allowing the subsequent steps of protein purification. The purification has been carried out in three different steps, using the AKTA purifier, with two different columns, three different dialysis conditions and all steps have been monitored with the SDS-PAGE electrophoresis. The protein obtained was aliquoted and aliquots were stored at -80°C in freezer for subsequent use.

2.1 SDS-PAGE electrophoresis

Protein electrophoresis is the movement of protein within an electric field. It is most commonly used to separate proteins for the purposes of analysis and purification.

The term electrophoresis refers to the movement of charged molecules in response to an electric field, resulting in their separation. In an electric field, proteins move toward the electrode of opposite charge. Factors affecting protein electrophoresis include the strength of the electric field, the temperature of the system, the pH, ion type, and concentration of the buffer as well as the size, shape and charge of the proteins (Garfin, D.E; *One dimensional gel electrophoresis*, 1990).

Protein electrophoresis can be performed in either liquid or gel-based media and can also be used to move proteins from one medium to another.

To know if in the different steps we obtained a good separation and which fraction contains our protein, we performed the SDS-PAGE electrophoresis where the gel serves as a size-selective sieve during separation. In most PAGE applications, the gel is mounted between two buffer chambers and the only electrical path between the two buffers is through the gel. Usually the gel has a vertical orientation, and it is cast with a comb that generates wells in which the samples are applied (Figure 2).

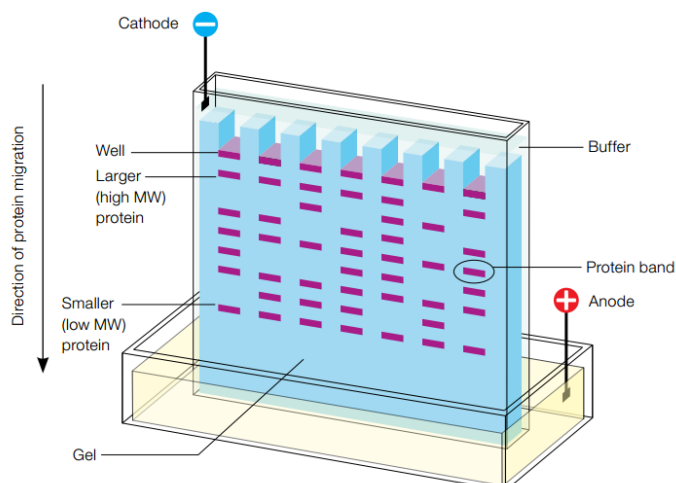


Figure 2: Electrophoresis protein separation system in the polyacrylamide gel.

Applying an electrical field across the buffer chambers forces the migration of protein into and through the gel. We used the SDS-PAGE, where in the PAGE system it has been incorporated the detergent sodium dodecyl sulfate (SDS) into a discontinuous denaturing buffer system, creating what has become the most popular form of protein electrophoresis, SDS-PAGE. With this system the proteins become fully denatured and separate from each other based on their molecular weight. In Figure 3 is reported an example of a gel where protein band patters can be visualized and subjected to qualitative and quantitative analysis.

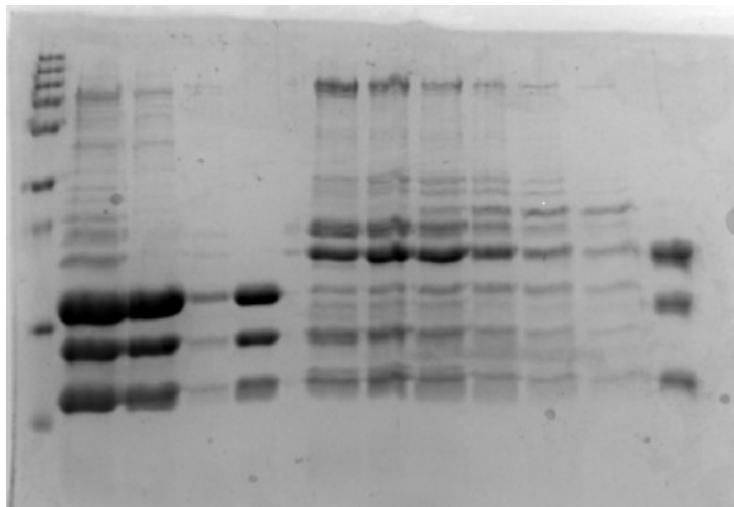


Figure 3: Example of proteins separated on a SDS-PAGE.

3.1 Isothermal titration calorimetry (ITC)

The protein obtained, and described in the previously paragraphs, was used to measure the binding affinity between the protein and specific compounds. To obtain this data we used the technique called Isothermal titration calorimetry (ITC). ITC is one of the most robust label- and immobilization-free biophysical techniques used to measure protein–ligand interactions in drug design. ITC allows the simultaneous determination of the binding constant (K_a) and as a result the free energy of binding ($\Delta G = -RT \ln K_a$), as well as the enthalpy of binding (ΔH), from which the binding entropy can be calculated ($T\Delta S = \Delta H - \Delta G$). These are all important parameters for structure-thermodynamics correlations. Most often ITC is used for protein – ligand interactions in drug design but it can also be used to measure interactions between almost any biochemicals, proteins, nucleic acids, lipids, carbohydrates, and other organic compounds. Despite the fact that most studies use ITC for affinity measurements, an advantage of ITC is that it is the only method that can provide direct determination of the binding enthalpy, which is a useful parameter for structure – thermodynamics correlations in the design of novel drug-like molecules.^[14-16]

References

1. Sezonov, G., D. Joseleau-Petit, and R. D'Ari, *Escherichia coli* physiology in Luria-Bertani broth. *J Bacteriol*, 2007. **189**(23): p. 8746-9.
2. Shiloach, J. and R. Fass, *Growing E. coli to high cell density--a historical perspective on method development*. *Biotechnol Adv*, 2005. **23**(5): p. 345-57.
3. Pope, B. and H.M. Kent, *High efficiency 5 min transformation of Escherichia coli*. *Nucleic Acids Res*, 1996. **24**(3): p. 536-7.
4. Rosano, G.L. and E.A. Ceccarelli, *Recombinant protein expression in Escherichia coli: advances and challenges*. *Front Microbiol*, 2014. **5**: p. 172.
5. Bolivar, F., et al., *Construction and characterization of new cloning vehicles. II. A multipurpose cloning system*. *Gene*, 1977. **2**(2): p. 95-113.
6. Minton, N.P., *Improved plasmid vectors for the isolation of translational lac gene fusions*. *Gene*, 1984. **31**(1-3): p. 269-73.
7. Der, S.D., et al., *Identification of genes differentially regulated by interferon alpha, beta, or gamma using oligonucleotide arrays*. *Proc Natl Acad Sci U S A*, 1998. **95**(26): p. 15623-8.
8. Camps, M., *Modulation of ColE1-like plasmid replication for recombinant gene expression*. *Recent Pat DNA Gene Seq*, 2010. **4**(1): p. 58-73.
9. Baneyx, F., *Recombinant protein expression in Escherichia coli*. *Curr Opin Biotechnol*, 1999. **10**(5): p. 411-21.
10. Graumann, K. and A. Premstaller, *Manufacturing of recombinant therapeutic proteins in microbial systems*. *Biotechnol J*, 2006. **1**(2): p. 164-86.
11. Korpimaki, T., J. Kurittu, and M. Karp, *Surprisingly fast disappearance of beta-lactam selection pressure in cultivation as detected with novel biosensing approaches*. *J Microbiol Methods*, 2003. **53**(1): p. 37-42.
12. Wu, J. and M. Filutowicz, *Hexahistidine (His6)-tag dependent protein dimerization: a cautionary tale*. *Acta Biochim Pol*, 1999. **46**(3): p. 591-9.
13. Perron-Savard, P., G. De Crescenzo, and H. Le Moual, *Dimerization and DNA binding of the Salmonella enterica PhoP response regulator are phosphorylation independent*. *Microbiology*, 2005. **151**(Pt 12): p. 3979-87.
14. Ciulli, A., et al., *Probing hot spots at protein-ligand binding sites: a fragment-based approach using biophysical methods*. *J Med Chem*, 2006. **49**(16): p. 4992-5000.
15. Linkuviene, V., et al., *Isothermal titration calorimetry for drug design: Precision of the enthalpy and binding constant measurements and comparison of the instruments*. *Anal Biochem*, 2016. **515**: p. 61-64.
16. Patel, S.G. and P.M. Bummer, *Thermodynamics of Aggregate Formation between a Non-Ionic Polymer and Ionic Surfactants: an Isothermal Titration Calorimetric Study*. *Int J Pharm*, 2016.